Journal of Research of the National Bureau of Standards Vol. 54, No. 4, April 1955 Research Paper 2579

Partially Balanced Incomplete Block Designs With Two Associate Classes and Two Treatments Per Block

Willard H. Clatworthy

In physical science experimentation the experimental material may divide naturally into groups of two objects (treatments) each. Thus, the experimental arrangement will involve what is known in the design of experiments as an incomplete block design. In this paper an investigation is made of a special kind of incomplete block design known as the partially balanced incomplete block design with two associate classes. In these designs the various comparisons of pairs of objects involve two kinds of precision.

An enumeration is made of all partially balanced incomplete block designs with two associate classes and two treatments per block where r, the number of times each treatment appears in the arrangement, is less than or equal to 10. Simple instructions are given for writing the experimental arrangements. These designs have a definite known method for analysis of the data. No attempt has been made to state which of the various designs are best, since it is felt that the best design must be determined for the particular investigation.

1. Introduction

It happens rather frequently in physical science experimentation, and occasionally in biological investigations, that the experimental material divides naturally into groups of two. For example, the comparison of the lengths of meter bars is conveniently made two at a time, the testing of experimental rubbers for automobile tires might be performed with the two halves of a tire made of different experimental rubber, or nutritional experiments might involve twins. Designs with two treatments per block have been studied by Yates [11][1], Kempthorne [10], Youden and Connor [9], and Bose and Nair [5].

The object of this paper is to investigate the class of partially balanced incomplete block (PBIB) designs with two associate classes having

(a) two treatments per block, and

(b) 10 or fewer replications of each treatment.

A complete enumeration has been made of all sets of parameter values for all designs of this class that satisfy the necessary conditions for PBIB designs with two associate classes set forth in [3, 4, 6, 7, 8]. Solutions (experimental arrangements) for all parameter sets given in the enumeration are contained in this paper with but four exceptions. In these four unsolved designs the number of treatment-pairs (blocks) is rather large, and an intensive search for solutions was not made.

Bose [1] has exhausted the class of PBIB designs with two associate classes and two replications of each treatment. Designs found in [1] that fall within the scope of this investigation are included here.

The great majority of the designs of the class under consideration may be classified according to four types discussed in [6], namely, group divisible designs, triangular designs, square designs, and cyclic designs.

2. Definition of a Partially Balanced Design With Two Associate Classes

A partially balanced incomplete block design with two associate classes is an arrangement of v treatments in b blocks, such that:

1. Each of the v treatments occurs r times in the arrangement, which consists of b blocks each of which contains k experimental units. No treatment appears more than once in any block.

2. Every pair among the v treatments occurs together in either λ_1 or λ_2 blocks (and are said to be ith associates, if they occur together in λ_i blocks, $i=1, 2$).

[1] Figures in brackets indicate the literature references at the end of this paper.

UNIVERSITY OF MICHIGAN LIBRARIES

3. There exists a relationship of association between every pair of the v treatments satisfying the following conditions:

a. Any two treatments are either first or second associates.

b. Each treatment has n_1 first and n_2 second associates.

c. Given any two treatments that are ith associates, the number of treatments common to the jth associates of the first and the kth associates of the second is p_{jk}^{i}, and this number is independent of the pair of treatments with which we start. Furthermore, $p_{jk}^{i}=p_{kj}^{i}$ $(i,j,k=1,2)$.

For partially balanced incomplete block designs with two associate classes, it is well-known that the following relationships are necessary:

$$vr=bk, \tag{1}$$

$$v=n_1+n_2+1, \tag{2}$$

$$\lambda_1 n_1+\lambda_2 n_2=r(k-1), \tag{3}$$

$$p_{11}^{1}+p_{12}^{1}+1=p_{11}^{2}+p_{12}^{2}=n_1, \tag{4}$$

$$p_{21}^{1}+p_{22}^{1}=p_{21}^{2}+p_{22}^{2}+1=n_2, \tag{5}$$

$$n_1 p_{12}^{1}=n_2 p_{11}^{1}, \qquad n_1 p_{22}^{1}=n_2 p_{12}^{2}. \tag{6}$$

The eight parameters v, b, r, k, λ_1, λ_2, n_1, and n_2 are known as the parameters of the first kind, and the parameters p_{jk}^{i} $(i,j,k=1,2)$ are called the parameters of the second kind. The parameters of the second kind may be displayed as elements of two symmetric matrices.

$$P_1=\begin{pmatrix} p_{11}^{1} & p_{12}^{1} \\ p_{21}^{1} & p_{22}^{1} \end{pmatrix} \quad \text{and} \quad P_2=\begin{pmatrix} p_{11}^{2} & p_{12}^{2} \\ p_{21}^{2} & p_{22}^{2} \end{pmatrix}. \tag{7}$$

For a general definition of a partially balanced incomplete block design with $m(\geq 1)$ associate classes and for a discussion of the classification, properties, and analysis of designs having $m=2$, the reader is referred to the excellent paper by Bose and Shimamoto [6]. The notation used in the present paper follows rather closely that in [6].

A design is said to be *connected* if for every two treatments, two blocks, or a block and a treatment, it is possible to pass from one to the other by means of a chain consisting alternately of blocks and treatments, such that every treatment of the chain occurs in each of the adjoining blocks. In this paper only designs possessing the property of connectedness are considered.

3. Group Divisible Designs With Two Treatments Per Block

In the group divisible designs the $v=mn$ treatments can be divided into m groups of n treatments each, such that any two treatments belonging to the same group are first associates, and any two treatments belonging to different groups are second associates. Bose and Shimamoto [6], who discovered the group divisible designs, showed that their association scheme is an $m\times n$ rectangular array of the v treatments in which the rows constitute groups. For these arrays they showed that the following relations hold:

$$n_1=n-1, \qquad n_2=n(m-1), \qquad (n-1)\lambda_1+n(m-1)\lambda_2=r(k-1), \tag{8}$$

and the parameters of the second kind are the elements of the symmetric matrices,

$$P_1=(p_{jk}^{1})=\begin{pmatrix} n-2 & 0 \\ 0 & n(m-1) \end{pmatrix}, \qquad P_2=(p_{jk}^{2})=\begin{pmatrix} 0 & n-1 \\ n-1 & n(m-2) \end{pmatrix}. \tag{9}$$

For the special case in which each block consists of two treatments $(k=2)$, each treatment of a

group is paired with each of the other $n-1$ treatments of the same group λ_1 times and with each of the treatments of the other $m-1$ groups λ_2 times to form the blocks of the design. Obviously, each of the $v=mn$ treatments occurs

$$r=(n-1)\lambda_1+n(m-1)\lambda_2 \tag{10}$$

times in the design that contains

$$b=mn[(n-1)\lambda_1+n(m-1)\lambda_2]/2 \tag{11}$$

blocks each of size $k=2$.

Note that for a given subclass of designs characterized by known values of r, $k=2$, b, λ_1, and λ_2, all designs of the subclass are determined by the sets of all integral values of m and n $(m,n\geq 2)$ satisfying (10) and (11).

For any PBIB design with two associate classes, Bose and Shimamoto define four computational constants c_1, c_2, H, and Δ by means of the following relations:

$$k^2\Delta=(rk-r+\lambda_1)(rk-r+\lambda_2)+(\lambda_1-\lambda_2)\{r(k-1)(p_{12}^1-p_{12}^2)+\lambda_2 p_{12}^1-\lambda_1 p_{12}^2\}, \tag{12}$$

$$kH=(2rk-2r+\lambda_1+\lambda_2)+(p_{12}^1-p_{12}^2)(\lambda_1-\lambda_2), \tag{13}$$

$$k\Delta c_1=\lambda_1(rk-r+\lambda_2)+(\lambda_1-\lambda_2)(\lambda_2 p_{12}^1-\lambda_1 p_{12}^2), \tag{14}$$

$$k\Delta c_2=\lambda_2(rk-r+\lambda_1)+(\lambda_1-\lambda_2)(\lambda_2 p_{12}^1-\lambda_1 p_{12}^2). \tag{15}$$

For group divisible designs with two treatments per block these expressions simplify to

$$c_1=2\lambda_1/(r+\lambda_1), \qquad c_2=2[(r+n\lambda_1)\lambda_2-(n-1)\lambda_1^2]/mn\lambda_2(r+\lambda_1), \tag{16}$$

$$H=n[\lambda_1+(2m-1)\lambda_2]/2, \tag{17}$$

and

$$\Delta=mn\lambda_2(r+\lambda_1)/4. \tag{18}$$

It is known that λ_2, the "between group λ" of group divisible designs, is never zero; hence there is no difficulty in evaluating c_2.

The efficiency, E, of group divisible designs with block size two, as compared with a randomized block design with the same number of treatments and replications, is given by

$$E=(nm-1)/[(n-1)(2-c_1)+n(m-1)(2-c_2)]. \tag{19}$$

Table 1 contains the parameters of all group divisible designs with two treatments per block and $2\leq r\leq 10$. The computational constants c_1, c_2, H, and Δ, and also E are given. Of course, there exist many other group divisible designs with $k\geq 3$, as well as designs with $k=2$ and $r>10$.

The construction of group divisible designs with two treatments per block by use of the groups (association schemes) is exceedingly simple. For example, let us construct design 2 of table 1. This design has parameters

$$v=6, \quad b=9, \quad r=3, \quad k=2, \quad m=2, \quad n=3, \quad \lambda_1=0, \quad \lambda_2=1.$$

Let the six treatments be represented by the integers 1, 2, · · ·, 6, and let the $m=2$ groups be

1	2	3
4	5	6

By the rule previously given for forming the blocks, no treatment of any group can occur in a block with any other treatment belonging to the same group (since $\lambda_1=0$), and each treatment

UNIVERSITY OF MICHIGAN LIBRARIES

TABLE 1. *Group divisible designs with two treatments per block and $2 \leq r \leq 10$*

Reference	v	b	r	m	n	λ_1	λ_2	c_1	c_2	H	Δ	E
1	4	4	2	2	2	0	1	0	1/2	3	2	3/5
2	6	9	3	2	3	0	1	0	1/3	9/2	9/2	5/9
3	6	12	4	3	2	0	1	0	1/3	5	6	15/26
4	8	16	4	2	4	0	1	0	1/4	6	8	7/13
5	4	8	4	2	2	0	2	0	1/2	6	8	3/5
6	4	8	4	2	2	2	1	2/3	1/3	5	6	9/14
7	10	25	5	2	5	0	1	0	1/5	15/2	25/2	9/17
8	4	10	5	2	2	1	2	1/3	13/24	7	12	36/55
9	4	10	5	2	2	3	1	3/4	1/8	6	8	3/5
10	8	24	6	4	2	0	1	0	1/4	7	12	14/25
11	9	27	6	3	3	0	1	0	2/9	15/2	27/2	6/11
12	12	36	6	2	6	0	1	0	1/6	9	18	11/21
13	4	12	6	2	2	0	3	0	1/2	9	18	3/5
14	6	18	6	2	3	0	2	0	1/3	9	18	5/9
15	6	18	6	3	2	2	1	1/2	1/4	7	12	10/17
16	4	12	6	2	2	4	1	4/5	−1/10	7	10	5/9
17	14	49	7	2	7	0	1	0	1/7	21/2	49/2	13/25
18	6	21	7	2	3	2	1	4/9	5/27	15/2	27/2	45/77
19	6	21	7	3	2	3	1	3/5	2/15	8	15	75/133
20	4	14	7	2	2	1	3	1/4	13/24	10	24	9/14
21	4	14	7	2	2	3	2	3/5	17/40	9	20	60/91
22	4	14	7	2	2	5	1	5/6	−1/3	8	12	18/35
23	10	40	8	5	2	0	1	0	1/5	9	20	45/82
24	12	48	8	3	4	0	1	0	1/6	10	24	33/62
25	16	64	8	2	8	0	1	0	1/8	12	32	15/29
26	6	24	8	3	2	0	2	0	1/3	10	24	15/26
27	8	32	8	2	4	0	2	0	1/4	12	32	7/13
28	4	16	8	2	2	0	4	0	1/2	12	32	3/5
29	6	24	8	2	3	1	2	2/9	10/27	21/2	27	45/76
30	8	32	8	4	2	2	1	2/5	1/5	9	20	35/62
31	4	16	8	2	2	2	3	2/5	8/15	11	30	45/68
32	6	24	8	3	2	4	1	2/3	0	9	18	15/28
33	4	16	8	2	2	4	2	2/3	1/3	10	24	9/14
34	4	16	8	2	2	6	1	6/7	−4/7	9	14	21/44
35	12	54	9	4	3	0	1	0	1/6	21/2	27	22/41
36	18	81	9	2	9	0	1	0	1/9	27/2	81/2	17/33
37	6	27	9	2	3	0	3	0	1/3	27/2	81/2	5/9
38	6	27	9	3	2	1	2	1/5	7/20	11	30	25/42
39	6	27	9	2	3	3	1	1/2	0	9	18	5/9
40	8	36	9	4	2	3	1	1/2	1/8	10	24	28/51
41	4	18	9	2	2	1	4	1/5	43/80	13	40	40/63
42	6	27	9	3	2	5	1	5/7	−1/7	10	21	35/69
43	4	18	9	2	2	5	2	5/7	13/56	11	28	28/45
44	12	60	10	6	2	0	1	0	1/6	11	30	33/61
45	15	75	10	3	5	0	1	0	2/15	25/2	75/2	21/40
46	20	100	10	2	10	0	1	0	1/10	15	50	19/37
47	10	50	10	2	5	0	2	0	1/5	15	50	9/17
48	4	20	10	2	2	0	5	0	1/2	15	50	3/5
49	8	40	10	2	4	2	1	1/3	1/8	10	24	14/25
50	9	45	10	3	3	2	1	1/3	4/27	21/2	27	36/65
51	10	50	10	5	2	2	1	1/3	1/6	11	30	27/49
52	8	40	10	4	2	4	1	4/7	1/28	11	28	98/185
53	4	20	10	2	2	2	4	1/3	13/24	14	48	36/55
54	4	20	10	2	2	4	3	4/7	19/42	13	42	63/95
55	6	30	10	3	2	6	1	3/4	−7/24	11	24	12/25
56	4	20	10	2	2	6	2	3/4	1/8	12	32	3/5
57	4	20	10	2	2	8	1	8/9	−19/18	11	18	27/65

must occur once in a block with each of the treatments not in its group (since $\lambda_2=1$). Thus, the $b=9$ blocks of the design are the treatment-pairs in the following columns:

$$\begin{array}{ccccccccc} 1 & 1 & 1 & 2 & 2 & 2 & 3 & 3 & 3 \\ 4 & 5 & 6 & 4 & 5 & 6 & 4 & 5 & 6 \end{array}$$

4. Triangular Designs With Blocks of Size Two

In [6] triangular designs are defined and discussed. Triangular designs have $v=n(n-1)/2$ treatments and an association scheme described as follows. The treatments are arranged in order and in a symmetrical fashion about the principal diagonal of an $n\times n$ array in which the principal diagonal is blanked out. For example, if $n=4$ and the $v=6$ treatments are denoted by the integers $1, \cdots, 6$, the association scheme is

$$\begin{array}{cccc} * & 1 & 2 & 3 \\ 1 & * & 4 & 5 \\ 2 & 4 & * & 6 \\ 3 & 5 & 6 & * \end{array}$$

Two treatments lying in the same column are first associates, whereas treatments that do not lie in the same column are second associates. Thus, in the above example, treatments 2, 3, 4, and 5 are first associates of treatment 1, whereas treatment 6 is the only second associate of treatment 1. In [6] it is shown that

$$n_1=2(n-2), \qquad n_2=(n-2)(n-3)/2, \tag{20}$$

$$P_1=(p_{ik}^1)=\begin{pmatrix} n-2 & n-3 \\ n-3 & (n-3)(n-4)/2 \end{pmatrix}, \tag{21}$$

and

$$P_2=(p_{ik}^2)=\begin{pmatrix} 4 & 2(n-4) \\ 2(n-4) & (n-4)(n-5)/2 \end{pmatrix}, \tag{22}$$

where $n\geqq 4$.

If, when the v treatments are arranged in an $n\times n$ array as described above, we form all possible treatment-pairs (blocks in the case $k=2$) by pairing each treatment of a row (or column) with every other treatment in the same row (or column), we obtain a design with parameters

$$\begin{array}{llll} v=n(n-1)/2, & r=2(n-2), & \lambda_1=1, & n_1=2(n-2), \\ b=n(n-1)(n-2)/2, & k=2, & \lambda_2=0, & n_2=(n-2)(n-3)/2, \end{array} \tag{23}$$

and parameters of the second kind given by (21) and (22).

For triangular designs the computational constants c_1, c_2, H, and Δ of (12), (13), (14), and (15) simplify to

$$c_1=4/n(n-1), \qquad c_2=-2(n-4)/n(n-1), \tag{24}$$

$$H=(3n-2)/2, \qquad \text{and} \qquad \Delta=n(n-1)/2. \tag{25}$$

The efficiency of a triangular design, as compared with a randomized block design with the same number of treatments and replications, is given by

$$E=n(n-1)(n+1)/2(n-2)(n^2+3n-2). \tag{26}$$

If, instead of forming the treatment-pairs for the blocks as described previously, we pair off each treatment with each of the treatments that does not lie in the same row or column

UNIVERSITY OF MICHIGAN LIBRARIES

of the association scheme, we obtain a triangular design whose parameters are

$$\begin{aligned} &v=n(n-1)/2, && r=(n-2)(n-3)/2, && \lambda_1=0, \\ &b=n(n-1)(n-2)(n-3)/8, && k=2, && \lambda_1=1, \end{aligned} \tag{27}$$

and (20), (21), and (22), where $n \geq 5$.

The constants c_1, c_2, H, and Δ for the latter triangular designs are given by

$$c_1=-8/n(n-1)(n-4), \qquad c_2=4/n(n-1), \tag{28}$$

$$H=(n^2-4n+2)/2, \qquad \text{and} \qquad \Delta=n(n-1)(n-2)(n-3)(n-4)/16, \tag{29}$$

and their efficiency is given by

$$E=(n_1+n_2)/[n_1(2-c_1)+n_2(2-c_2)]. \tag{30}$$

Table 2 gives the parameters of all triangular designs with $k=2$ and $2 \leq r \leq 10$, along with the corresponding values of c_1, c_2, H, Δ, and E. Obviously, triangular designs with $k=2$ and $r>10$ can be found, as can designs with $k \geq 3$.

TABLE 2. *Triangular designs with two treatments per block and $2 \leq r \leq 10$*

Reference	v	b	r	n	λ_1	λ_2	c_1	c_2	H	Δ	E
1	6	12	4	4	1	0	1/3	0	5	6	15/26
2	10	30	6	5	1	0	1/5	−1/10	13/2	10	10/19
3	15	60	8	6	1	0	2/15	−2/15	8	15	105/208
4	21	105	10	7	1	0	2/21	−1/7	19/2	21	42/85
5	10	15	3	5	0	1	−2/5	1/5	7/2	5/2	5/11
6	15	45	6	6	0	1	−2/15	2/15	7	45/4	105/212
7	21	105	10	7	0	1	−4/63	2/21	23/2	63/2	126/250
8	6	24	8	4	2	0	1/3	0	10	24	15/26
9	10	30	6	5	0	2	−2/5	1/5	7	10	5/11

Construction of triangular designs with two treatments per block is easily done by use of the association scheme for the design and the rules for formation of the blocks stated earlier. For example, the association scheme for design 2 of table 2 is

*	1	2	3	4
1	*	5	6	7
2	5	*	8	9
3	6	8	*	10
4	7	9	10	*

Since $\lambda_1=1$ and $\lambda_2=0$, the $b=30$ blocks of the design are formed by writing all pairs of numbers lying in the same row (or column) of the association scheme:

1 2	1 5	2 5	3 6	4 7
1 3	1 6	2 8	3 8	4 9
1 4	1 7	2 9	3 10	4 10
2 3	5 6	5 8	6 8	7 9
2 4	5 7	5 9	6 10	7 10
3 4	6 7	8 9	8 10	9 10

5. Designs With Square Association Schemes

Consider $v=s^2$ treatments arranged in a square array of side s. Let this $s\times s$ array be the association scheme of the design. We shall form blocks of size k by forming all possible distinct k-plets from the treatments lying in each of the rows and in each of the columns of the array. From one row (or column) it is possible to form C_k^s distinct k-plets, where C_k^s represents the number of combinations of s things taken k at a time, k and s being restricted in this application by $2\leq k\leq s$. In this manner it is possible to form $b=2sC_k^s$ blocks, each of size k, and each of the $v=s^2$ treatments will appear once in each of $r=2C_{k-1}^{s-1}$ blocks. Two treatments lying in the same row or in the same column of the association scheme are first associates, while two treatments not lying in the same row or in the same column are second associates. Thus,

$$n_1=2(s-1) \qquad \text{and} \qquad n_2=(s-1)^2. \tag{31}$$

Two treatments that are first associates occur together in C_{k-2}^{s-2} blocks (when $s=k=2$, we define C_0^0 to be unity), while two treatments that are second associates do not occur together in any block. Hence,

$$\lambda_1=C_{k-2}^{s-2} \qquad \text{and} \qquad \lambda_2=0. \tag{32}$$

It is easy to verify that the matrices P_1 and P_2 of (33) give the correct values for the parameters of the second kind. Thus, we have a two-parameter family of designs with

$$\begin{aligned} &v=s^2, \quad r=2C_{k-1}^{s-1}, \quad \lambda_1=C_{k-2}^{s-2}, \quad n_1=2(s-1), \quad P_1=\begin{pmatrix} s-2 & s-1 \\ s-1 & (s-1)(s-2) \end{pmatrix}, \\ &b=2sC_k^s, \quad k=k, \quad \lambda_2=0, \quad n_2=(s-1)^2, \quad P_2=\begin{pmatrix} 2 & 2(s-2) \\ 2(s-2) & (s-2)^2 \end{pmatrix}, \end{aligned} \tag{33}$$

where $s\geq k\geq 2$.

The expressions for e_1, e_2, H, and Δ simplify, in this type of design, to

$$e_1=k/s^2, \qquad e_2=-k(s-2)/s^2, \tag{34}$$

$$H=\frac{3s}{2}\,C_{k-2}^{s-2}, \qquad \text{and} \qquad \Delta=2(s/k)^2. \tag{35}$$

The efficiency of these square designs, as compared with randomized block designs with the same number of treatments and replications, is

$$E=s(s+1)(k-1)/k(s-1)(s+3). \tag{36}$$

In the special case $s=k$, the set of parameters (33) becomes

$$\begin{aligned} &v=s^2, \quad r=2, \quad \lambda_1=1, \quad n_1=2(s-1), \quad P_1=\begin{pmatrix} s-2 & s-1 \\ s-1 & (s-1)(s-2) \end{pmatrix}, \\ &b=2s, \quad k=s, \quad \lambda_2=0, \quad n_2=(s-1)^2, \quad P_2=\begin{pmatrix} 2 & 2(s-2) \\ 2(s-2) & (s-2)^2 \end{pmatrix}, \end{aligned} \tag{37}$$

which is the family of familiar simple square lattice designs with $r=2$ replications.

Putting $k=2$ in (33), we obtain the family of square designs with two treatments per block, the parameters of which are

$$\begin{aligned} &v=s^2, \qquad r=2(s-1), \qquad \lambda_1=1, \qquad n_1=2(s-1), \\ &b=s^2(s-1), \qquad k=2, \qquad \lambda_2=0, \qquad n_2=(s-1)^2, \end{aligned} \tag{38}$$

UNIVERSITY OF MICHIGAN LIBRARIES

where $s \geq 2$, and the parameters of the second kind are given by (33).

All of the designs discussed in this section are of the type known as Latin square designs with two constraints [6].

Setting $s=2, 3, \cdots, 6$ in (38) we obtain the first five designs of table 3. Designs 6, 7, 8, and 9 are n-plicates of design 1, i. e., their solutions are obtained by writing the solution of design 1, $n=2, 3, 4, 5$ times, respectively. Design 11 is obtained by pairing each treatment with the treatments not lying in the same row or column of the square association scheme. If the associate classes of design 11 are renamed, so that $\lambda_1=1$ and $\lambda_2=0$, it is seen that it is a Latin-square type with $i=3$ constraints.

TABLE 3. *Square designs with two treatments per block and $2 \leq r \leq 10$*

Reference	v	b	r	s	λ_1	λ_2	c_1	c_2	H	Δ	E
1	4	4	2	2	1	0	1/2	0	3	2	3/5
2	9	18	4	3	1	0	2/9	−2/9	9/2	9/2	1/2
3	16	48	6	4	1	0	1/8	−1/4	6	8	10/21
4	25	100	8	5	1	0	2/25	−6/25	15/2	25/2	15/32
5	36	180	10	6	1	0	1/18	−2/9	9	18	7/15
6	4	8	4	2	2	0	1/2	0	6	8	3/5
7	4	12	6	2	3	0	1/2	0	9	18	3/5
8	4	16	8	2	4	0	1/2	0	12	32	3/5
9	4	20	10	2	5	0	1/2	0	15	50	3/5
10	9	36	8	3	2	0	2/9	−2/9	9	18	1/2
11	16	72	9	4	0	1	−1/16	1/8	10	24	80/123

Again, the association scheme and the rule for formation of the blocks provide the method of construction that holds for square designs with $k=2$ and $r>10$, as well as for the designs of table 3. To illustrate the construction of square designs, the association scheme for design 2 of table 3 may be represented by the 3×3

$$\begin{array}{ccc} 1 & 2 & 3 \\ 4 & 5 & 6 \\ 7 & 8 & 9 \end{array}$$

array of integers $1, 2, \cdots, 9$. Since $\lambda_1=1$ and $\lambda_2=0$, the $b=18$ blocks of the design are formed by pairing every number with every other number lying in the same row or column. Thus, the 18 blocks are

$$\begin{array}{cccccccccc} \underline{1\ 2} & \underline{4\ 5} & \underline{7\ 8} & \underline{1\ 4} & \underline{2\ 5} & \underline{3\ 6} \\ \underline{1\ 3} & \underline{4\ 6} & \underline{7\ 9} & \underline{1\ 7} & \underline{2\ 8} & \underline{3\ 9} \\ \underline{2\ 3} & \underline{5\ 6} & \underline{8\ 9} & \underline{4\ 7} & \underline{5\ 8} & \underline{6\ 9} \end{array}$$

6. Cyclic Designs With Two Treatments Per Block

Another type of partially balanced design defined and discussed in [6] is the cyclic type. Let the v treatments be represented by the integers $1, 2, \cdots, v$. Then the first associates of treatment i $(i=1,2, \cdots, v)$ are

$$i+d_1,\ i+d_2, \cdots, i+d_{n_1} \pmod{v}, \tag{39}$$

where the d's satisfy the conditions:

1. The d's are all different and $0<d_j<v$ $(j=1,2, \cdots, n_1)$;
2. Among the $n_1(n_1-1)$ differences d_j-d_k $(j\neq k;\ j,k=1,2, \cdots, n_1)$ reduced mod v, each of the numbers $d_1, d_2, \cdots, d_{n_1}$ occurs α times and each of the numbers $e_1, e_2, \cdots, e_{n_2}$ occurs β times, where $d_1, \cdots, d_{n_1}, e_1, \cdots, e_{n_2}$ are all the numbers $1, 2, \cdots, v-1$, $\alpha=p_{11}^1$, and $\beta=p_{11}^2$.

In the special case of PBIB designs with two associate classes and $k=2$, determination of a difference set $d_1, d_2, \cdots, d_{n_1}$ satisfying 1 and 2 above is equivalent to construction of the design, since each of the treatment-pairs $(i, i+d_j)$ reduced mod v $(i=1,2, \cdots,v; j=1,2, \cdots,n_1$ is a block occurring λ_1 times, while each of the treatment-pairs $(i, i+e_k)$ reduced mod v $(i=1,2, \cdots,v; k=1,2, \cdots,n_2)$ is a block occuring λ_2 times.

In table 4 are listed 11 designs having cyclic solutions.

TABLE 4. *Cyclic type designs with two treatments per block and $2 \leq r \leq 10$*

Reference	v	b	r	λ_1	λ_2	n_1	n_2	α	β	c_1	c_2	H	Δ	E
1	5	5	2	1	0	2	2	0	1	2/5	−2/5	5/2	5/4	1/2
2	5	10	4	2	0	2	2	0	1	2/5	−2/5	5	5	1/2
3	5	15	6	3	0	2	2	0	1	2/5	−2/5	15/5	45/4	1/2
4	5	15	6	2	1	2	2	0	1	26/55	2/5	15/2	55/4	55/86
5	5	20	8	4	0	2	2	0	1	2/5	−2/5	10	20	1/2
6	5	20	8	3	1	2	2	0	1	46/95	14/95	10	95/4	19/32
7	5	25	10	5	0	2	2	0	1	2/5	−2/5	25/2	125/4	1/2
8	5	25	10	3	2	2	2	0	1	14/29	2/29	25/2	145/4	29/50
9	5	25	10	3	2	2	2	0	1	14/31	10/31	25/2	155/4	31/50
10	13	39	6	1	0	6	6	2	3	2/13	−2/13	13/2	39/4	1/2
11	17	68	8	1	0	8	8	3	4	2/17	−2/17	17/2	17	1/2

The designs 1 to 9 of table 4 have the difference set $d_1=2$ and $d_2=3$ (mod 5). These designs belong to the family having parameters

$$\begin{aligned} &v=5, && r=2(\lambda_1+\lambda_2), && \lambda_1, && n_1=2, && P_1=\begin{pmatrix}0 & 1\\ 1 & 1\end{pmatrix},\\ &b=5(\lambda_1+\lambda_2), && k=2, && \lambda_2, && n_2=2, && P_2=\begin{pmatrix}1 & 1\\ 1 & 0\end{pmatrix}. \end{aligned} \tag{40}$$

Designs of (40) have a geometrical representation that provides an association scheme. Number the vertices of the five-pointed star 1, 2, 3, 4, 5, in clockwise order. Each line of the

star connecting two vertices is a block occuring λ_1 times, while two vertices not connected by a line is a block occurring λ_2 times, where λ_1 and λ_2 are nonnegative integers satisfying (39).

Design 10 of table 4 has the difference set,

$$d_1=2,\ d_2=5,\ d_3=6,\ d_4=7,\ d_5=8,\ d_6=11 \pmod{13}.$$

Since $\lambda_1=1$ and $\lambda_2=0$, each of the treatment-pairs $(i, i+d_j)$ reduced mod 13 $(i=1,2, \cdots,13; j=1,2, \cdots,6)$ occurs once to give the $b=39$ blocks:

1 3	2 4	3 5	4 9	5 11	6 13	9 11
1 6	2 7	3 8	4 10	5 12	7 9	10 12
1 7	2 8	3 9	4 11	5 13	7 12	11 13
1 8	2 9	3 10	4 12	6 8	7 13	
1 9	2 10	3 11	5 7	6 11	8 10	
1 12	2 13	4 6	5 10	6 12	8 13	

332243—55——2

UNIVERSITY OF MICHIGAN LIBRARIES

Design 11 of table 4 has the difference set

$$d_1=3,\ d_2=5,\ d_3=6,\ d_4=7,\ d_5=10,\ d_6=11,\ d_7=12,\ d_8=14,$$

which, when developed mod 17, will yield a table of first associates for the treatments 1 to 17, where 0 is replaced with 17. Since $\lambda_1=1$ and $\lambda_2=0$, pairing each of the treatments with each of its first associates will yield 68 distinct treatment-pairs, which are the blocks of the design.

7. Other Designs With Two Treatments Per Block

In table 5 are listed 8 sets of parameter values, 4 sets of which are unsolved.

TABLE 5. *Other designs with two treatments per block and $2\leq r\leq 10$*

Reference	v	b	r	λ_1	λ_2	n_1	n_2	p_{11}^1	p_{11}^2	c_1	c_2	H	Δ	E
1	16	40	5	1	0	5	10	0	2	1/8	−3/16	6	8	12/25
2	16	80	10	2	0	5	10	0	2	1/8	−3/16	12	32	12/25
3	16	80	10	1	0	10	5	6	6	1/8	−1/12	10	24	18/35
*4	21	105	10	1	0	10	10	4	5					
*5	26	130	10	1	0	10	15	3	4					
6	27	135	10	1	0	10	16	1	5	2/27	−2/27	12	135/4	117/236
*7	50	175	7	1	0	7	42	0	1					
*8	56	280	10	1	0	10	45	0	2					

We shall now give a construction for design 1. Let θ represent any treatment of the design, let the $n_1=5$ first associates of θ be $a, b, \cdots, e$, and let the $n_2=10$ second associates of θ be the integers 1, 2, $\cdots$, 10. Since $\lambda_1=1$, $\lambda_2=0$, and $p_{11}^1=0$, the five treatments that appear in the blocks containing a common treatment must be second associates of each other, and since $p_{11}^2=2$, any pair of these treatments must have just two common first associates. It is easily seen that the following 25 blocks satisfy these requirements:

θ a a 1 b 1 c 2 d 3 e 4

θ b a 2 b 5 c 5 d 6 e 7

θ c a 3 b 6 c 8 d 8 e 9

θ d a 4 b 7 c 9 d 10 e 10

θ e

Reapplying the above requirement, it is seen that no treatment-pairs can be formed from treatments within the following groups:

$$(1,2,3,4),\quad (1,5,6,7),\quad (2,5,8,9),\quad (3,6,8,10),\quad (4,7,9,10).$$

Hence, the three remaining blocks containing 1 must contain 8, 9, and 10; the three remaining blocks containing 2 must contain 6, 7, and 10; the remaining blocks containing 3 must contain 5, 7, and 9; the remaining blocks containing 4 must contain 5, 6, and 8. This gives the following blocks:

1 8 2 6 3 5 4 5

1 9 2 7 3 7 4 6

1 10 2 10 3 9 4 8

The remaining three blocks must contain 5, 6, $\cdots$, 10. Reasoning as before, it is clear

that these blocks are

$$\underline{5\ 10},\quad \underline{6\ 9},\quad \text{and}\quad \underline{7\ 8}.$$

This gives the $b=40$ blocks of design 1. The reader can check the constancy of the p_{ik}^{j} $(i,j,k=1,2)$ for all treatment-pairs of the design.

The solution for design 2 of table 5 consists of the blocks of design 1 written twice.

Let us now develop some theory that will enable us to construct design 3 of table 5.

Consider any PBIB design with 2 associate classes and 2 treatments per block, and let its parameters be denoted by v, b, r, $k=2$, λ_1, λ_2, n_1, n_2, and p_{ik}^{j} $(i,j,k=1,2)$. Let us adopt the convention $\lambda_1>\lambda_2\geq 0$. The blocks of this design are some b treatment-pairs from among the $v(v-1)/2$ distinct treatment-pairs that can be formed from the v treatments. The b blocks will not all be different unless $\lambda_1=1$ and $\lambda_2=0$. Let D represent this design.

Let us form a design D' from D as follows: If a treatment-pair (α,β) occurs in λ_1 blocks of D, let (α,β) occur in λ_2 blocks of D'; if (α,β) occurs in λ_2 blocks of D, let (α,β) occur in λ_1 blocks of D'. We shall call design D' the *pair-complement of design* D.

Let the parameters of design D' be represented by the usual letters carrying primes. Any treatment α will occur in λ_1 blocks with each of its n_1 first associates in design D and will consequently occur in λ_2 blocks with each of these n_1 treatments in design D'. Similarly, α will occur in λ_1 blocks in D' with each of the n_2 second associates of α in D. If we put $\lambda_2'=\lambda_2$, then clearly,

$$v'=v,\quad k'=2,\quad \lambda_1'=\lambda_1,\quad \lambda_2'=\lambda_2,\quad n_1'=n_2,\quad n_2'=n_1. \tag{41}$$

Consequently, α occurs in

$$r'=\lambda_2 n_1+\lambda_1 n_2 \tag{42}$$

blocks in D', and D' will contain

$$b'=v(\lambda_2 n_1+\lambda_1 n_2)/2 \tag{43}$$

blocks. A bit of reflection on the parameters of the second kind for D' reveals that

$$P_1'=(p_{ik}^{1\prime})=\begin{pmatrix} p_{22}^{2} & p_{21}^{2} \\ p_{12}^{2} & p_{11}^{2} \end{pmatrix} \tag{44}$$

and

$$P_2'=(p_{ik}^{2\prime})=\begin{pmatrix} p_{22}^{1} & p_{21}^{1} \\ p_{12}^{1} & p_{11}^{1} \end{pmatrix}. \tag{45}$$

It is easy to verify that the parameters of D' satisfy the necessary relations among the parameters set forth in [4].

Consideration of the association schemes of group divisible, triangular, Latin square, and cyclic designs with two treatments per block shows that if design D is one of these types, then its pair-complement D' is of the same type. It should also be noted that the existence of D as a connected design does not guarantee that D' will be a connected design. For instance, if $p_{21}^{2}=\lambda_2=0$, then D' will be a disconnected design of the group divisible type.

The parameters of design 1 are

$$\begin{aligned} &v=16,\quad r=5,\quad \lambda_1=1,\quad n_1=5,\quad P_1=\begin{pmatrix} 0 & 4 \\ 4 & 6 \end{pmatrix}, \\ &b=40,\quad k=2,\quad \lambda_2=0,\quad n_2=10,\quad P_2=\begin{pmatrix} 2 & 3 \\ 3 & 6 \end{pmatrix}. \end{aligned} \tag{46}$$

UNIVERSITY OF MICHIGAN LIBRARIES

If design 1 is design D, then its pair-complement D' will have parameters

$$\begin{aligned} &v'=16, \quad r'=10, \quad \lambda_1'=1, \quad n_1'=10, \quad P_1'=\begin{pmatrix}6 & 3\\ 3 & 2\end{pmatrix}, \\ &b'=80, \quad k'=2, \quad \lambda_2'=0, \quad n_2'=5, \quad P_2'=\begin{pmatrix}6 & 4\\ 4 & 0\end{pmatrix}. \end{aligned} \tag{47}$$

But (47) is design 3 of table 5. Hence, design 3 is the pair-complement of design 1.

After a change of notation the $b=80$ blocks of design 3 may be written as follows:

1 7	2 3	3 4	4 6	5 10	7 8
1 8	2 4	3 5	4 7	5 11	7 9
1 9	2 5	3 6	4 9	5 13	7 10
1 10	2 6	3 8	4 10	5 15	7 11
1 11	2 11	3 9	4 12	6 7	7 12
1 12	2 12	3 10	4 13	6 8	7 13
1 13	2 13	3 14	4 16	6 9	8 9
1 14	2 14	3 15	5 6	6 11	8 10
1 15	2 15	3 16	5 7	6 12	8 11
1 16	2 16	4 5	5 8	6 14	8 14
					8 15
9 10	9 16	10 16	11 14	12 14	13 16
9 12	10 13	11 12	11 15	12 16	14 15
9 14	10 15	11 13	12 13	13 15	14 16
					15 16

An examination of the pair-complements of the designs discussed in this paper will show that they are either

a. Disconnected designs in which we have no interest,

b. Designs with $r>10$,

c. Self pair-complementary, i. e., have the same parameters as D, or

d. Other designs that are included in this paper.

We shall next prove a theorem that will enable us to construct design 6 of table 5.

Suppose a construction exists for a design D that has parameters v, b, r, $k=3$, $\lambda_1=1$, $\lambda_2=0$, n_1, n_2, and p_{ik}^j $(i,j,k=1,2)$. We shall form a design D^* from design D as follows: If $B_j=(\alpha,\beta,\gamma)$ is a block of D, then the treatment-pairs (α,β), (α,γ), and (β,γ) shall be blocks of D^*. Obviously, any treatment-pair (θ,π) that occurs in λ_i blocks of D will also occur in $\lambda_i^*=\lambda_i$ blocks of D^*, $(i=1,2)$. Any treatment of D^* will consequently have the same ith associates as it has in D. Hence, the parameters of the second kind p_{ik}^{j*} $(i,j,k=1,2)$ of D^* will be the same as the corresponding parameters of D. Thus, D^* is a two-associate class PBIB design with parameters,

$$\begin{aligned} &v^*=v, \quad r^*=2r, \quad \lambda_1^*=1, \quad n_1^*=n_1, \quad P_1^*=(p_{ik}^1), \\ &b^*=3b, \quad k^*=2, \quad \lambda_2^*=0, \quad n_2^*=n_2, \quad P_2^*=(p_{ik}^2). \end{aligned} \tag{48}$$

This proves the theorem:

THEOREM. *If a solution for design D having parameters* v, b, r, $k=3$, $\lambda_1=1$, $\lambda_2=0$, n_1, n_2, *and* p_{ik}^j $(i,j,k=1,2)$ *exists, then a solution for design* D^*, *whose parameters are given by* (48), *also exists and consists of all distinct treatment-pairs that can be formed from the treatments within the blocks of* D.

Now Bose and Clatworthy [2] have solved the design whose parameters are

$$v=27, \quad r=5, \quad \lambda_1=1, \quad n_1=10, \quad P_1=\begin{pmatrix}1 & 8\\ 8 & 8\end{pmatrix},$$
$$b=45, \quad k=3, \quad \lambda_2=0, \quad n_2=16, \quad P_2=\begin{pmatrix}5 & 5\\ 5 & 10\end{pmatrix}. \tag{49}$$

The blocks of design (49) are:

		1 2 3		
		1 4 5		
		1 6 7		
		1 8 9		
		1 10 11		
2 12 13	4 12 20	6 20 15	8 20 17	10 20 19
2 14 15	4 14 22	6 22 13	8 24 13	10 26 13
2 16 17	4 16 24	6 16 27	8 18 23	10 16 23
2 18 19	4 18 26	6 18 25	8 14 27	10 14 25
3 20 21	5 13 21	7 24 19	9 22 19	11 22 17
3 22 23	5 15 23	7 17 26	9 15 26	11 15 24
3 24 25	5 17 25	7 14 21	9 16 21	11 18 21
3 26 27	5 19 27	9 12 23	9 12 25	11 12 27

Thus, by the theorem, design 6 of table 5, having parameters

$$v^*=27, \quad r^*=10, \quad \lambda_1^*=1, \quad n_1^*=10, \quad P_1^*=P_1,$$
$$b^*=135, \quad k^*=2, \quad \lambda_2^*=0, \quad n_2^*=16, \quad P_2^*=P_2,$$

has a solution that may be obtained by forming the three distinct treatment-pairs from the treatments in each of the blocks of design (49).

8. The Enumeration Problem

There exist many sets of parameters for PBIB designs with two associate classes, $k=2$ and $2\leq r\leq 10$, that satisfy the necessary relations set forth in [4] and restated in [6]. However, not all such sets of parameters have solutions (constructions). The writer has obtained an exhaustive enumeration of the sets of parameters for the class of designs investigated in this paper by use of theory developed in reference [7]. Those parameter sets that fail to satisfy the necessary conditions for the existence of solutions given in [3, 6, and 8] were discarded. The remaining sets of parameters appear in this paper. Constructions are given for all designs for which parameters are listed in tables 1 to 5, with four exceptions. These four designs are the designs of table 5 marked with asterisks. For these designs, b is rather large, and consequently an intensive search for solutions was not made.

UNIVERSITY OF MICHIGAN LIBRARIES

For suggestions leading to the construction of designs 3 and 6 of table 5, the writer is indebted to W. J. Youden.

9. References

[1] R. C. Bose, Partially balanced incomplete block designs with two associate classes involving only two replications, Calcutta Statistical Association Bulletin **3,** 120 (1951).
[2] R. C. Bose and W. H. Clatworthy, Some classes of partially balanced designs. (Accepted for publication in Annals of Mathematical Statistics).
[3] R. C. Bose and W. S. Connor, Combinatorial properties of group divisible incomplete block designs, Annals of Mathematical Statistics **23,** 367 (1952).
[4] R. C. Bose and K. R. Nair, Partially balanced incomplete block designs, Sankhyā **4,** 337 (1939).
[5] R. C. Bose and K. R. Nair, Partially balanced designs with two plots per block, Annals of Mathematical Statistics **23,** 639 (1952) (Abstract).
[6] R. C. Bose and T. Shimamoto, Classification and analysis of partially balanced incomplete block designs with two associate classes, Journal of the American Statistical Association **47,** 151 (1952).
[7] W. H. Clatworthy, Symmetrical partially balanced incomplete block designs with two associate classes and three and four replications. (Publication pending.)
[8] W. S. Connor and W. H. Clatworthy, Some theorems for partially balanced designs, Annals of Mathematical Statistics **25,** 100 (1954).
[9] W. J. Youden and W. S. Connor, New experimental designs for paired observations, J. Research NBS **53,** 191 (1954) RP2532.
[10] O. Kempthorne, A class of experimental designs using blocks of two plots, Annals of Mathematical Statistics **24,** 76 (1953).
[11] F. Yates, Incomplete randomized designs, Annals of Eugenics **7,** 121 (1936).

WASHINGTON, June 24, 1954.

Journal of Research of the National Bureau of Standards Vol. 54, No. 4, April 1955 Research Paper 2580

Solid-State Reactions and Dielectric Properties in the Systems Magnesia-Zirconia-Titania and Lime-Zirconia-Titania [1]

L. W. Coughanour, R. S. Roth, S. Marzullo, and F. E. Sennett

A study of solid-state reactions and dielectric properties was made for the ternary systems MgO-ZrO_2-TiO_2 and CaO-ZrO_2-TiO_2. The compatibility relations were determined for each, and an estimate of the extent of the solid-solution areas was obtained. One ternary compound having the formula $CaO{\cdot}ZrO_2{\cdot}2TiO_2$ was discovered. An X-ray diffraction powder pattern of this compound is included.

Ceramic dielectric-test pieces were prepared from compositions within these systems. Data are given for the values of K and Q at 50 kilocycles per second, and at 1 and 20 megacycles per second. The variations of these values with changes in temperature were observed at a frequency of 1 megacycle per second.

1. Introduction

This is the fourth paper on a program of study of solid-state reactions occurring in various ceramic-oxide systems, and of the properties of dielectrics obtainable from those systems. It covers the systems MgO-ZrO_2-TiO_2 and CaO-ZrO_2-TiO_2. Portions of the binary boundary-systems have been studied previously by other investigators. The MgO-TiO_2 dielectrics have been described by Rieke and Ungewiss [1] [2] and by Shelton, et al.[2]. The properties of CaO-TiO_2 dielectrics have been determined by Bunting, et al. [3], and a limited amount of data on the ZrO_2-TiO_2 and MgO-ZrO_2 dielectrics have been obtained by Shelton [4]. The MgO-ZrO_2 bodies were found to have a dielectric constant (K) of less than 20 and a positive temperature coefficient of K. The ZrO_2-TiO_2 specimens have K values of less than 100 and have a negative temperature coefficient. Rieke and Ungewiss [1] have reported on the ceramic and dielectric properties of specimens in the MgO-ZrO_2-TiO_2 system, but no literature references were found pertaining to the ternary system CaO-ZrO_2-TiO_2.

2. Materials and Methods

2.1. Materials

The following substances were used as sources of the component oxides in the study of solid-state reactions:

MgO—Water-clear crystals of periclase of over 99-percent purity, ground to pass a 325-mesh sieve, using a mullite mortar and pestle.

CaO—Reagent grade calcium carbonate of nominal 99.5-percent purity.

TiO_2—A highly purified grade of rutile of over 99.9-percent purity.

ZrO_2—Dense zirconia of over 99-percent purity, calcined at 1,450° C, ground in a steel-ball mill, acid-treated, washed, and dried.

The substances used in the fabrication of the dielectric-test compositions were the following:

MgO—The same as used in the study of solid-state reactions.

TiO_2—The same grade as used for solid-state reactions was used in the MgO-ZrO_2-TiO_2 system.

TiO_2—A less highly purified grade of rutile, designated TMO, was used in the CaO-ZrO_2-TiO_2 system. This material had a purity of 98.7 percent, the principal impurities being SiO_2 and Al_2O_3.

CaO:TiO_2—A commercial grade of perovskite. This material had a purity of 96.5-percent, the principal impurities being MgO, SiO_2, and Al_2O_3.

CaO:ZrO_2—A commercial grade of calcium zirconate. This material was about 96-percent pure, and the principal impurities were SiO_2, Al_2O_3, and HfO_2.

ZrO_2—The same as used in the study of solid-state reactions.

2.2. Sample Preparation

Compositions are designated on a mole-ratio basis. No corrections were made for the percentage of purity of the raw materials.

The raw materials in sufficient amounts to yield 10-g samples were weighed to the nearest milligram, and thoroughly mixed in the dry state. The compositions were then mixed with about 5 weight percent of a 5 weight percent starch-solution binder, and 1-in.-diameter disks were formed at a pressure of 5,000 lb/in^2. The pressed disks, resting on platinum foil, were calcined for 4 hr at 1,000° to 1,200° C in an oxidizing atmosphere. After the calcined disks were pulverized, using a mullite mortar and pestle, the samples were ready to be used either for the solid-state studies or for forming dielectric-test specimens, depending upon the raw materials chosen.

2.3. Study of Solid-State Reactions

In the study of solid-state reactions, two methods of heat treatment were used. In many cases, a conventional platinum-wound quench furnace was used. The temperature in the furnace was measured with a Pt versus Pt–10-percent-Rh thermocouple and was

[1] This study was sponsored by the Office of Ordnance Research, Department of the Army.

[2] Figures in brackets indicate the literature references at the end of this paper.

UNIVERSITY OF MICHIGAN LIBRARIES

controlled by a modified Roberts-type controller. The quenching technique was used in order that high-temperature solid solutions could be observed. For quench tests a small amount of the prepared sample was placed in a platinum envelope, which was then suspended in the furnace. The test temperature ranged from 1,200° to 1,550° C and was maintained constant for a given length of time. Equilibrium conditions were usually reached in less than 3 hr. After this reaction time, the sample was quenched, usually in air. In some cases, water or carbon tetrachloride was used as the quenching medium.

Alternatively, samples were heated to temperatures as high as 1,750° C, in an oxide-resistor furnace [5], and were cooled relatively slowly. The quenched or slowly cooled specimens were then analyzed by X-ray diffraction and petrographic methods.

These procedures and methods of sample selection are, in general, similar to those discussed by Foster [6a]. In the interpretation and plotting of the results, the discussions of Foster [6a] and Barrett [6b] were applied.

2.4. Preparation of Dielectric-Test Specimens

The calcined mixtures were moistened with about 5 weight percent of starch-solution binder, and disks about ⅛ in. thick and ½ to 1½ in. in diameter were formed at a pressure of 10,000 to 15,000 lb/in^2. The pressed disks were fired for ½ to 1 hr on platinum foil in an oxidizing atmosphere, and were cooled relatively slowly. Maturing temperatures varied from 1,400° to 1,650° C, depending upon the composition and the raw materials. For maturing temperatures up to 1,550° C, a platinum-wound resistance furnace was used. Temperatures were measured with a Pt versus Pt–10-percent-Rh thermocouple and were controlled by an automatic commercial instrument. For maturing temperatures higher than 1,550° C, an oxide-resistor furnace [5] was used. This furnace was manually controlled, and temperatures were measured with a calibrated optical pyrometer.

A specimen was considered to be properly matured when its equivalent water absorption was 0.1 percent or less of the dry weight. The absorption was determined by placing the weighed sample in carbon tetrachloride. The liquid was boiled for 5 hr and allowed to cool; the specimen was removed from the liquid, quickly surface-dried, and weighed in a stoppered bottle. From the gain in weight, the equivalent water absorption was calculated.

Some compositions could not be properly matured, in which case, dielectric tests were performed on test pieces having the lowest obtainable absorption value.

2.5. Determination of Dielectric Properties

The test specimens were coated on each side with a silver paste and fired to 750° C to give silver electrodes about 3 to 5 mils thick. The specimens were then cooled overnight. Preliminary determinations were made at a temperature of 25° ±0.5° C, and at a controlled relative humidity of 40 percent or less.

At frequencies between 50 kc and 20 Mc and at temperatures between 25° and 250° C, the dielectric constant (K) and the Q-value (when greater than 10, the Q-value is very nearly equal to the reciprocal of the power factor) were determined by measurements on a Q-meter.

For measurements at temperatures greater than 25° C, the specimens were placed on an electric hotplate covered by a muffle and were connected to the Q-meter by 10-in. leads. The temperature was controlled by means of a variable autotransformer and was measured by means of a thermocouple inserted into a silvered ceramic disk adjacent to the specimen. Correction factors for the capacitance and inductance of the lead wires were applied.

For measurements in the temperature range between −50° and 0° C, the specimens were placed in an insulated chamber cooled by dry ice. The temperature was controlled by a thermostat and was measured by means of a liquid-in-glass thermometer. The measurements were made at a frequency of 1 Mc and were obtained by using a type 820A twin-T impedance circuit combined with a model HRO–50T radio receiver. Corrections were applied for the capacitance and inductance of the lead wires.

3. Results of Solid-State Reaction Studies

3.1. The MgO-ZrO_2-TiO_2 System

The four binary compounds occurring in the boundary systems are $2MgO{\cdot}TiO_2$, $MgO{\cdot}TiO_2$, $MgO{\cdot}2TiO_2$ [7], and ZrO_2-TiO_2 [8]. There are no binary compounds in the MgO-ZrO_2 system [9]. For the study of the ternary fields, 31 selected compositions were subjected to suitable heat treatment and, after quenching or cooling, were analyzed by X-ray and petrographic methods. The data resulting from these tests are listed in table 3. The compatibility relations derived from these data, together with the location of the compositions, are indicated in figure 1. No ternary compounds were observed, and the binary joins established for the subsolidus equilibrium relations are MT_2-ZT,[3] MT_2-ZrO_2, MT-ZrO_2, and M_2T-ZrO_2. The estimated solid-solution areas are indicated in figure 2. No attempt was made to locate the solid-solution limits with a high degree of accuracy. The heat treatment of samples was not uniform from one part of the system to another; therefore, figure 2 is not to be considered an isothermal section of the diagram. The figure does, however, indicate the general trends of solid-solution formation within the system at temperatures below the solidus.

[3] M = MgO, C = CaO, Z = ZrO_2, and T = Tio_2. Thus, in this shorthand notation, MT_2 = $MgO{\cdot}2TiO_2$.

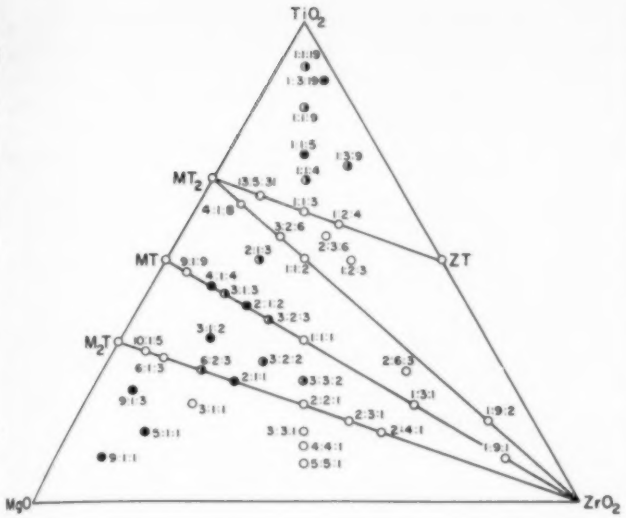

FIGURE 1. *Compatibility relations in the system* MgO-ZrO_2-TiO_2.

The prepared compositions are indicated and plotted according to mole ratios.
○, Compositions used in the study of solid-state reactions;
●, compositions used in the study of dielectric properties;
◑, compositions used for both studies.

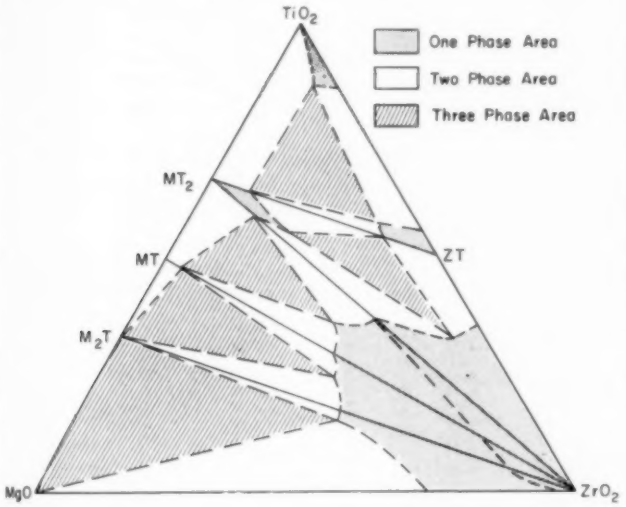

FIGURE 2. *Estimated trends of solid-solution development in the system* MgO-ZrO_2-TiO_2 *over the temperature range 1,400° to 1,750° C.*

The dashed line near the ZrO_2 apex of the figure indicates the approximate location of a two-phase area, which theoretically would separate the cubic ZrO_2 field on the left from the tetragonal ZrO_2 field on the right in a true isothermal section of the phase diagram.

In the binary system MgO-ZrO_2, single-phase cubic ZrO_2 solid solutions are obtained by quenching the specimens from a temperature in excess of 1,400° C, as indicated in table 1. Relatively slow cooling from the same temperature results in an exsolution process giving cubic ZrO_2 and some monoclinic ZrO_2, and MgO. Very slow cooling from high temperatures, or quenching from 1,200° C, results in only MgO and monoclinic ZrO_2 with no cubic ZrO_2. No quenched specimens contained both cubic and monoclinic ZrO_2. It is assumed that the tetragonal ZrO_2 modification cannot be retained at room temperature by quenching and that all monoclinic ZrO_2 found in the

TABLE 1. *Results of study of solid-state reactions in the system* MgO-ZrO_2-TiO_2

Mole ratio M:Z:T	Binary join or ternary field	Heat treatment [a]		Phases identified by X-ray and/or petrographic means (all in solid-solution form, unless otherwise indicated)
		Time	Temperature	
		hr	*° C*	
13:5:31	MT_2-ZT	2	1,500	MT_2+ZT+trace TiO_2.
1:1:3	do	1	1,550	MT_2+ZT.
1:2:4	do	1	1,600	Do.
4:1:8	MT_2-ZrO_2	2	1,500	MT_2+trace MT (no ZrO_2 at all).
3:2:6	do	2	1,500	MT_2+monoclinic ZrO_2+trace ZT.
1:1:2	do	28	[b] 1,500	Do.
1:1:2	do	2	1,525	MT_2+monoclinic ZrO_2.
1:9:2	do	1	1,670	monoclinic ZrO_2+trace MT_2.
9:1:9	MT-ZrO_2	2	1,500	MT+trace monoclinic ZrO_2.
3:1:3	do	2	1,525	MT+monoclinic ZrO_2+trace MT_2.
3:2:3	do	1	1,610	MT+monoclinic ZrO_2+trace cubic ZrO_2.
1:1:1	do	½	1,625	MT+monoclinic ZrO_2.
1:1:1	do	72	[b] 1,400	MT+cubic ZrO_2.
1:3:1	do	½	1,750	Cubic ZrO_2+monoclinic ZrO_2+trace MT.
1:9:1	do	½	1,700	Monoclinic ZrO_2+trace cubic ZrO_2.
10:1:5	M_2T-ZrO_2	2	1,500	M_2T[c]+small amount cubic ZrO_2.
6:1:3	do	2	1,500	M_2T [c]+cubic ZrO_2.
6:2:3	do	1	1,610	Do.
2:2:1	do	½	1,750	M_2T[c]+cubic ZrO_2.
2:2:1	do	72	[b] 1,200	M_2T[c]+monoclinic ZrO_2[c].
2:3:1	do	½	1,700	Cubic ZrO_2+trace M_2T[c].
2:4:1	do	½	1,750	Cubic ZrO_2.
1:1:4	MT_2-ZT-TiO_2	1	1,425	MT_2+ZT+TiO_2.
1:1:9	do	1	1,425	MT_2+TiO_2+trace ZT.
1:1:19	do	2	1,550	TiO_2+MT_2.
1:3:9	do	1	1,425	TiO_2+MT_2+ZT.
2:3:6	MT_2-ZT-ZrO_2	2	1,500	MT_2+ZT.
1:2:3	do	5	1,450	MT_2+ZT+monoclinic ZrO_2.
2:1:3	MT-MT_2-ZrO_2	4	1,450	MT_2+cubic ZrO_2+MT.
2:6:3	do	16	[b] 1,500	Cubic ZrO_2+monoclinic ZrO_2.
3:2:2	M_2T-MT-ZrO_2	½	1,625	M_2T[c]+MT+cubic and monoclinic ZrO_2.
3:3:2	do	1	1,610	M_2T[c]+cubic ZrO_2.
3:3:1	MgO-M_2T-ZrO_2	½	1,650	Cubic ZrO_2+MgO[c]+trace M_2T[c].
5:5:1	do	½	1,650	Cubic ZrO_2+MgO[c].
1:9:0	MgO-ZrO_2	1	1,670	Cubic ZrO_2+monoclinic ZrO_2.
1:9:0	do	72	[b] 1,490	Cubic ZrO_2.
1:9:0	do	80	[b] 1,200	Monoclinic ZrO_2+small amount MgO.[c]
1:4:0	do	1	1,610	Cubic ZrO_2+small amounts of MgO[c] and monoclinic ZrO_2.
1:1:0	do	1	1,610	Cubic ZrO_2+monoclinic ZrO_2+MgO.[c]
1:1:0	do	48	[b] 1,515	Cubic ZrO_2+MgO.[c]
1:1:0	do	80	[b] 1,200	Monoclinic ZrO_2+MgO.[c]

[a] Each sample had been calcined at least once prior to the recorded heat treatment and cooled slowly, unless otherwise indicated.
[b] The specimen was quenched from the temperature indicated.
[c] No solid-solution formation was noted in this substance.

X-ray patterns is actually tetragonal ZrO_2 at temperatures above 1,000° C. Data were obtained by the quenching technique for compositions in the MgO-ZrO_2 system. These data indicate that for compositions higher in MgO content than 10 mole percent, there is no two-phase region of tetragonal and cubic ZrO_2 at temperatures above 1,500° C. The apparent disagreement of these results with those of Duwez, Odell, and Brown [9a] is believed to be due to their having obtained their data from "rapidly cooled," but not quenched, specimens.

Within the ternary system, cubic ZrO_2 solid solutions can be found which are stable to a greater or lesser extent, depending on the TiO_2 content of the specimen. Samples on the M_2T-ZrO_2 join show cubic ZrO_2 solid solutions with stability relations similar to those in the MgO-ZrO_2 system. However, compositions on the MT-ZrO_2 join must be cooled faster than those on the MgO-ZrO_2 and M_2T-ZrO_2 joins in order to maintain the cubic solid solutions. Furnace-cooled specimens, although actually cooled fairly rapidly, show little or no cubic ZrO_2, but the same materials, when quenched, show only cubic ZrO_2 solid solutions, with no monoclinic ZrO_2. All samples in the two-phase region of the MT_2-ZrO_2 join showed MT_2 and monoclinic ZrO_2. Even quenched samples did not contain cubic ZrO_2.

3.2. The CaO-ZrO_2-TiO_2 System

The binary compounds occurring in the boundary-systems are CaO·TiO_2 and 3CaO·2TiO_2 [10,8b], ZrO_2·TiO_2 [8], and CaO·ZrO_2 [11].

For the investigation of the ternary fields, 22 selected samples were quenched from various temperatures and were examined by X-ray diffraction and petrographic means. From the results of these tests, which are listed in table 2, a ternary compound, CZT_2, was discovered and the arrangement of composition triangles was determined. The binary joins found to exist in the subsolidus temperature range were CT-CZT_2, CZT_2-TiO_2, CZT_2-ZT, CZT_2-ZrO_2, CT-ZrO_2, CT-CZ, and C_3T_2-CZ. These compatibility relations, together with the location of pre-

TABLE 2. *Results of study of solid-state reaction in the system* CaO-ZrO_2-TiO_2

Mole ratio C:Z:T	Binary join or ternary field	Heat treatment [a]		Phases identified by X-ray and/or petrographic means (ss=solid solution)
		Time	Temperature	
		hr	*° C*	
1:1:2	CT-CZT_2	24	1,450	CZT_2.
2:1:3	do	2.5	1,450	CT+CZT_2 (little or no ss).
1:2:3	CZT_2-ZT	24	1,450	CZT_2+ZT (small amount ss).
1:4:5	do	3	1,450	Do.
1:1:4	CZT_2-TiO_2	3	1,450	CZT_2 ss+TiO_2 ss.
1:4:2	CZT_2-ZrO_2	3	1,500	CZT_2 ss+monoclinic ZrO_2 ss.
1:1:1	CT-ZrO_2	3	1,550	CT+cubic ZrO_2 ss.
1:4:1	do	3	1,550	Cubic ZrO_2 ss.
2:1:1	CT-CZ	5	1,550	(CT-CZ) ss.
5:2:2	C_3T_2-CZ	5	1,550	(C_3T_2-CZ) ss+small amount CaO.
9:6:2	do	3	1,550	(C_3T_2-CZ) ss.
7:1:4	do	3	1,550	C_3T_2+(C_3T_2-CZ) ss+small amount CaO.
3:1:6	CT-CZT_2-TiO_2	3	1,400	CT ss+CZT_2 ss+TiO_2 ss.
1:3:6	CZT_2-ZT-TiO_2	14	1,450	CZT_2 ss+ZT ss+TiO_2 ss.
2:2:3	CT-CZT_2-ZrO_2	16	1,450	CZT_2 ss+CT+monoclinic ZrO_2 ss.
2:9:6	CZT_2-ZT-ZrO_2	43	1,450	CZT_2+ZT ss+monoclinic ZrO_2 ss.
2:2:1	CT-CZ-ZrO_2	16	1,450	(CT-CZ) ss+cubic ZrO_2 ss.
3:4:1	do	3	1,550	Do.
2:4:1	do	3	1,550	Small amount (CT-CZ) ss+cubic ZrO_2 ss.
6:1:4	CT-CZ-C_3T_2	3	1,550	(CT-CZ) ss+small amount C_3T_2.
4:1:1	C_3T_2-CZ-CaO	3	1,550	(C_3T_2-CZ) ss+CaO.
16:1:4	do	3	1,550	C_3T_2+(C_3T_2-CZ) ss+CaO.

[a] Each sample was quenched, in air, from the temperature indicated. Each sample had been previously calcined at least once.

TABLE 3. *X-ray powder diffraction pattern of the compound* CaO·ZrO_2·2TiO_2, *using* Cu $K\alpha_1$ *radiation*

2θ	d	R.I.[a]	2θ	d	R.I.[a]
14.28	6.2	7	74.98	1.27	3
15.68	5.6	6	75.63	1.26	10
16.99	5.2	8	76.19	1.25	5
19.53	4.5	4	76.74	1.24	3
20.41	4.35	4	80.96	1.18	4
22.42	3.96	14	81.72	1.177	9
23.54	3.78	5	82.38	1.169	16
24.59	3.62	3	82.70	1.166	15
25.16	3.57	2	84.50	1.146	7
25.87	3.44	3	84.62	1.144	7
26.76	3.33	14	85.28	1.137	17
27.59	3.23	26	85.70	1.133	7
29.04	3.07	2	86.84	1.121	8
29.39	3.04	3	87.00	1.119	8
30.51	2.93	100	87.49	1.114	5
30.75	2.91	78	87.81	1.111	8
32.07	2.79	56	88.09	1.108	7
33.26	2.69	3	88.46	1.104	7
35.83	2.50	54	90.69	1.083	2
36.03	2.49	19	91.83	1.072	3
37.68	2.39	5	92.57	1.066	5
38.48	2.34	4	94.83	1.046	5
39.39	2.29	21	95.97	1.037	5
39.55	2.28	14	96.25	1.036	6
40.57	2.22	4	96.58	1.032	7
40.77	2.21	3	96.94	1.029	7
42.23	2.14	7	97.25	1.026	10
42.74	2.11	4	97.87	1.022	6
43.50	2.08	5	98.49	1.017	4
44.32	2.04	8	100.99	0.9883	3
44.48	2.04	10	101.32	.9959	5
45.07	2.01	16	101.76	.9928	5
47.76	1.90	13	102.98	.9843	4
48.05	1.89	9	103.68	.9796	10
48.37	1.88	6	104.92	.9714	7
48.82	1.86	7	105.76	.9659	5
50.23	1.81	27	106.17	.9634	4
50.72	1.79	67	107.88	.9528	5
51.32	1.78	10	108.33	.9501	5
51.63	1.77	15	109.82	.9413	2
52.28	1.75	7	110.96	.9348	4
52.52	1.74	66	113.76	.9197	5
52.64	1.74	58	115.53	.9106	5
52.99	1.73	4	115.90	.9088	5
53.47	1.71	7	117.11	.9028	9
54.01	1.69	5	119.16	.8932	6
55.39	1.66	6	120.09	.8890	5
55.74	1.65	4	120.37	.8878	6
56.12	1.64	3	122.88	.8769	4
57.57	1.59	4	125.19	.8676	12
58.06	1.59	5	126.28	.8634	11
58.26	1.58	7	126.45	.8628	9
59.69	1.55	8	127.61	.8584	5
59.97	1.54	32	128.00	.8569	7
60.57	1.53	12	128.79	.8541	7
60.78	1.52	20	129.95	.8501	6
61.22	1.51	42	131.26	.8456	6
62.76	1.48	17	132.82	.8405	7
62.94	1.48	24	133.62	.8379	7
63.26	1.47	14	143.76	.8104	5
63.81	1.46	15	145.92	.8056	4
65.33	1.43	3	146.35	.8047	2
65.88	1.42	6	147.53	.8022	9
66.87	1.39	2	148.59	.8001	10
69.25	1.36	8	148.96	.7994	7
69.69	1.35	7	149.71	.7979	9
70.44	1.34	4	160.63	.7815	6
71.93	1.31	7	163.75	.7781	4

[a] R.I. is the intensity of the diffraction peaks relative to the strongest peak.

pared compositions, are shown in figure 3. The compound CZT_2 forms large well-developed crystals when heated. Its optical properties are biaxial negative with optic axial angle $(2V)=80°$ to 85°, and indices of refraction $\alpha\cong2.23$, $\beta\cong2.27$, and $\gamma\cong2.30$. It has a distorted pyrochlore-type structure, with orthorhombic or lower symmetry. Its X-ray powder pattern is given in table 3. The composition of this compound may be written as $(Ca, Zr)Ti_2O_7$ to show its relation to the pyrochlore structure [12], which is (Na, Ca) (Nb, Ta)O_6F or $A_2B_2X_7$. This is believed to be the first published paper on a compound having a pyrochlore-type structure with no pentavalent ions as essential elements in the B position of the structure.

The indexed powder pattern for $CaZrO_3$ is given in table 4. It has been indexed as orthorhombic with:

$$a\cong\sqrt{2}\times\text{pseudo cube}=5.587\text{ A},$$
$$b\cong\ 2\times\text{pseudo cube}=8.008\text{ A},$$
$$c\cong\sqrt{2}\times\text{pseudo cube}=5.758\text{ A},$$

in a manner similar to that done for $CaTiO_3$ and $CaSnO_3$ [13].

The estimated solid-solution limits for this system are shown in figure 4. Here, also, the figure is not intended to represent an isothermal section of the diagram, but to show only approximate solid-solution areas, as samples within the system are heated to subsolidus temperatures.

The relative stability relations of the cubic ZrO_2 solid solutions within this system are essentially similar to those in the MgO-ZrO_2-TiO_2 system. The cubic solid solution in the CaO-ZrO_2 system is more stable than that in the MgO-ZrO_2 system. Its stability also decreases with increasing TiO_2 content. Quenched specimens on the CT-ZrO_2 join show cubic ZrO_2 solid solution, while those on the CZT_2-ZrO_2 join show only monoclinic ZrO_2.

TABLE 4. *Indexed X-ray powder pattern of the orthorhombic compound* $CaO{\cdot}ZrO_2$, *using* $CuK\alpha_1$ *radiation*

2θ	d	R.I.*	hkl	2θ	d	R.I.*	hkl
22.19	4.00	84	101	75.60	1.26	4	402
24.84	3.58	5	111	75.82	1.25	4	252
31.06	2.88	40	002	78.39	1.22	3	224
31.56	2.83	100+	121	79.92	1.20	4	422/153
32.02	2.79	50	200	82.44	1.169	4	044
35.73	2.51	4	201	84.50	1.146	3	440
37.30	2.41	6	130	86.13	1.128	2	314
37.50	2.40	6	211	88.40	1.125	2	105
38.42	2.34	2	022	87.70	1.112	4	343/262
39.30	2.29	3	220	90.40	1.086	3	125
40.62	2.22	5	131	91.16	1.078	4	244
41.88	2.16	4	122	91.49	1.075	8	163
45.22	2.00	74	202/040	92.49	1.066	9	361
46.34	1.96	4	032	92.62	1.065	8	442
46.67	1.94	3	212	93.42	1.058	5	521
50.23	1.81	14	103	100.43	1.002	3	404
50.91	1.79	24	222	100.70	1.000	2	080
50.93	1.79	26	141	103.20	0.9828	4	145
51.57	1.77	9	301	103.70	.9795	3	305
55.54	1.65	29	123	104.78	.9723	4	424
55.89	1.64	26	042	105.18	.9697	3	181
56.50	1.63	16	240	108.11	.9514	4	305
56.78	1.62	40	321	109.10	.9455	4	106
61.75	1.50	3	133	109.23	.9448	5	363
64.70	1.44	4	004	109.62	.9425	4	280
65.87	1.42	20	242	110.25	.9359	4	523
66.93	1.40	5	400	111.60	.9313	2	182
69.32	1.35	4	024	118.55	.8960	5	444
69.89	1.34	8	143	119.02	.8939	3	282
70.50	1.33	2	060	120.86	.8856	3	226
70.97	1.33	4	341	122.70	.8777	2	143/471
71.50	1.32	3	420	126.74	.8617	3	165
73.99	1.28	4	204	130.67	.8476	6	501/316
74.82	1.27	14	323	137.35	.8269	3	246
74.89	1.27	16	161	143.86	.8102	6	642

* R.I. is the intensity of the diffraction peaks relative to the strongest peak.

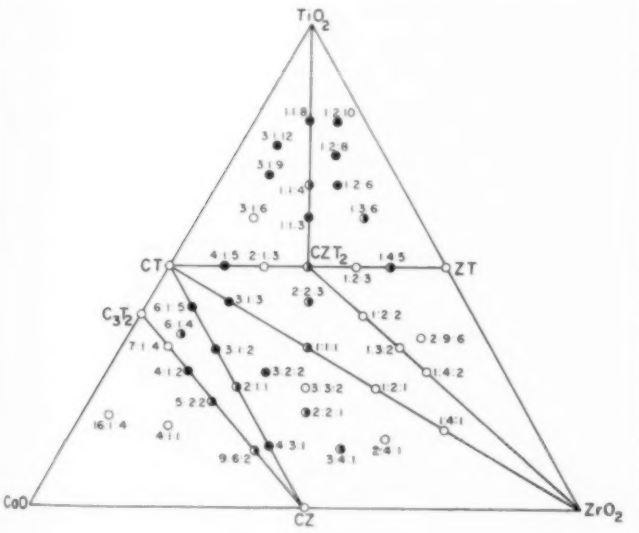

FIGURE 3. *Compatibility relations in the system* CaO-ZrO_2-TiO_2.
The compositions studied are indicated and plotted according to mole ratios.
○, Compositions used in the study of solid-state reactions;
●, compositions used in the study of dielectric properties;
◑, compositions used for both studies.

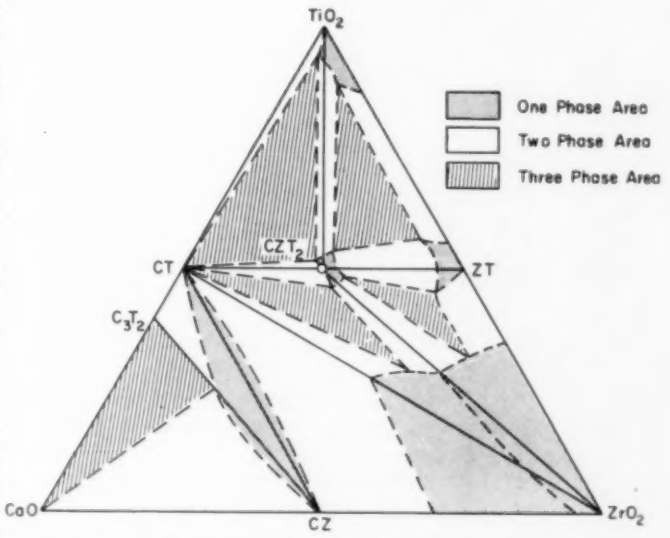

FIGURE 4. *Estimated trends of solid-solution development in the system* CaO-ZrO_2-TiO_2 *over the temperature range 1,450° to 1,550° C.*
The dashed line near the ZrO_2 apex of the figure indicates the approximate location of a two-phase area which theoretically would separate the cubic ZrO_2 field on the left from the tetragonal ZrO_2 field on the right in a true isothermal section of the phase diagram.

4. Results of Dielectric Testing

4.1. The System MgO-ZrO_2-TiO_2

The dielectric properties obtained for test specimens from the MgO-ZrO_2-TiO_2 system are listed in tables 5, 6, and 7.

In the MT_2-ZT-TiO_2 field of the system, K varied from 40 to 80, and the average temperature coefficients of the dielectric constant (TCK) were found to be negative. In the other areas of the system, K was found to vary between 15 and 20 and the TCK-values were positive and between 100 and 200 ppm/°C. The Q-values were, for the most part, high in all parts of the system. These results are in general agreement with those reported by Riecke and Ungewiss [1]. The values of the observed properties for any given specimen composition, as expected, seemed to be an average of the values for the appropriate end members.

TABLE 5. *Results of dielectric testing in the system* MgO-ZrO_2-TiO_2

Mole ratio M:Z:T	Binary join or ternary field	Heat treatment		Linear shrinkage	Equivalent water absorption	Dielectric constant, K, at 25° C and—			Reciprocal, Q, of power factor at 25° C and—		
		Time	Temperature			50 kc	1 Mc	20 Mc	50 kc	1 Mc	20 Mc
		hr	*° C*	*%*	*%*						
4:1:4	MT-ZrO_2	2	1,500	13.2	0.06	17	18	18	500	5,000	6,000
3:1:3	do	1	1,550	13.0	.13	18	18	17	30	400	4,000
2:1:2	do	1	1,550	13.0	.04	17	18	17	200	3,000	10,000
3:2:3	do	2	1,560	11.6	.21	18	17	17	200	3,000	5,000
6:2:3	M_2T-ZrO_2	½	1,625	11.2	.00	19	19	19	400	1,000	800
2:1:1	do	½	1,625	10.0	.00	20	20	20	300	1,000	600
1:1:19	MT_2-ZT-TiO_2	2	1,425	14.8	.10	76	76	76	700	10,000	1,000
1:1:9	do	2	1,425	16.4	.00	75	75	75	6,000	10,000	1,400
1:1:5	do	2	1,425	15.6	.00	52	52	52	4,000	10,000	3,000
1:1:4	do	2	1,425	15.5	.10	42	41	41	150	2,000	3,000
1:3:19	do	1	1,500	14.6	.23	80	79	79	200	1,300	4,000
1:3:9	do	1	1,500	13.8	.10	65	64	65	70	700	2,000
2:1:3	MT-MT_2-ZrO_2	1	1,550	13.2	.55	18	18	18	500	2,000	820
3:1:2	M_2T-MT-ZrO_2	1	1,550	11.0	.04	16	17	17	170	1,000	1,000
3:2:2	do	½	1,650	11.0	.12	21	21	21	400	700	600
3:3:2	do	½	1,650	9.6	.02	28	28	28	400	700	500
9:1:3	MgO-M_2T-ZrO_2	½	1,625	11.0	.15	14	14	14	100	2,000	3,000
9:1:1	do	1	1,550	11.6	.08	13	13	13	80	1,000	2,000
5:1:1	do	1	1,610	11.2	.09	15	16	15	200	1,000	1,000
3:1:1	do	1	1,635	16.3	.05	20	20	20	1,000	900	430

TABLE 6. *Variation of dielectric constant with temperature of some specimens in the system* MgO-ZrO_2-TiO_2

Mole ratio M:Z:T	Binary join or ternary field	Value of K at 1 Mc and—							Average temperature coefficient of K from −50° to 250° C
		−50° C	0° C	50° C	100° C	150° C	200° C	250° C	
									ppm/° C
2:1:1	M_2T-ZrO_2	19.4	19.5	19.7	19.8	19.9	20.1	20.2	+135
1:1:4	MT_2-ZT-TiO_2	41.9	41.3	40.7	40.0	39.3	39.0	38.6	−280
1:1:5	do	53.5	52.5	51.3	50.2	49.2	49.2	47.5	−410
1:1:9	do	78.5	76.2	73.2	70.7	68.6	66.4	64.7	−650
2:1:3	MT-MT_2-ZrO_2	17.5	17.7	17.8	17.9	18.1	18.2	18.3	+150
3:1:1	MgO-M_2T-ZrO_2	19.4	19.5	19.6	19.8	19.9	20.0	20.2	+130
9:1:1	do	14.6	14.9	15.0	15.1	15.2	15.3	15.4	+180
9:1:3	do	17.8	17.9	18.1	18.2	18.3	18.4	18.6	+150

TABLE 7. *Variation of Q with temperature of some specimens in the system* MgO-ZrO_2-TiO_2

Mole ratio M:Z:T	Binary join or ternary field	Value of Q at 1 Mc and—						
		−50° C	0° C	50° C	100° C	150° C	200° C	250° C
2:1:1	M_2T-ZrO_2	570	620	470	580	630	430	280
1:1:4	MT_2-ZT-TiO_2	5,000	5,000	5,000	5,000	5,000	3,000	800
1:1:5	do	10,000	10,000	5,000	8,000	8,000	6,000	3,000
1:1:9	do	10,000	10,000	8,000	5,000	4,000	3,500	3,000
2:1:3	MT-MT_2-ZrO_2	4,000	4,000	3,000	2,500	2,200	1,700	850
3:1:1	MgO-M_2T-ZrO_2	840	930	970	940	840	690	520
9:1:1	do	1,400	1,400	1,400	1,950	1,400	900	710
9:1:3	do	1,900	1,900	2,400	1,610	1,950	1,090	700

4.2. The System CaO-ZrO_2-TiO_2

The dielectric properties obtained for specimens from this system are given in tables 8, 9, and 10.

The value of K varied from about 164 for the compound CT to about 24 for the compound CZ. The ternary compound CZT_2 was found to have a K of about 48. The TCK varied from large negative values for compositions high in CT to small positive values for compositions high in CZT_2 or CZ. Bodies having a low TCK can be obtained by proper adjustment of the composition. This fact is illustrated in figure 5 for some specimens along the CZT_2-TiO_2 join. It is probable that more precise adjustment of the ratio of TiO_2 to CZT_2 would result in a body having a zero average TCK value. The Q-values of specimens in this system are generally lower than those of specimens in the MgO-ZrO_2-TiO_2 system. In this system also, the properties of a specimen of given composition seemed to be an average of the properties of the end members of the appropriate join or composition triangle.

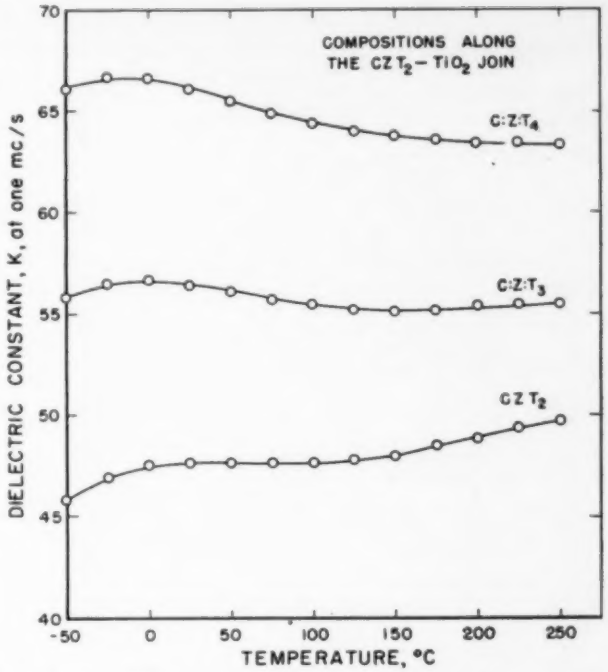

FIGURE 5. *Effect of temperature variations on the dielectric constant of some compositions on the* CZT_2-TiO_2 *join.*

TABLE 8. *Results of dielectric testing in the system* CaO-ZrO_2-TiO_2

Mole ratio C:Z:T	Binary join or ternary field	Heat treatment		Equivalent water absorption	Linear shrinkage	Dielectric constant K, at 25° C and—			Reciprocal, Q, of power factor, at 25° C and—		
		Time	Temperature			50 kc	1 Mc	20 Mc	50 kc	1 Mc	20 Mc
		hr	*°C*	*%*	*%*						
4:1:5	CT-CZT_2	1	1,475	0.11	16.2	99	98	97	300	260	50
1:1:2	do	1	1,425	.08	13.9	47.8	47.6	47.6	200	190	30
1:1:2	CZT_2-TiO_2	1	1,425	.08	13.9	47.8	47.6	47.6	200	190	30
1:1:3	do	1	1,425	.06	15.9	56.5	56.4	55.6	320	230	30
1:1:4	do	1	1,400	.01	14.1	68	66	65	330	250	70
1:1:8	do	1	1,425	.04	12.2	86	86	86	600	300	60
1:1:2	CZT_2-ZT	1	1,425	.08	13.9	47.8	47.6	47.6	200	190	30
1:4:5	do	1	1,450	.14	13.5	39.9	39.6	39.6	330	440	70
1:0:1	CT-ZrO_2	1	1,500	.08	16.8	16.4	16.4	16.4	2,000	9,000	600
3:1:3	do	1	1,400	.00	16.4	88	87	86.5	340	350	110
1:1:1	do	1	1,450	.00	15.8	64.7	64.6	64.4	200	560	240
1:0:1	CT-CZ	1	1,500	.08	16.8	164	164	164	2,000	9,000	600
6:1:5	do	1	1,500	.05	13.8	106	106	106	1,000	3,000	2,000
3:1:2	do	1	1,550	.00	12.1	86	86	86	2,000	1,500	2,000
2:1:1	do	1	1,500	.02	13.3	64	63	63	2,000	2,000	980
4:3:1	do	1	1,500	.04	11.2	40	40	40	1,000	2,000	1,000
1:1:0	do	1	1,500	.17	15.0	24	24	24	130	100	1,000
4:1:2	C_3T_2-CZ	1	1,550	.16	18.0	74.4	74.3	74.2	1,000	1,300	510
5:2:2	do	1	1,550	.13	14.9	68.6	68.4	68.1	1,000	2,000	380
9:6:2	do	1	1,500	.04	13.5	44	44	44	8,000	10,000	2,000
3:1:9	CT-CZT_2-TiO_2	1	1,250	.35	13.9	92	91	89	50	110	55
3:1:12	do	1	1,350	.10	13.8	98	97	96	120	310	80
1:3:6	CZT_2-ZT-TiO_2	1	1,450	.03	16.6	56.6	56.4	56.1	440	440	66
1:2:6	do	1	1,450	.00	14.4	63.3	62.9	62.5	480	380	40
1:2:8	do	1	1,425	.03	15.7	79	78	78	600	500	70
1:2:10	do	1	1,450	.03	13.7	77	76	76	800	600	90
2:2:3	CT-CZT_2-ZrO_2	1	1,475	.04	12.8	38.6	38.0	37.1	100	130	30
3:2:2	CT-CZ-ZrO_2	1	1,450	.09	.....	62.2	61.7	61.7	700	750	440
3:4:1	do	1	1,460	.13	13.7	39	38	37	100	250	250
2:2:1	do	1	1,450	.00	17.1	59.0	58.6	58.4	380	380	320
6:1:4	CT-CZ-C_3T_2	1	1,500	.00	15.9	97.2	97.1	97.0	1,000	960	330

TABLE 9. *Variation of K with temperature in the system* $CaO\text{-}ZrO_2\text{-}TiO_2$

Mole ratio C:Z:T	Binary join or ternary field	Value of K at 1 Mc and—							Average temperature coefficient of K from −50° to 250° C
		−50° C	0° C	50° C	100° C	150° C	200° C	250° C	
									ppm/°C
4:1:5	CT-CZT_2	104	100	96	93	90	87	85	−670
1:1:2	do	45.8	47.5	47.6	47.6	48.0	48.9	49.7	+270
1:1:2	CZT_2-TiO_2	45.8	47.5	47.6	47.6	48.0	48.9	49.7	+270
1:1:3	do	55.8	56.7	56.1	55.5	55.1	55.7	55.5	
1:1:4	do	66.1	66.6	65.5	64.4	63.8	63.5	63.4	−140
1:1:8	do	68.0	86.7	62.5	82.2	80.4	78.9	77.6	−420
1:4:5	CZT_2-ZT	39.0	39.6	39.6	39.6	39.7	39.9	40.1	+90
1:0:1	CT-ZrO_2	184	172	152	141	133	125	120	−1,350
3:1:3	do	75	90	84	80	78	76	74	−820
1:1:1	do	66	65	64	62	62	61	60	−300
6:1:5	CT-CZ	120	110	102	96	91	87	84	−1,200
3:1:2	do	96	89	83	78	74	71	68	−780
4:3:1	do	42.1	40.7	39.4	38.2	37.5	36.7	36.2	−500
1:1:0	do	23.6	23.7	23.8	23.9	24.0	24.1	24.2	+85
4:1:2	C_3T_2-CZ	80	76	72	69	67	65	63	−800
5:2:2	do	73	69	67	65	63	61	59	−790
9:6:2	do	47	45	44	43	42	41	40	−480
3:1:9	CT-CZT_2-TiO_2	95	92	89	86	83	81	79	−610
3:1:12	do	103	99	95	92	88	86	84	−670
1:3:6	CZT_2-ZT-TiO_2	56.6	56.8	56.1	55.5	55.2	55.1	55.1	−90
1:2:6	do	64.1	63.5	62.5	61.1	60.4	60.0	59.7	−250
1:2:8	do	80.8	79.1	77.0	75.0	73.4	72.4	71.5	−410
1:2:10	do	79	77	75	73	71	69	69	−470
2:2:3	CT-CZT_2-ZrO_2	36.2	37.7	38.2	38.5	39.0	39.8	40.6	+390
3:2:2	CT-CZ-ZrO_2	68	64	61	59	57	55	54	−810
3:4:1	do	39.3	38.6	38.0	37.6	37.3	37.2	37.3	−170
2:2:1	do	63	60	58	56	55	54	53	−600
6:1:4	CT-CZ-C_3T_2	108	100	94	90	86	82	80	−990

TABLE 10. *Variation of Q with temperature in the system* $CaO\text{-}ZrO_2\text{-}TiO_2$

Mole ratio C:Z:T	Binary join or ternary field	Value of Q at 1 Mc and—						
		−50° C	0° C	50° C	100° C	150° C	200° C	250° C
4:1:5	CT-CZT_2	60	140	280	230	130	90	70
1:1:2	do	25	90	240	140	60	50	60
1:1:2	CZT_2-TiO_2	25	90	240	140	60	50	60
1:1:3	do	30	110	300	210	80	70	90
1:1:4	do	40	110	320	200	100	80	100
1:1:8	do	50	120	370	450	280	150	100
1:4:5	CZT_2-ZT	60	210	490	300	140	110	100
1:0:1	CT-ZrO_2	760	4,000	3,500	2,500	1,700	170	40
3:1:3	do	180	240	200	180	120	100	100
1:1:1	do	310	390	390	100	50	100	230
6:1:5	CT-CZ	2,000	2,000	3,000	2,000	2,000	2,000	500
3:1:2	do	1,000	870	1,100	1,100	890	570	190
4:3:1	do	800	1,000	2,000	2,000	2,000	900	900
1:1:0	do	800	800	700	900	600	500	400
4:1:2	C_3T_2-CZ	1,100	760	880	650	320	120	35
5:2:2	do	1,200	1,000	900	480	400	180	60
9:6:2	do	1,000	2,000	3,000	3,000	3,000	3,000	2,000
3:1:9	CT-CZT_2-TiO_2	70	120	260	330	210	160	110
3:1:12	do	110	180	380	400	270	210	140
1:3:6	CZT_2-ZT-TiO_2	60	200	510	300	130	100	100
1:2:6	do	60	180	360	250	120	90	90
1:2:8	do	70	230	520	380	160	130	120
1:2:10	do	90	290	440	350	190	140	140
2:2:3	CT-CZT_2-ZrO_2	30	60	110	100	60	40	40
3:2:2	CT-CZ-ZrO_2	690	600	480	390	300	240	140
3:1:1	do	270	250	240	210	18	140	90
2:2:1	do	420	380	340	280	260	200	120
6:1:4	CT-CZ-C_3T_2	560	590	820	740	330	110	30

5. Summary

An investigation of solid-phase reactions in the systems MgO-ZrO_2-TiO_2 and CaO-ZrO_2-TiO_2 was conducted. Compatibility relations were established and solid-solution areas were estimated for each system. No ternary compounds were observed in the MgO-ZrO_2-TiO_2 system. In the CaO-ZrO_2-TiO_2 system, a ternary compound having the formula $CaO{\cdot}ZrO_2{\cdot}2TiO_2$ was discovered, and its optical properties and X-ray diffraction pattern were determined.

The X-ray diffraction powder pattern for the compound $CaO{\cdot}ZrO_2$ was obtained and indexed as orthorhombic.

Dielectric-test samples were prepared and tested in each system. The dielectric constant varied between 15 and 165, depending upon the composition of the specimen. The average temperature coefficient of K between $-50°$ and $150°$ C varied from large negative values to small positive values, also depending upon the composition of the fired piece.

6. References

[1] R. Rieke and A. Ungewiss, Ber. deut. keram. Ges. **17,** 237 (1936).

[2] George R. Shelton, Ansel S. Creamer, and Elmer N. Bunting, J. Research NBS **41,** 17 (1948), RP1899.

[3] Elmer N. Bunting, George R. Shelton, and Ansel S. Creamer, J. Research NBS **43,** 237 (1949), RP2025.

[4] George R. Shelton (unpublished data).

[5] S. M. Lang and R. F. Geller, J. Am. Ceram. Soc. **34,** 193 (1951).

[6] (a) Wilfrid R. Foster, Bull. Am. Ceram. Soc. **30,** 291 (1951).
(b) Charles S. Barrett, Structure of metals, ch. 10 (McGraw-Hill Book Co., Inc., New York, N. Y.) (1943).

[7] (a) L. W. Coughanour and V. A. DeProsse, J. Research NBS **51,** 85 (1953), RP 2435.
(b) H. Sigurdson and S. S. Cole, J. Metals **1,** No. 12, Transaction 905 (1949).
(c) Y. Tanaka, Bul. Chem. Soc. Japan **60,** 212 (1939).
(d) W. Jander and K. Bunde, Z. anorg. Chem. **239,** 418 (1938).
(e) W. Büssem, C. Schusterius, and A. Ungewiss, Ber. deut. keram. Ges. **18,** 433 (1937).

[8] (a) Frank H. Brown, Jr. and Pol Duwez, J. Am. Ceram. Soc. **37,** 129 (1954).
(b) L. W. Coughanour, R. S. Roth, and V. A. DeProsse, J. Research NBS **52,** 37 (1954), RP2470.

[9] (a) Pol Duwez, Francis Odell, and Frank H. Brown, Jr., J. Am. Ceram. Soc. **35,** 107 (1952).
(b) S. M. Lang, L. H. Maxwell, and R. F. Geller, J. Research NBS **43,** 429 (1949), RP 2034.
(c) N. A. Zhirnova, J. Appl. Chem. (U. S. S. R.) **12,** 1279 (1939).
(d) F. Ebert and E. Cohn, Z. anorg. u. allgem. Chem. **213,** 321 (1933).

[10] (a) R. C. De Vries, Rustum Roy, and E. F. Osborn, Paper presented at 1953 convention Am. Ceram. Soc. (April 28, 1953).
(b) H. G. Fisk, Jr., J. Am. Ceram. Soc. **34,** 9 (1951).
(c) P. S. Mamykin and B. A. Loshkarev, Ogneupory **15,** 215 (1950).
(d) L. D. Ershov, Trudy Giprotsementa, No. 1 (1940).
(e) I. Parga-Pondahl and K. Bergt, Tonind.-Ztg. **53,** 1000 (1933).

[11] (a) H. von Wartenberg and W. Gurr, Z. anorg u. allgem. Chem. **196,** 381 (1931).
(b) O. Ruff, F. Ebert, and E. Stephan, Z. anorg. u allgem. Chem. **180,** 219 (1929).

[12] O. Rosen and A. Westgren, Geol. Fören. Fork. **60,** 226 (1938).

[13] L. W. Coughanour, R. S. Roth, S. Marzullo, and F. E. Sennett, J. Research NBS **54,** 149 (1955) RP2576.

WASHINGTON, November 2, 1954.

Journal of Research of the National Bureau of Standards Vol. 54, No. 4, April 1955 Research Paper 2581

Synthesis of α-D-Glucose-2-C^{14}, α-D-Mannose-2-C^{14}, and α-D-Galactose-2-C^{14} [1]

Horace S. Isbell, Harriet L. Frush, and Robert Schaffer

α-D-Glucose-2-C^{14}, α-D-mannose-2-C^{14}, and α-D-galactose-2-C^{14} have been synthesized from the corresponding 1-C^{14}-labeled pentoses in yields of 50, 18, and 36 percent, respectively. The methods are adaptations of those previously employed in the syntheses of the 1-labeled sugars, but include certain improvements, among them, the use of sodium acid oxalate as a buffer in the reduction of D-mannono-γ-lactone, and the elimination of the crystallization of D-lyxose-1-C^{14}.

1. Introduction and Discussion of Synthetic Procedures

To confirm and extend fundamental knowledge obtained by research workers in many fields by use of 1-C^{14}-labeled sugars a supply of sugars labeled at other positions is required. The present paper describes the preparation of some 2-C^{14}-labeled sugars from D-arabinose-1-C^{14} and D-lyxose-1-C^{14} [1,2].[2] In each case, the labeled pentose was allowed to react with nonradioactive sodium cyanide, and the next higher sugars were prepared by methods similar to those previously developed for the production of the 1-C^{14}-labeled sugars [1,2,3,4,5]. However, the procedure formerly employed for the reduction of D-mannono-γ-lactone [3] involved the addition and removal of benzoic acid, a step that caused considerable trouble. Consequently, the sodium amalgam reduction of D-mannono-γ-lactone was studied further, and a procedure developed for the production of D-mannose in high yield by the use of sodium acid oxalate as a buffer.

In contrast with the procedure previously reported for the preparation of D-lyxose-1-C^{14} [2], no attempt was made to crystallize the labeled D-lyxose used for the preparation of the nitriles of D-galactonic-2-C^{14} acid and D-talonic-2-C^{14} acid. The accompanying diagrams show the steps of the syntheses and the yields of the products based on the activities of the D-arabinose-1-C^{14} and D-lyxono-γ-lactone-1-C^{14}, used as starting materials.

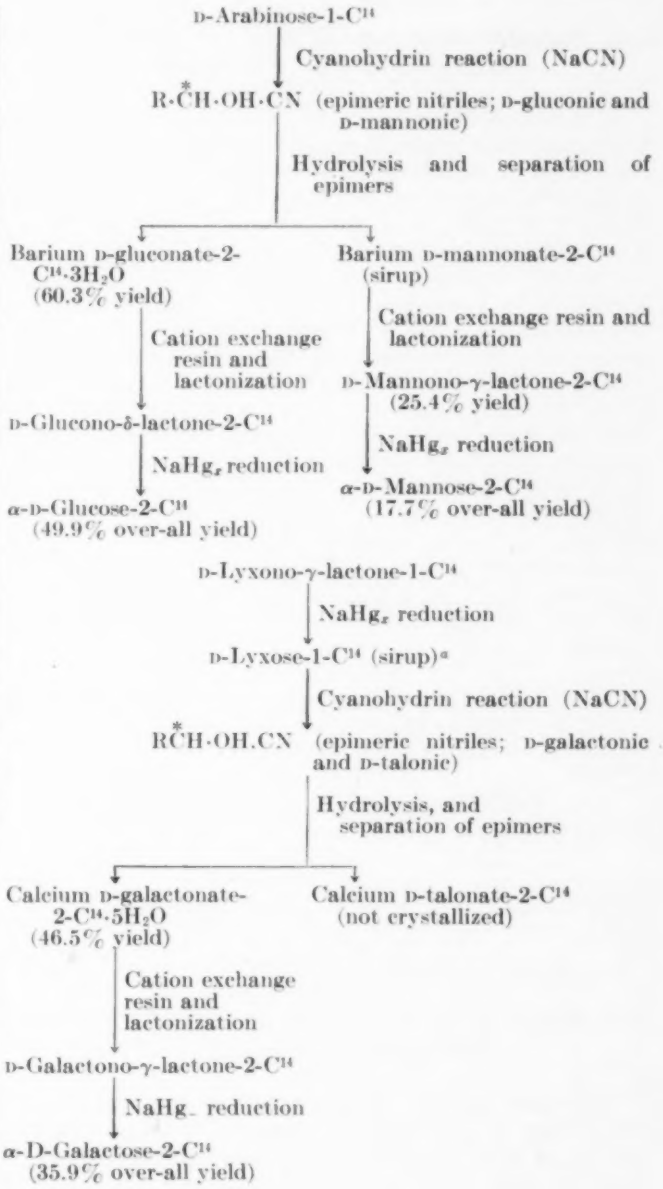

2. Experimental Procedures

2.1. Barium D-Gluconate-2-C^{14} Trihydrate and D-Mannono-γ-lactone-2-C^{14}

A solution containing 3.49 millimoles (mM) of D-arabinose-1-C^{14}, with 680 microcuries (μc) of activity, and 3.6 mM of sodium cyanide in 25 ml of water was allowed to stand at room temperature for 3 days. The reaction products were then treated by the procedures described for the preparation of barium

[1] This work is part of a project on the development of methods for the synthesis of radioactive carbohydrates, sponsored by the U. S. Atomic Energy Commission. This paper is based on the work described in an AEC report.

[2] Figures in brackets indicate the literature references at the end of this paper.

[a] Sirup used without crystallization.

D-gluconate-1-C^{14} and D-mannono-γ-lactone-1-C^{14} [3].

The crystalline barium D-gluconate-2-C^{14} trihydrate had an activity of 339 μc. By the use, in three portions, of a total of 1,030 mg of nonradioactive barium D-gluconate trihydrate as carrier, an additional quantity of 71 μc was separated. Thus the radiochemical yield of barium D-gluconate-2-C^{14} from D-arabinose-1-C^{14} was 60.3 percent.

The mother liquor from the preparation of barium D-gluconate-2-C^{14}, after removal of barium, and lactonization, gave 116 mg of crystalline D-mannono-γ-lactone-2-C^{14} having an activity of 126 μc. By means of a total of 297 mg of carrier, used in 3 portions, the total radiochemical yield was increased to 173 μc, corresponding to 25.4 percent of the original D-arabinose-1-C^{14}.

2.2. Preparation of α-D-Glucose-2-C^{14} from Barium D-Gluconate-2-C^{14} Trihydrate

A 1.035-mM quantity of barium D-gluconate-2-C^{14} trihydrate, having an activity of 400 μc, was converted to D-glucono-δ-lactone-2-C^{14} by the method previously described [3]. In the earlier work, a mixture of oxalic acid and sodium oxalate was used in the sodium amalgam reduction of the lactone to the sugar; crystalline sodium acid oxalate was later found to be more convenient [1]. Table 1 reports the results of a series of reductions of D-glucono-δ-lactone in the presence of crystalline sodium acid oxalate. The conditions of experiment 2 were followed in the reduction of D-glucono-δ-lactone-2-C^{14}. The product, separated as crystalline α-D-glucose without carrier by the procedure given for the production of α-D-glucose-1-C^{14}, weighed 296 mg and had an activity of 314 μc. Additional material obtained by use of carrier amounted to 17 μc. Thus the radiochemical yield of α-D-glucose-2-C^{14} from barium D-gluconate-2-C^{14} trihydrate was 82.8 percent, and the over-all yield from D-arabinose-1-C^{14} was 49.9 percent.[3]

TABLE 1. *Reduction of D-glucono-δ-lactone[a] by sodium amalgam in the presence of sodium acid oxalate*

Experiment	Sodium acid oxalate monohydrate	$NaHg_x$ (5 percent)	Yield of D-glucose (by analysis)
	g	*g*	*%*
1	0.6	1.65	87.2
2	1.0	2.3	90.6
3	1.5	3.45	87.9
4	2.0	4.6	83.4

[a] 1.0 mM of lactone in 20 ml of water.

2.3. Preparation of α-D-Mannose-2-C^{14} from D-Mannono-γ-lactone-2-C^{14}

The procedure for the preparation of α-D-mannose-1-C^{14} from D-mannono-γ-lactone-1-C^{14} was simplified by use of sodium acid oxalate as a buffer in place of benzoic acid. The experiments reported in table 2 show that a maximum yield of sugar is obtained by use of 27.6 g of 5-percent sodium amalgam per millimole of lactone in the presence of 12 g of sodium acid oxalate.

TABLE 2. *Reduction of D-mannono-γ-lactone[a] by sodium amalgam in the presence of sodium acid oxalate*

Experiment	Sodium acid oxalate monohydrate	$NaHg_x$ (5 percent)	Yield of D-mannose (by analysis)
	g	*g*	*%*
1	1.0	2.3	25.5
2	2.0	4.6	43.9
3	4.0	[b] 9.2	56.5
4	6.0	[b] 13.8	67.8
5	8.0	[c] 18.4	88.3
6	12.0	[c] 27.6	91.6
7	16.0	[c] 36.8	88.6

[a] 1.0 mM of lactone in 20 ml of water.
[b] Added in 4.5-g quantities at 1-hr intervals. Mercury was removed before each new addition.
[c] Added in 9.2-g quantities at 1-hr intervals. Mercury was removed before each new addition.

For the preparation of α-D-mannose-2-C^{14}, a 1.4-mM composite sample of D-mannono-γ-lactone-2-C^{14}, having an activity of 294 μc, was reduced in the presence of 16.8 g of sodium acid oxalate, by use of 39 g of 5-percent sodium amalgam in three portions. Salts were removed by precipitation with alcohol and use of ion-exchange resins, as previously described. The crystalline sugar was prepared by concentrating the solution, dissolving the sirup in methanol, and adding 2-propanol. The crystalline α-D-mannose-2-C^{14}, obtained without carrier, weighed 158 mg and had an activity of 185 μc; by use of nonradioactive α-D-mannose as carrier, an additional 20 μc of the sugar was obtained. Thus the radiochemical yield from D-mannono-γ-lactone-2-C^{14} was 69.7 percent and the over-all yield from D-arabinose-1-C^{14} was 17.7 percent.[4] By elution of the resin used for removal of the salts, 49 μc of crude D-mannonic-2-C^{14} acid was reclaimed.

2.4. Calcium D-Galactonate-2-C^{14} Pentahydrate

Calcium D-galactonate-2-C^{14} pentahydrate can be prepared readily from crystalline β-D-lyxose-1-C^{14} by the process developed for the production of calcium D-galactonate-1-C^{14} [4]. However, by starting the synthesis with a solution of D-lyxose-1-C^{14}, without separation of the crystalline sugar, considerable saving of time and material can be made. In the present study, the D-lyxose-1-C^{14} was obtained by reduction [2] of 3 mM of D-lxyono-γ-lactone-1-C^{14} containing 1,918 μc of carbon-14. The solution of D-lyxose was concentrated to 25 ml and cooled to 0° C. Six millimoles of sodium bicarbonate and 6 ml of aqueous 0.5 *N* sodium cyanide were added, and the solution was stored at room temperature. After 4 days, the reaction mixture was treated by the procedure described for the preparation of calcium D-galactonate-1-C^{14}. The calcium D-galactonate-2-C^{14} pentahydrate obtained without carrier weighed

[3] Based on the percentage yield of barium D-gluconate-2-C^{14} from D-arabinose-1-C^{14}.

[4] Based on the percentage yield of D-mannono-γ-lactone-2-C^{14} from D-arabinose-1-C^{14}.

240 mg and had an activity of 593 μc. Additional salt, obtained by use of carrier, amounted to 299 μc. Thus the radiochemical yield of calcium D-galactonate-2-C^{14} pentahydrate was 892 μc or 46.5 percent of the original D-lyxono-γ-lactone-1-C^{14}. The residual liquor, containing approximately 1,000 μc of carbon-14 largely in the form of calcium D-talonate-2-C^{14}, was set aside for future use.

2.5. Preparation of α-D-Galactose-2-C^{14} From Calcium D-Galactonate-2-C^{14} Pentahydrate

A solution of D-galactonic-2-C^{14} acid was prepared from 763 mg of calcium D-galactonate-2-C^{14} pentahydrate having an activity of 803 μc. The acid was lactonized, and reduced by the procedure developed for the preparation of α-D-galactose-1-C^{14} [4]; a total of 18 g of 4.2-percent sodium amalgam and 6.6 g of sodium acid oxalate was used. The sugar solution after removal of salts, and concentration, gave crystalline α-D-galactose-2-C^{14} that, once recrystallized, had an activity of 567 μc. By means of 400 mg of nonradioactive sugar, used in two portions as carrier, additional sugar containing 54 μc was obtained. Thus the total radiochemical yield of α-D-galactose-2-C^{14} was 621 μc or 77.3 percent of the calcium D-galactonate-2-C^{14} pentahydrate; the overall yield was 35.9 percent.[5] Extraction with aqueous acetic acid of the mixed resin column used for deionization of the sugar solution liberated 117 μc of activity. This material, largely D-galactonic-2-C^{14} acid, was stored for use in a subsequent preparation.

WASHINGTON, December 21, 1954.

3. References

[1] H. L. Frush and H. S. Isbell, J. Reasearch NBS **51,** 307 (1953) RP2458.

[2] H. S. Isbell, H. L. Frush, and N. B. Holt, J. Research NBS **53,** 325 (1954) RP2550.

[3] H. S. Isbell, J. V. Karabinos, H. L. Frush, N. B. Holt, A. Schwebel, and T. T. Galkowski, J. Research NBS **48,** 163 (1952) RP2301.

[4] H. S. Isbell, H. L. Frush, and N. B. Holt, J. Research NBS **53,** 217 (1954) RP2536.

[5] H. S. Isbell, U. S. Patents 2,606,918 (1952), 2,632,005 (1953); H. S. Isbell and J. V. Karabinos, J. Research NBS **48,** 438 (1952) RP2334; H. L. Frush and H. S. Isbell, J. Research NBS **50,** 133 (1953) RP2400; **51,** 167 (1953) RP2446.

[5] Based on the percentage yield of calcium D-galactonate-2-C^{14} from D-lyxono-γ-lactone-1-C^{14}.

...nal of Research of the National Bureau of Standards Vol. 54, No. 4, April 1955 Research Paper 2582

The System of Lime, Silica, and Water at 180° C

Richard B. Peppler

Solid-liquid equilibria in the system CaO-SiO_2-H_2O were investigated at 180° C. Only four compounds were found to be stable in equilibrium with the liquid: Xonotlite ($5CaO \cdot 5SiO_2 \cdot H_2O$, hillebrandite ($2CaO \cdot SiO_2 \cdot H_2O$), α-quartz, and $Ca(OH)_2$. The metastable equilibrium curves of gyrolite ($2CaO \cdot 3SiO_2 \cdot 2H_2O$) and a particular silica gel were determined. The results also suggested several other metastable compounds. Supplementary experiments of six months' duration with oxide mixtures confirmed the stability at 180° C of only two ternary compounds, xonotlite and hillebrandite.

1. Introduction

The system CaO-SiO_2-H_2O has been the subject of many investigations. Under hydrothermal conditions, this system yields a number of crystalline compounds [1]. However, only tentative and qualitative compatibility diagrams have been published to date. Most investigators have concerned themselves primarily with the identities of the products obtained. The goal of the present investigation has been not only to identify the products formed, but also to determine the quantitative equilibrium relationships as accurately as possible.

The importance of studies of this system to an understanding of the setting of portland cement, the pozzolanic reaction, and the formation of sand-lime bricks is apparent. The 180° C isotherm of this system was chosen for investigation because of its direct applicability to steam-cured portland-cement products.

2. Apparatus and Procedure

Stainless-steel autoclaves of ½- to 1-liter capacity were used. These have been described in detail elsewhere [2]. Briefly, each consisted of two similar vessels separated by a filter disk. In each experiment, one vessel was filled with solid and liquid phases in the proportion of 2 g of solid per liter of liquid, and the autoclave was assembled. It was heated in an electric oven maintained at 180° ±2° C for the desired period of time. When the autoclave was removed, filtration was accomplished by inverting it in cold water and condensing the vapors in the "empty" vessel.

The solid reaction products were washed with alcohol and ether, and dried at 45° C. Afterward they were examined petrographically and X-ray powder patterns were obtained. In some cases, differential thermal-analysis (DTA) curves and absorption tests with methylene blue were made.

The filtrate was analyzed for lime and silica. The lime was determined gravimetrically by precipitation as the oxalate and ignition to the oxide. Silica was determined gravimetrically except where its concentration was less than 0.01 g/liter. In such cases, it was determined colorimetrically as the silicomolybdate, using a standard sodium chromate solution as a color reference.

The solutions of CaO were prepared by igniting reagent quality $CaCO_3$ overnight at 950° C and dissolving the resulting CaO in ordinary distilled water.

A commercial silica gel was used as a source of silica. It was found to contain 0.05 percent of Na_2O and 0.01 percent of K_2O and to have an HF residue of 0.35 percent and an ignition loss at 1,100° C of 6.50 percent. An air alutriation stack was used to fractionate some of the gel into two parts, one of particle size above 10 μ and the other below 10 μ. It was found that the reactivities of the two fractions were not significantly different at 180° C; consequently, the unfractionated gel was used throughout this investigation.

In some cases, crystalline calcium hydrosilicates were used as the initial solid phases. The compounds for this purpose were synthesized by hydrothermal treatment of oxide mixtures in a Morey bomb as follows: Gyrolite ($2CaO \cdot 3SiO_2 \cdot 2H_2O$) from a 2:3 molar ratio of CaO to SiO_2 at 350° C, 6 days, 163-atm pressure; xonotlite ($5CaO \cdot 5SiO_2 \cdot H_2O$) from a 1:1 molar ratio of CaO to SiO_2 at 380° C, 17 days, 235-atm pressure; and hillebrandite ($2CaO \cdot SiO_2 \cdot H_2O$) from a 2:1 molar ratio of CaO to SiO_2 at 242° C, 7 days, 34-atm pressure. Petrographic examination and X-ray diffraction patterns identified the products as the compounds indicated. The experimental conditions for these syntheses were suggested by the work of Flint, McMurdie, and Wells [2].

Metastable solutions were prepared by heating silica gel with a solution of $Ca(OH)_2$ at 90° C for 3 weeks, filtering, and mixing the clear filtrate with $Ca(OH)_2$ solutions.

Contamination of the liquid phases by attack on the autoclaves occurred in most experiments. The soluble iron introduced into solution was, however, less than 1 ppm. Chromium was a worse offender. As much as 30 ppm as calcium chromate would sometimes be found in the liquid phase. In such cases, chromium was removed as the hydroxide prior to the determination of calcium oxide, and its color after conversion to chromate, was matched with the standard chromate color reference prior to the determination of silica colorimetrically.

The effect of carbon dioxide, as judged by the observed quantity of calcite in the solid phases, was negligible.

3. Phase Equilibria at 180° C

3.1. Approach From Undersaturation

Data pertaining to this phase of the investigation are presented in table 1, (A). Silica gel was mixed with saturated solutions of lime water in such proportions as to give initial molar ratios of CaO to SiO_2 from 0.00 to 3.00. These mixtures were heated at 180° C from 4 to 15 days. The crystalline products were so fine-grained that only an average or a range of indices of refraction could be obtained, as indicated in column 6. Because of the small differences among the published refractive indices of the calcium hydrosilicates, and the uncertainty that exists in several cases, the data obtained did not suffice to identify the products.

An X-ray powder pattern was obtained for each solid reaction product. The strong family resemblance of the calcium hydrosilicates and the ambiguity in published patterns of them made identification difficult. In general, the patterns published by Flint and McMurdie [3] and Taylor and Bessey [1] were used as references. However, to decide upon the identity of the principal phases in the reaction products, the patterns of the compounds synthesized at higher temperatures were arbitrarily taken as standard.

In no case was a single pure phase obtained, as judged by the X-ray patterns. One or two principal phases would be indicated, but there would always be a minority of ambiguous lines. The principal compounds are indicated in column 8 (table 1). the minor compounds are not indicated. In general, they were compounds having the CaO to SiO_2 ratio that was present in the initial mixture. Thus in experiments 2, 3, and 4 (CaO/SiO_2=0.26 to 0.63), okenite ($CaO{\cdot}2SiO_2{\cdot}2H_2O$) was indicated; in experiment 5 (CaO/SiO_2=0.80), the compound $4CaO{\cdot}5SiO_2{\cdot}5H_2O$; in experiment 6 ($CaO/SiO_2$=1.05),

TABLE 1. *Solubility relationships in the system* $CaO\text{-}SiO_2\text{-}H_2O$ *at 180° C*

1	2	3	4	5	6	7	8	9
Experiment	Initial molar ratio CaO/SiO_2	Time	Final CaO	Final SiO_2	Refractive index of solid phases	Relative amount solid dyed	Identity of solid phases	Identity of product after DTA
A. Silica gel+$Ca(OH)_2$ solutions (from undersaturation)								
		Days	*g/liter*	*g/liter*				
1	0.00	6	0.00	0.75	1.45		Silica gel	$\alpha-CaO{\cdot}SiO_2$+
2	.26	4	.05	.53	Range 1.42 to 1.54	Large	Xonotlite+gyrolite+silica gel	$\beta-CaO{\cdot}SiO_2$+ α-quartz.
3	.26	12	.03	.32	Range 1.46 to 1.54	do	do	Do.
4	.63	7	.02	.20	Range 1.54 to 1.59; Bulk 1.54 to 1.55	do	do	Do.
5	.80	7	.02	.08	Average 1.57	Small	Gyrolite+xonotlite	$\alpha-CaO{\cdot}SiO_2$+ $\beta-CaO{\cdot}SiO_2$ (no α-quartz).
6	1.05	13	.02	.09	Range 1.57 to 1.59	Medium	Xonotlite	Do.
7	1.50	15	.09	.008	Average 1.61	Small	Hillebrandite	$\beta-2CaO{\cdot}SiO_2$+ $\beta-CaO{\cdot}SiO_2$.
8	1.73	7	.07	.008	Range 1.58 to 1.61	Very small or none.	do	$\beta-2CaO{\cdot}SiO_2$.
9	2.00	11	.05	.007	Average 1.60	None	do	Do.
10	3.00	14	.17	.002	Average 1.60	do	Hillebrandite+$Ca(OH)_2$	$\beta-2CaO{\cdot}SiO_2$+ CaO.
B. Metastable solutions (from supersaturation)								
1	2	3	4	5	6	7	8	
11	0.32	7	0.02	0.13	Average 1.54	Large	$CaO{\cdot}SiO_2{\cdot}H_2O$+xonotlite+$4CaO{\cdot}5SiO_2{\cdot}5H_2O$.	
12	.50	10	.03	.003	Range 1.58 to 1.60	do	Xonotlite.	
13	.67	9	.08	.002	Average 1.57; Fibers 1.58 to 1.59	do	Hillebrandite+?	
14	.80	8	.06	.01	Granules 1.59 to 1.60	do	Hillebrandite+?	
15	1.00	8	.02	.01	do	Medium	Do.	
16	1.50	8	.02	.01	Average 1.60	None	Xonotlite+hillebrandite.	
17	1.67	8	.02	.01	Average 1.55	do	Do.	
18	1.97	13	.09	.001	Average 1.59 to 1.60	do	Hillebrandite.	
19	2.82	13	.06	.002	do	do	Hillebrandite+$Ca(OH)_2$.	
C. Compounds as initial solid phases								
Experiment	Initial phases			Time	Final CaO	Final SiO_2	Product	
				Days	*g/liter*	*g/liter*		
20	Hillebrandite+sat. $Ca(OH)_2$			19	0.15	0.002	Hillebrandite+$Ca(OH)_2$.	
21	Hillebrandite+xonotlite+H_2O			7	.08	.005	Hillebrandite+xonotlite.	
22	Xonotlite+gyrolite+H_2O			10	.03	.02	Xonotlite.	
23	Silica gel+gyrolite+H_2O			3	.03	.13	Gyrolite+silica gel.	
24	Flint+xonotlite water			8	.02	.096	α-quartz+xonotlite.	
25	Flint+H_2O			8	.00	.04	α-quartz.	

crestmoreite ($2CaO \cdot 2SiO_2 \cdot H_2O$) and "CSH I"; in experiment 7 ($CaO/SiO_2 = 1.50$), afwillite ($3CaO \cdot 2SiO_2 \cdot 3H_2O$); 8 ($CaO/SiO_2 = 1.73$), foshagite ($5CaO \cdot 3SiO_2 \cdot 3H_2O$); 9 ($CaO/SiO_2 = 2.00$), "CSH II"; and 10 ($CaO/SiO_2 = 3$), $3CaO \cdot SiO_2 \cdot 3H_2O$. The lines indicating these compounds were generally weak and constituted less than 10 percent of the number of lines in the pattern.

The solid reaction products were treated with a saturated alcoholic solution of methylene blue hydrochloride for 24 hr. washed free of excess dye, and examined microscopically. The relative proportion of dyed particles, indicating unreacted silica gel, is given in column 7 of table 1. In general, the amount of unreacted silica decreased as the molar ratio of CaO to SiO_2 increased. This is to be expected. The low value in experiment 5 appears to be unusual. It confirms the X-ray and microscopic data, however. Experiment 5 was the first experiment in which no silica gel was observed microscopically in the reaction product.

Differential thermal-analysis (DTA) curves were obtained of the solid reaction products in each case. These are presented in figure 1. The identities of the products after the DTA heat treatment were determined by X-ray powder patterns, and are given in table 1, (A), column 9.

It is known that the ultimate decomposition products of gyrolite when heated to 1,000° C are pseudowollastonite ($\alpha - CaO \cdot SiO_2$) and α-quartz, and that those of xonotlite are a mixture of pseudowollastonite and wollastonite ($\beta - CaO \cdot SiO_2$) [4]. The uncombined silica gel in the reaction products evidently transforms to α-quartz.

As the molar CaO to SiO_2 ratio increased (experiments 1 to 5), the proportion of wollastonite in the products of DTA heat treatment increased. This indicates that the proportion of xonotlite in the original reaction product had increased. It also confirms the refractive index data (column 6), which indicate that the average index of refraction had increased from that of the unaltered silica gel (1.42) through that of gyrolite (1.54) to that of xonotlite (1.59). The microscopic examinations also showed that gyrolite predominated in experiments 2, 3, and 4, and xonotlite in experiments 5 and 6.

The DTA curves, figure 1, show a family resemblance among the products of experiments 2 to 6 (CaO to SiO_2 molar ratios of 0.26 to 1.05). This agrees with the fact that these products are all mixtures of unaltered silica gel, gyrolite, and xonotlite, as indicated by the optical and X-ray data. The endothermic break from 100° to 300° C is evidently the dehydration of the unreacted silica gel. The characteristic exothermic break at 800° to 850° C is evidently associated with the crystallization of wollastonite. The increased size of this break for experiment 3 over that of experiment 2 indicates that the reaction in the autoclave had proceeded further in 12 days than in 4, which agrees with the observation that there was less uncombined silica in the former case. The diminishing size of this break thereafter may possibly be related to the increasing proportion of wollastonite.

It may be observed that the DTA curves of the products of experiments 7 to 10 also constitute a group, being similar to each other but differing from the first group. The endothermic break for the dehydration of silica gel is absent, correlating with the observation that the amount of silica gel, as determined by dye absorption, was negligible in the corresponding reaction products. The characteristic endothermic break between 500° and 600° C is evidently associated with the dehydration of hille-

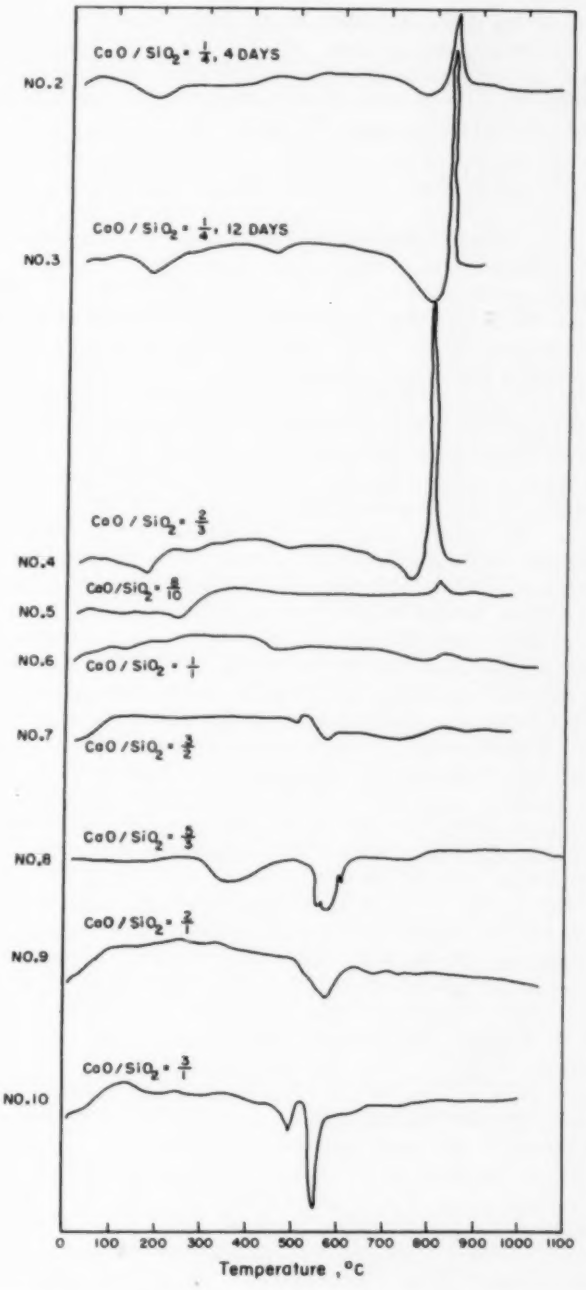

FIGURE 1. *Differential thermal analysis curves of solid reaction products obtained by an approach to equilibrium from undersaturation.*

brandite to β-$2CaO{\cdot}SiO_2$. In the case of experiment 10, the additional endothermic break at 500° C is associated with the dehydration of excess $Ca(OH)_2$. The increasing size of the β-$2CaO{\cdot}SiO_2$ break with increasing CaO/SiO_2 ratio may possibly be related to an increasing proportion of hillebrandite in the product. The optical and X-ray data also indicated that hillebrandite was the main product in experiments 7 to 10.

The X-ray pattern of the reaction product of experiment 7 indicated the presence of another hydrosilicate other than hillebrandite. This was confirmed by the presence of a minor amount of wollastonite in the product after DTA heat treatment. The X-ray patterns of the reaction product of experiment 10 indicated the presence of $Ca(OH)_2$ before and of CaO after the DTA heat treatment.

3.2. Approach from Supersaturation

A series of metastable solutions of silica gel in lime water was prepared as described in section 2. These metastable solutions were held at 180° C from 7 to 13 days. Data pertaining to this phase of the investigation are presented in table 1, (B), and are shown graphically in figure 2.

Referring to table 1, it may be observed that the products of these precipitation experiments do not have the CaO to SiO_2 molar ratios of the initial mixtures. In the case of experiment 11, the principal products in the solid phase appeared to be a mixture of a very small amount of xonotlite with the compounds $4CaO{\cdot}5SiO_2{\cdot}5H_2O$ and $CaO{\cdot}SiO_2{\cdot}H_2O$, the former predominating. As these two compounds were not found in the approach from undersaturation, they may be metastable with respect to xonotlite. The observed index, 1.54, coincides with that of $4CaO{\cdot}5SiO_2{\cdot}5H_2O$ [2]. The only other hydrosilicates obtained from supersaturation were xonotlite and hillebrandite, regardless of the initial molar CaO to SiO_2 ratio. Apparently, whatever the immediate products of precipitation may be, they are all metastable with respect to xonotlite and hillebrandite. This is in accord with the results reported in section 3.1.

The paths of precipitation in these experiments judged by initial and final points are indicated in figure 3. It may be observed that there are two groups of precipitates, namely, those formed when the initial CaO to SiO_2 ratio was less than 1, and those formed when the initial CaO to SiO_2 ratio was greater than 1. In the former group, the precipitates had a CaO to SiO_2 ratio of from 1 to 2. The hydrosilicate having this ratio, okenite, was not observed. As no calcium hydrosilicate richer in silica is known, the precipitates must have consisted of silica and other hydrosilicates. In the second group, the precipitates had a CaO to SiO_2 ratio slightly lower than 2 to 1, indicating the presence of some other phases less rich in lime, in addition to hillebrandite. The path of precipitation of the mixture with a ratio of 2.8 has a slope indicating lime in excess of hillebrandite.

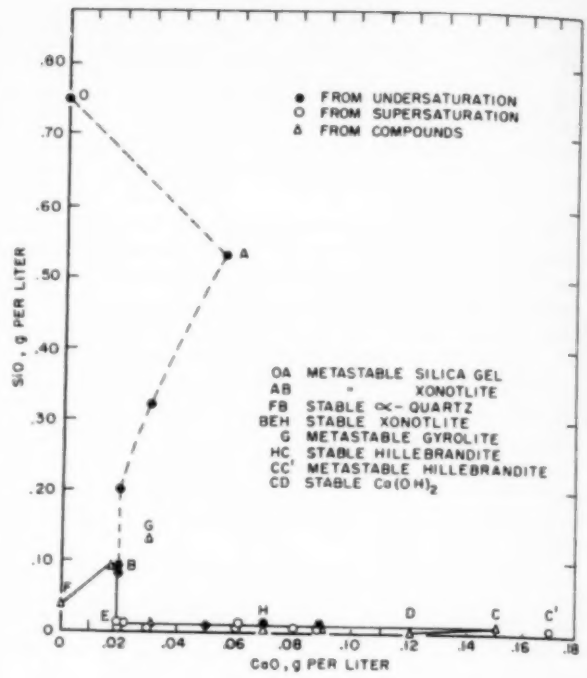

FIGURE 2. *Phase equilibria in the system* $CaO{\cdot}SiO_2{\cdot}H_2O$ *at 180° C.*

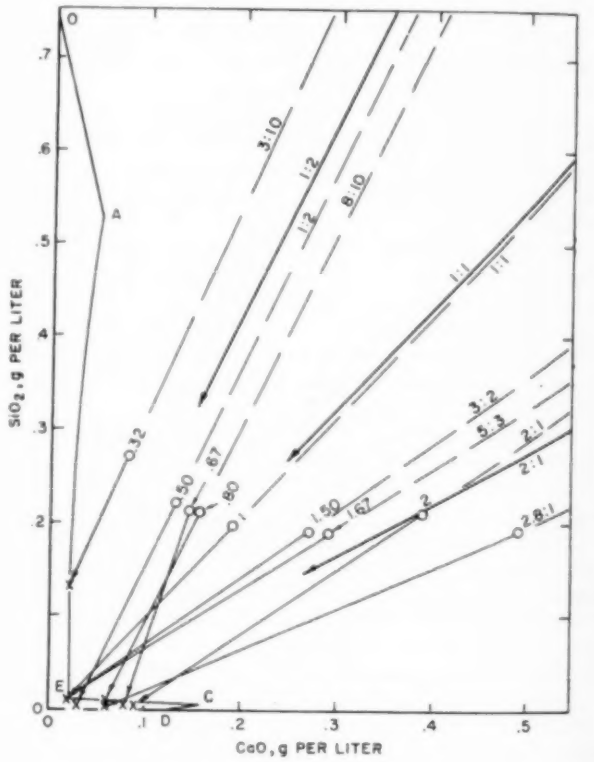

FIGURE 3. *Precipitation from supersaturated solutions in the system* $CaO{\cdot}SiO_2{\cdot}H_2O$ *at 180° C.*

Figure 2 indicates that the data obtained from supersaturation, when plotted, give points falling reasonably well on the solubility curves determined by an approach from undersaturation. The composition of the liquid phase in experiments 15, 16, and 17 (point E) appeared to define the xonotlite-hillebrandite invariant point, which the experiments in the preceding section did not; but subsequent experiments indicated this point to represent metastable equilibrium.

The results of dye-absorption tests on the solid reaction products, similar to those described in section 3.1 are shown in column 7. A similar trend of decrease in the uncombined silica is indicated, but the transition to complete combination after 1 to 1 CaO to SiO_2 ratio is sharper.

The compositions of the liquid phases are indicated in columns 4 and 5 of table 1. The plot of these data in figure 2 indicates that a metastable gyrolite–silica-gel invariant point exists above and to the right of A; that the metastable equilibrium curve for gyrolite lies to the right of AB, which approximates the xonotlite equilibrium curve; and that a stable hillebrandite-$Ca(OH)_2$ invariant point exists at C′. Point D is the solubility of $Ca(OH)_2$ as CaO in water alone at 180° C, as taken from a graph of Peppler and Wells [5]. Evidently a xonotlite-hillebrandite invariant point must exist between points A and C′ on the curve AEC′.

3.3. Experiments With Compounds

For this phase of the investigation, hillebrandite, xonotlite, and gyrolite and α-quartz were used. A washed flint was used as the α-quartz. It was found to have 0.004 percent of Fe_2O_3 and an HF residue of less than 0.02 percent. The X-ray powder pattern showed only α-quartz.

The data are presented in table 1, (C), and are shown graphically in figure 2. Experiment 20 established the hillebrandite-$Ca(OH)_2$ invariant point, point C, figure 2, at 0.15 g/liter of CaO, whereas experiment 10 (table 1, A) gave 0.17. The agreement is reasonable under the circumstances and is further confirmation that hillebrandite is a stable phase in this system at 180° C.

Experiment 21 was an attempt to establish the hillebrandite-xonotlite invariant point directly. The composition of the liquid phase, point H, figure 2, does not agree with the point E, established by precipitation from supersaturated solutions. Point H may be considered as the probable xonotlite-hillebrandite invariant point, because it was defined directly from the two compounds. Point E may be a metastable invariant point.

In experiment 22, a mixture of xonotlite and gyrolite after 10 days gave only xonotlite, confirming the previous conclusion that gyrolite is metastable with respect to xonotlite and silica at 180° C. In experiment 23, the gyrolite did not have time to convert to xonotlite. The composition of the liquid phase of this experiment is indicated in figure 2 as point G. It seems probable that an area to the right of AB represents metastable gyrolite.

Experiment 24 was designed to establish the stable xonotlite-α-quartz invariant point.

The solubility of α-quartz alone (experiment 6) was found to be 0.04 g/liter, and a straight line joining point F, representing this composition with the point B, is taken as the stable equilibrium curve of α-quartz.

3.4. Experiments With Oxide Mixtures

Certain experiments of 6 months' duration were undertaken in an attempt to determine beyond any reasonable doubt what compounds are stable in the system CaO-SiO_2-H_2O at 180° C. A series of 10 mixtures of CaO and silica gel, whose molar CaO to SiO_2 ratio varied from 0.10 to 4.00, was placed in platinum thimbles, and the thimbles were placed in an autoclave with an excess of water in such a manner that the solid and liquid phases were not in contact. The autoclave was held at 180° C for 6 months.

When the products were removed from the autoclave, they were dried for 1 hr at 110° C and examined microscopically. The sizes of the crystalline reaction products were so minute that only average indices of refraction could be obtained. It was necessary to resort to X-ray powder patterns to establish their identities. The patterns so obtained were compared with the standard patterns mentioned earlier. The results are presented in table 2.

Table 2 shows that only two calcium hydrosilicates were obtained, namely, xonotlite and hillebrandite. The unreacted silica gel, indicated as another product in experiments 1, 2, and 3, was not physically distinct from xonotlite. The xonotlite, rather, was uniformly dispersed in the silica gel, so that the whole mass appeared to be homogeneous and to have a very light grey color between crossed nicols. The X-ray patterns corresponding to these preparations indicated that the gel had partially transformed to α-quartz.

In the case of experiments 9 and 10 (table 2), the $Ca(OH)_2$ was physically distinct from the hydrosilicate, and of relatively large particle size. Thus, the appearance of the products obtained after 6 months of hydrothermal treatment was very close to that of the products obtained in a few days when the solid and liquid phases were in contact.

TABLE 2. *Pastes heated at 180° C for 6 months*

Experiment	CaO to SiO_2 ratio	Identity by X-ray patterns
	M	
1	0.100	Xonotlite+silica gel.
2	.500	Do.
3	.667	Do.
4	.800	Xonolite.
5	1.000	Do.
6	1.500	Hillebrandite+xonotlite.
7	1.667	Hillebrandite.
8	2.000	Do.
9	3.000	Hillebrandite+$Ca(OH)_2$.
10	4.000	Do.

4. Discussion

The 180° C isotherm of the system CaO-SiO_2-H_2O appears to be more, rather than less, complex than the room temperature isotherm. Although the compounds at 180° C are definitely crystalline and give reasonably sharp X-ray patterns, it is difficult to identify them. The number of compounds that can exist metastably in this system appears to be at a maximum at or near 180° C [1, 2] and would include nearly all the calcium hydrosilicates that have been described. The determination of the phase equilibria of these metastable phases is beyond the scope of the present investigation. Certain conclusions, however, may be drawn.

When the initial CaO to SiO_2 molar ratio is 0.8 or less and silica is initially a solid phase, the two combine to form metastable gyrolite. It transforms then into xonotlite with a rapidity that apparently depends on the CaO to SiO_2 molar ratio, as evidenced by the fact that the proportion of xonotlite increases in the reaction products with increasing CaO to SiO_2 ratio (table 1, A). At low CaO to SiO_2 ratio, the transformation is not complete at the end of 12 days (experiment 3). Other phases may first form that are in turn metastable with respect to gyrolite, as indicated by the minority of lines in the powder patterns that match lines of the powder patterns of other compounds more closely. In the presence of excess reactive silica, however, these minor phases apparently exist only transitorily.

When the initial molar CaO to SiO_2 ratio was 1.05 (and silica gel was the solid phase), the only product at the end of 13 days was xonotlite (experiment 6). It is possible that gyrolite first formed and then converted to xonotlite, because a mixture of gyrolite and xonotlite converted in 10 days to xonotlite (experiment 22). This latter experiment establishes conclusively that xonotlite, and not gyrolite, is the stable phase.

Certain analogies can be drawn between the phase equilibria in the system CaO-SiO_2-H_2O at room temperature [4, 6] and those at 180° C. At room temperature, available evidence indicates that only two stable ternary compounds, CSH I and C_2SH II, a monocalcium and a dicalcium silicate hydrate, exist. These are analogous, as regards CaO to SiO_2 ratio, to xonotlite and hillebrandite, found to be stable at 180° C.

At room temperature, the compound CSH I has been found to vary in CaO to SiO_2 ratio from 0.8 to 1.5, and the compound C_2SH II, to vary from 1.4 to 1.9 [7]. In the present study, all compositions from CaO to SiO_2 ratio up to 1.5 gave xonotlite, and higher CaO to SiO_2 ratios gave hillebrandite. The CaO to SiO_2 ratio of the solid reaction products was not determined in this investigation. Kalousek, Logiudice, and Dodson [8], however, prepared synthetic hillebrandite, as well as the α- and γ-dicalcium silicate hydrate, in the range 175° to 250° C, in which the CaO to SiO_2 molar ratios varied from 1.5 to 2.4 and possibly extended to 3.0 for synthetic hillebrandite (β-hydrate). For each hydrate, almost identical X-ray patterns were obtained over the range of varying CaO to SiO_2 ratio. This situation is directly analogous to that found at room temperature, where a varying CaO to SiO_2 ratio, within the limits mentioned above, does not affect the X-ray patterns.

Several previous investigators have prepared dicalcium silicate hydrate ($10CaO{\cdot}5SiO_2{\cdot}6H_2O$) [2, 8, 9, 10, 11], and it has been isolated in steam-cured mortars [12]. This suggests that it might be the stable dicalcium silicate hydrate at 180° C. The present investigation, however, indicates that hillebrandite is the stable dicalcium silicate hydrate. Kalousek, Logiudice, and Dodson [8] found that the α-hydrate, prepared at 175° C, began to convert to the β-hydrate (hillebrandite) when the temperature was raised. Their work indicates that many variables such as type of silica and condition of mixing, helped to determine what hydrate was produced, so that they were not able to assign definite ranges of temperature over which the various hydrates are stable. These same authors found that at 175° C, when the CaO to SiO_2 ratio fell below 1.8, xonotlite appeared. This is in accord with the results obtained in the present investigation.

Recent work of Heller and Taylor [13] indicates that hillebrandite is the stable dicalcium cilicate hydrate at 180° C. They found that $Ca(OH)_2$ and silica in 2:1 ratio at 180° C for 30 days gave hillebrandite. The α-hydrate was formed below and the γ-hydrate above 180° C. These results were not conclusive, however, because in another experiment they obtained all three hydrates.

The present investigation also is in accord with other recent work of Heller and Taylor [14], which demonstrates that CSH I and afwillite are metastable at 180° C.

Returning to the group of experiments (table 1, A) where the initial molar CaO to SiO_2 ratio is 1.50 to 3.00, it is apparent that no stable compound more lime-rich than dicalcium silicate hydrate forms. The hydrate $3CaO{\cdot}SiO_2{\cdot}2H_2O$ was prepared by Flint, McMurdie, and Wells [2] at and above 200° C. In experiment 10, a few weak lines in the X-ray pattern indicated the presence of this hydrosilicate, but they resembled the lines of $Ca(OH)_2$ too closely to prove the existence of the hydrosilicate at 180° C. The same authors found that $CaO{\cdot}SiO_2{\cdot}H_2O$ formed at 150° C and xonotlite at 175° C from a CaO and SiO_2 mixture of 1:1 molar ratio. This would indicate that the compound $CaO{\cdot}SiO_2{\cdot}H_2O$ is metastable with respect to xonotlite near 180° C. The results of the present investigation are in accord. However, Flint, McMurdie, and Wells [2] found that the compound $4CaO{\cdot}5SiO_2{\cdot}5H_2O$ formed between 150° C [2] and 275° C and persisted in this range from 7 to 42 days. This suggests that it is a stable phase at 180° C because it was found to transform to xonotlite only at 300° C. In the present investigation, this compound was found to be metastable with respect to xonotlite at 180° C. Flint, McMurdie, and Wells used lime-silica gels in their experiments, and these gels were steamed out of contact with the liquid

phase. Apparently, the rates of reaction of these materials are different, depending on whether they are in contact with the liquid or vapor phase. In the present investigation, for example, the products after hydrothermal treatment of oxide mixtures for 6 months exhibited about the same degree of crystal growth and reaction as had corresponding liquid-contact experiments in 1 to 2 weeks. In the experiments from supersaturation, (table 1, B) the products of experiment 1 were the two compounds mentioned above ($4CaO{\cdot}5SiO_2{\cdot}5H_2O$ and $CaO{\cdot}SiO_2{\cdot}H_2O$) and xonotlite, with respect to which the first two are evidently metastable.

The results of the present investigation are in accord with those of Flint, McMurdie, and Wells [2] as regards the silica-rich compounds. These authors found gyrolite at 150° to 400° C and xonotlite from 175° to 390° C, and were unable to prepare okenite in this temperature range.

Several properties of the solid phases of this system used qualitatively in this investigation might, in principle, be used to estimate quantitatively the rate of reaction. These include refractive index, dye absorption. DTA curves, and X-ray patterns of the products before and after DTA heat treatment.

5. Summary

Phase equilibria in the system $CaO{\cdot}SiO_2{\cdot}H_2O$ were investigated at 180° C. Only two stable ternary compounds were found, namely, xonotlite and hillebrandite. Two other stable binary compounds found were α-quartz and $Ca(OH)_2$. The metastable equilibrium curves of gyrolite and of a silica gel was determined approximately. The results suggested several other metastable compounds. Treating oxide mixtures with CaO to SiO_2 ratios of 0.1 to 4.0 with steam for 6 months at 180° C yielded xonotlite and hillebrandite as the only hydrosilicates.

6. References

[1] H. F. W. Taylor and G. E. Bessey, A review of hydrothermal reactions in the system $CaO{\cdot}SiO_2{\cdot}H_2O$, Mag. of Concrete Research **2,** 15 (July 1950).

[2] E. P. Flint, H. F. McMurdie, and L. S. Wells, Formation of hydrated calcium silicates at elevated temperatures and pressures, J. Research NBS **21,** 617 (1938) RP1147.

[3] H. F. McMurdie and E. P. Flint, X-Ray patterns of hydrated calcium silicates, J. Research NBS **31,** 225 (1943) RP1560.

[4] J. D. Bernal and L. Heller, Third International Symposium on the Chemistry of Cement (Cement and Concrete Assoc., London, England, Sept. 1952).

[5] R. B. Peppler and L. S. Wells, The system of lime, alumina, and water from 50° to 250° C, J. Research NBS **52,** 75 (1954) RP2476.

[6] H. H. Steinour, The system $CaO{\cdot}SiO_2{\cdot}H_2O$ and the hydration of the calcium silicates (Bul. 18, Portland Cement Assoc.) Chem. Rev. **40,** 391 (1947).

[7] H. F. W. Taylor, Hydrated calcium silicates, Pt. I, Compound formation at ordinary temperatures, J. Chem. Soc., 3682 (Dec. 1950).

[8] G. L. Kalousek, J. S. Logiudice, and V. H. Dodson, Studies on the lime-rich crystalline solid phases in the system lime-silica water, J. Am. Ceram. Soc. **37,** 7 (Jan. 1954).

[9] V. A. Vigfusson, G. N. Bates, and T. Thorvaldson, Hydrothermal syntheses of calcium hydrosilicates, Can. J. Research **2,** 520 (1934).

[10] G. E. Bessey, The calcium aluminate and silicate hydrates, Proc. Symposium on Chem. of Cements, p. 178 (Stockholm, Sweden, 1938).

[11] S. Nagai, Hydrothermale synthesen von calcium-silikaten, Z. anorg. u. allgem. Chem. **206,** 177 (1932); **207,** 321 (1932).

[12] T. Thorvaldson and G. R. Shelton, Steam curing of portland cement mortars, a new crystalline substance, Can. J. Research **1,** 148 (1929).

[13] L. Heller and H. F. W. Taylor, Hydrated calcium silicates, Pt. IV, Hydrothermal reactions—lime: silica ratio 2:1 and 3:1, J. Chem. Soc., 2535 (1952).

[14] L. Heller and H. F. W. Taylor, Hydrated calcium silicates, Pt. II, Hydrothermal reactions—lime: silica ratio 1:1, J. Chem. Soc., 2397 (Sept. 1951).

WASHINGTON, December 15, 1954.

Journal of Research of the National Bureau of Standards Vol. 54, No. 4, April 1955 Research Paper 2583

An Algorithm for Solving the Transportation Problem[1]

A. Gleyzal[2]

This article describes a new computational scheme for solving the transportation problem (described below) in which combinatorial ideas, rather than the theory of linear inequalities, play the major role. Whether the algorithm is superior to other methods previously employed or proposed must await computational experience, but preliminary inspection is encouraging.

1. Introduction

The transportation problem (stated for integers) is the following: Let C be an $m \times n$ matrix of integers c_{ij}, and let $a_1, \ldots, a_m$, $b_1, \ldots, b_n$ be positive integers such that $a_1 + \ldots + a_m = b_1 + \ldots + b_n$. We are required to find an $m \times n$ matrix $X = (x_{ij})$ such that[3]

(a) x_{ij} is a nonnegative integer,

$$\sum_{j=1}^{n} x_{ij} = a_i \qquad (i = 1, \ldots, m),$$

$$\sum_{i=1}^{m} x_{ij} = b_j \qquad (j = 1, \ldots, n),$$

and the linear form $l_c(x) = \sum_{i,j} c_{ij} x_{ij}$ is a minimum for all matrices satisfying (a) and (b).

Definitions: A matrix X satisfying (a) and (b) is called a *selection*. If X and Y are selections, we say $X(C) \leqq Y(C)$ (read "X is preferable to Y with respect to C") if $l_c(x) \leqq l_c(y)$. If $l_c(x) < l_c(y)$, we say $X(C) \lessdot Y(C)$ ("X is strongly preferable to Y with respect to C"). It is clear that the relation $\leqq$ is transitive. If X is preferable to all selections with respect to C (i. e., X solves the problem), it is said to be *optimal*.

If X is a selection, and i, j are indices such that $x_{ij} \geqq 1$, then c_{ij} is called an *X-selected element* of C. If $r_1, \ldots, r_m$, $s_1, \ldots, s_n$ are integers and $D = (d_{ij}) = (c_{ij} + r_i + s_j)$, then $C \sim D$ ("C and D are equivalent"). It is easy to see that $\sim$ is an equivalence relation. Further, one may prove that if $C \sim D$, then $X(C) \leqq Y(C)$ if and only if $X(D) \leqq Y(D)$, and $X(C) \lessdot Y(C)$ if, and only if, $X(D) \lessdot Y(D)$. Since throughout the computation subsequently described we work only with matrices equivalent to C, we shall henceforth write $X(C) \leqq Y(C)$ as $X \leqq Y$ (similarly, $X \lessdot Y$).

A *closed circuit* is a set of selected elements of the form $c_{i_1 j_1}, c_{i_1 j_2}, c_{i_2 j_2}, c_{i_2 j_3}, \ldots, c_{i_t j_t}, c_{i_t j_1}$, where $i_1, \ldots, i_t$ are distinct indices and $j_1, \ldots, j_t$ are distinct indices.

2. Summary of the Computation

The computation consists of two parts, which are performed alternately until an optimal selection is obtained. It will be seen that the algorithm itself yields the information that the optimal selection has been reached.

As a preliminary, we begin with some selection X. In part I, we find a matrix $D \sim C$ and a selection $Y \leqq X$ such that the Y-selected elements of D are 0. In part II, we discover if Y is optimal, and if not, obtain a selection $Z \lessdot Y$. Putting Z in place of X, we begin again with part I and continue. As there are only a finite number of selections, it is clear from the fact that $Z \lessdot Y \leqq X$, that this process terminates in a finite number of steps, and we thus arrive at an optimal selection.

3. Summary of Part I

With the pair of matrices C, X, we associate a pair of nonnegative integers (c_x, x) defined as follows: c_x is the number of nonzero X-selected elements of C, x is the number of nonzero elements of X.

If $c_x = 0$, we are finished with part I (set $D = C$, $Y = X$). If not, we construct, starting with a nonzero X-selected element of C a "tree I", which we discover to be either in case IA or case IB. If in case IA, we find a matrix C' such that $C' \sim C$ and the number of nonzero X-selected elements of C' is less than c_x. If in case IB, we find a selection X' preferable to X such that the set of nonzero elements of X' is a *proper* subset of the set of nonzero elements of X. Thus, after completing IA or IB, we have a matrix $C' \sim C$ and a selection $X' \leqq X$ such that

$$c_{x'} \leqq c_x, \quad x' \leqq x, \tag{1}$$

[1] A code of this method in the case of the "personnel problem," using an 8×8 matrix, has recently been composed for SWAC (National Bureau of Standards, Western Automatic Computer). For a variant of the method in this case, which is also applicable to matrices consisting of nonintegers, see Theodore S. Motzkin, The assignment problem (Proceedings of the American Mathematical Society Sixth Symposium for Applied Mathematics, 1954).

[2] Present address: Naval Ordnance Laboratory, White Oak, Silver Spring, Md.

[3] Other references to this problem and references to further literature are given by: George B. Dantzig, Maximimization of a linear function of variables subject to linear inequalities (Simplex Method), chapter XXI, and Application of the Simplex Method to a transportation problem, chapter XXIII, both included in Activity analysis of production and allocation, edited by T. C. Koopmans (John Wiley & Sons, Inc., New York, N. Y., 1951); Merrill M. Flood, On the Hitchcock distribution problem, Pacific J. Math. 3, 369-386 (1953).

and strict inequality holds in at least one of the two.

If $c'_{x'}>0$, we begin again, obtaining C'', X'', and so on. By virtue of (1), this cannot continue indefinitely. But we cannot have $x^{(n)}=0$, for this is inconsistent with (b); therefore, for some n, $c_{x^{(n)}}=0$. Hence, the desired result of part I is achieved.

4. Summary of Part II

In part II, we begin with a pair of matrices D, Y such that $d_{ij}=0$. Let e_D be the minimum of all elements of D that are *not* Y-selected. Let f_D be the number of elements of D equal to e_D.

If $e_D \geqq 0$, then, clearly, Y is optimal. Assume the contrary, therefore. Starting with an element $d_{i_1 j_1}$ of D such that $d_{i_1 j_1}=e_D$, we construct a "tree II." We examine this tree and discover whether we are in case IIA or case IIB. If in case IIA, we construct a matrix $D' \sim D$ such that the Y-selected elements of D' are 0, $e_{D'}>e_D$ (and the behavior of f_D is unspecified), or

$$e_{D'}=e_D, \qquad f_{D'}<f_D, \tag{2}$$

and we put D' in place of D and begin again with part II. It is obvious from (2) that we cannot continue to be in case IIA indefinitely, for eventually we would obtain $e_{D^{(\infty)}} \geqq 0$, which implies that Y is optimal. Therefore, if Y is not optimal, we must at some stage enter case IIB. If in case IIB, we find a selection $Z \lessdot Y$, and go back to part I, with any matrix equivalent to C (C itself, if convenient) replacing C, and Z replacing X.

5. Detail of Part I

Assume $c_{i_0 j_0}$ is an X-selected element of C that is not zero. We define, inductively, the following "family tree I":

1. The "founder" is $c_{i_0 j_0}$ ("first generation").

2. Assume now that we have defined the kth generation, for $k=1, \ldots, s$. We now define the $(s+1)$th generation; i. e., the union, over all members of the sth generation of the "children" of each member of the sth generation. The "children" of such a member are: if s is odd, all *other* X-selected elements in the same row of C as the given member; if s is even, all *other* X-selected elements in the same column of C as the given member. If the $(s+1)$th generation is vacuous, the tree terminates with the sth generation, and we say we are in case IA; if the $(s+1)$th generation contains at least one member of a previous generation (possibly the sth) the tree terminates with the $(s+1)$th generation, and we say we are in case IB. If the tree does not terminate, we continue. The tree must terminate, of course, after a finite number of generations.

Case IA: In this case, we shall show how to construct numbers $r_1, \ldots, r_m$, $s_1, \ldots, s_n$ such that $C'=(c'_{ij})=(c_{ij}+r_i+s_j) \sim C$, and $c'_z<c_z$ (indeed, all the elements of C' corresponding to the elements of the tree will be zero).

Associated with each element of the tree, define inductively the following numbers $N(t)$:

$$N(c_{i_0 j_0})=-c_{i_0 j_0}.$$

If p is the parent of t, define

$$N(t)=-t-N(p).$$

We note that because we are in IA, rather than IB, every element has a unique parent. Now, let α be any row index of some element $c_{\alpha\beta}$ of an odd generation: for each such α, define $r_\alpha=N(c_{\alpha\beta})$. Observe that because we are in case IA, this definition is unambiguous. For suppose $c_{\alpha\beta_1}$ and $c_{\alpha\beta_2}$ were two elements of row α, each occurring in an odd generation, then it follows from the definition of the tree that since $c_{\alpha\beta_1}$ occurs in an odd generation, $c_{\alpha\beta_2}$ is its child. Similarly, $c_{\alpha\beta_1}$ is the child of $c_{\alpha\beta_2}$. This would mean that we were in case IB.

For every index $i=1, \ldots, m$, which is not a row index of an element of an odd generation, define $r_i=0$. Similarly, let β be any column index appearing in some element $c_{\alpha\beta}$ of an even generation: for each such β, define $s_\beta=N(c_{\alpha\beta})$. For each index $j=1, \ldots, n$, which is not a column index of an element of an even generation, define $s_j=0$.

It is now easily seen that C' has the desired property.

Case IB: In this case, we shall show how to find a selection $X' \leqq X$ such that $x'<x$. We first show how to find among the members of the tree a closed circuit. Let k be defined by the statement that the $(k+1)$th generation is the first one that contains an element e of the rth generation, where $r<k+1$, and let e_k be a member of the kth generation whose child is e_r. (Although the knowledge is not necessary for the subsequent argument, it is convenient to note that $k+1>3$.) In other words, it is at the $(k+1)$th generation that we discover that we are in case IB. Hence each member of generations k, $k-1$, $\ldots$, 2 has a unique parent in the preceding generation, for if a member of the tree has two parents in the preceding generation, then all three members are in the same row or column, one of the parents would be a child of the other parent, and we would have arrived at case IB earlier.

Now let e_{k-1} be the unique parent in the $(k-1)$th generation of e_k, e_{k-2} be the unique parent in the $(k-2)$th generation of e_{k-1}, etc. There are two possibilities: either (a) e_r is an ancestor of e_k, or (b) e_r is not an ancestor of e_k. If (a) holds, then clearly $e_k, e_{k-1}, e_{k-2}, \ldots, e_{r+1}, e_r$ is a closed circuit. If (b) holds, let s be defined by the statement that the sth generation is the last generation that contains a common ancestor e_s of both e_k and e_r. Let e'_{r-1} be the parent of e_r in the $(r-1)$th generation, e'_{r-2} the parent of e'_{r-1}, and so on until we reach e_s. From this "line of descent" $e_r, e'_{r-1}, e'_{r-2}, \ldots, e'_{s+1}, e_s$ and the previous $e_k, e_{k-1}, e_{k-2}, \ldots, e_{s+1}, e_s$, noting that

e'_{s+1}, e_s, e_{s+1} are in the same row or column, it is easy to see that

$$e_k, e_{k-1}, e_{k-2}, \ldots, e_{s+1}, e'_{s+1}, \ldots, e'_{r-2}, e'_{r-1}, e_r$$

is a closed circuit. For the definition of k implies that the same row or column index occurs only in consecutive elements of this cycle, and if we consider these elements as arranged in a cyclic order, the construction of the tree and definition of k imply that the same row or column index occurs only in consecutive elements.

Let us denote this closed circuit by

$$c_{i_1 j_1}, c_{i_1 j_2}, \ldots, c_{i_t j_1},$$

as explained in the introductory definitions.

Let

$$\Sigma_1 = c_{i_1 j_1} + c_{i_2 j_2} + \ldots + c_{i_t j_t},$$

$$\Sigma_2 = c_{i_1 j_2} + c_{i_2 j_3} + \ldots + c_{i_t j_1}.$$

Either $\Sigma_1 \leqq \Sigma_2$ or $\Sigma_1 > \Sigma_2$. Assume the former, and let $x_2 = \min(x_{i_1 j_2}, \ldots, x_{i_t j_1})$.

Consider the new selection X'

$$x'_{i_1 j_1} = x_{i_1 j_1} + x_2, \ldots, x'_{i_t j_t} = x_{i_t j_t} + x_2,$$

$$x'_{i_1 j_2} = x_{i_1 j_2} - x_2, \ldots, x'_{i_t j_1} = x_{i_t j_1} - x_2.$$

For all other pairs of indices i, j, $x'_{ij} = x_{ij}$.

It is easy to verify that X' is a selection (i. e., satisfies (a) and (b), that $X' \leqq X$, and $x' < x$.

If $\Sigma_1 > \Sigma_2$, let $x_1 = \min(x_{i_1 j_1}, \ldots, x_{i_t j_t})$. Consider the new selection X'.

$$X'_{i_1 j_1} = x_{i_1 j_1} - x_1, \ldots, x'_{i_t j_t} = x_{i_t j_t} - x_1$$

$$X'_{i_1 j_2} = x_{i_1 j_2} + x_1, \ldots, x'_{i_t j_1} = x_{i_t j_1} + x_1.$$

For all other pairs of indices i, j, $x'_{ij} = x_{ij}$. Then it is easy to verify that X' is a selection, $X' \leqq X$, $x' < x$. This completes the discussion of part I.

6. Detail of Part II

Assume $d_{i_1 j_1}$ is an element of D that is *not* Y-selected, and such that $0 > d_{i_1 j_1} = e_D =$ minimum of all elements of D not selected by Y. We construct inductively, the following "family tree II".

1. The founder is $d_{i_1 j_1}$.

2. Assume now that we have defined the kth generation, for $k = 1, \ldots, s$. We now define the $(s+1)$th generation, the union, over all members of the sth generation of the children of each member of the sth generation. These are the children: If s is odd, $s > 1$ and there exists a Y-selected element of D whose column index is j_1, then this element is its child, the tree terminates, and we say we are in case IIB. If no such element exists or if $s = 1$, then the children consist of all Y-selected elements in the same row as the parent member, omitting, however, those whose column index is the same as that of a member of generations $1, \ldots, s$. If s is even, the children of a member are all nonpositive elements of D in the same column as the member, omitting, however, those whose row index is the same as that of a member of generations of $1, \ldots, s$.

Eventually, the tree must terminate, and if it does not terminate in case IIB, we say we are in case IIA.

Case IIA: In this case, we shall show how to construct numbers $r_1, \ldots, r_m, s_1, \ldots, s_n$ such that $D' = (d'_{ij}) = (d_{ij} + r_i + s_j) \sim D$, and D' has the properties (2).

Let α be any row index appearing in some number $d_{\alpha\beta}$ of an odd generation. For all such α, define $r_\alpha = +1$. For any index $i = 1, \ldots, m$ not included in $[\alpha]$, define $r_i = 0$. Similarly, let β be any column index appearing on some member $d_{\alpha\beta}$ of an even generation. For all such β, define $s_\beta = -1$. For any index $j = 1, \ldots, n$ not included in $\{\beta\}$, define $s_j = 0$.

We now show that D' has the properties (2). First, the Y-selected elements of D' are 0: For if d_{ij} is such an element, and if i resp. j appears as a row resp. column index of a member of an odd resp. even generation, then j resp. i appears as a column resp. row index of a member of an even resp. odd generation; hence, $r_i + s_j = 0$. Second, if $d_{ij} < 0$ and $s_j = -1$, then by our construction $r_i = 1$; hence the minimum of the elements of D' is not less than the minimum of the elements of D. In addition, because we are in case IIA, $d'_{i_1 j_1} = d_{i_1 j_1} + 1 > e_D$. These two statements imply the remainder of (2).

Case IIB: Because we are in case IIB, it is clear how to find a closed circuit in the tree containing $d_{i_1 j_1}$. Let us denote this circuit by

$$d_{i_1 j_1}, \ldots, d_{i_t j_1}.$$

Then $d_{i_1 j_2}, d_{i_2 j_3}, \ldots, d_{i_t j_1}$ are Y-selected elements of D. Consider the new selection Z:

$$Z_{i_1 j_1} = y_{i_1 j_1} + 1, \ldots, z_{i_t j_t} = y_{i_t j_t} + 1,$$

$$Z_{i_1 j_2} = y_{i_1 j_2} - 1, \ldots, z_{i_t j_1} = y_{i_t j_1} - 1.$$

For all other pairs of indices i, j, define $z_{ij} = y_{ij}$.

Then it is easy to verify that Z is a selection. Further, because all elements of the circuit are nonpositive, $d_{i_1 j_2} = \ldots = d_{i_t j_1} = 0$, and $d_{i_1 j_1} < 0$, it follows that $Z \leqq X$.

7. An Example

Consider the transportation problem with

$$C = \begin{pmatrix} 2595 \\ 8358 \\ 7314 \\ 5972 \end{pmatrix},$$

and $a_t = (3,2,3,3)$, $b_j = (3,5,2,1)$. For purposes of

illustration, we assume an initial selection matrix,

$$X=\begin{pmatrix}2100\\0020\\0300\\1101\end{pmatrix}.$$

It is convenient to indicate the selection by dots placed above the elements of the matrix C, as follows,

$$\begin{pmatrix}\ddot{2} & \dot{5} & 9 & 5\\ 8 & 3 & \ddot{5} & 8\\ 7 & \dddot{3} & 1 & 4\\ \dot{5} & \dot{9} & 7 & \dot{2}\end{pmatrix}$$

The steps in the solution and the operations associated with cases IA, IB, IIA, and IIB will be clear from the following: [4]

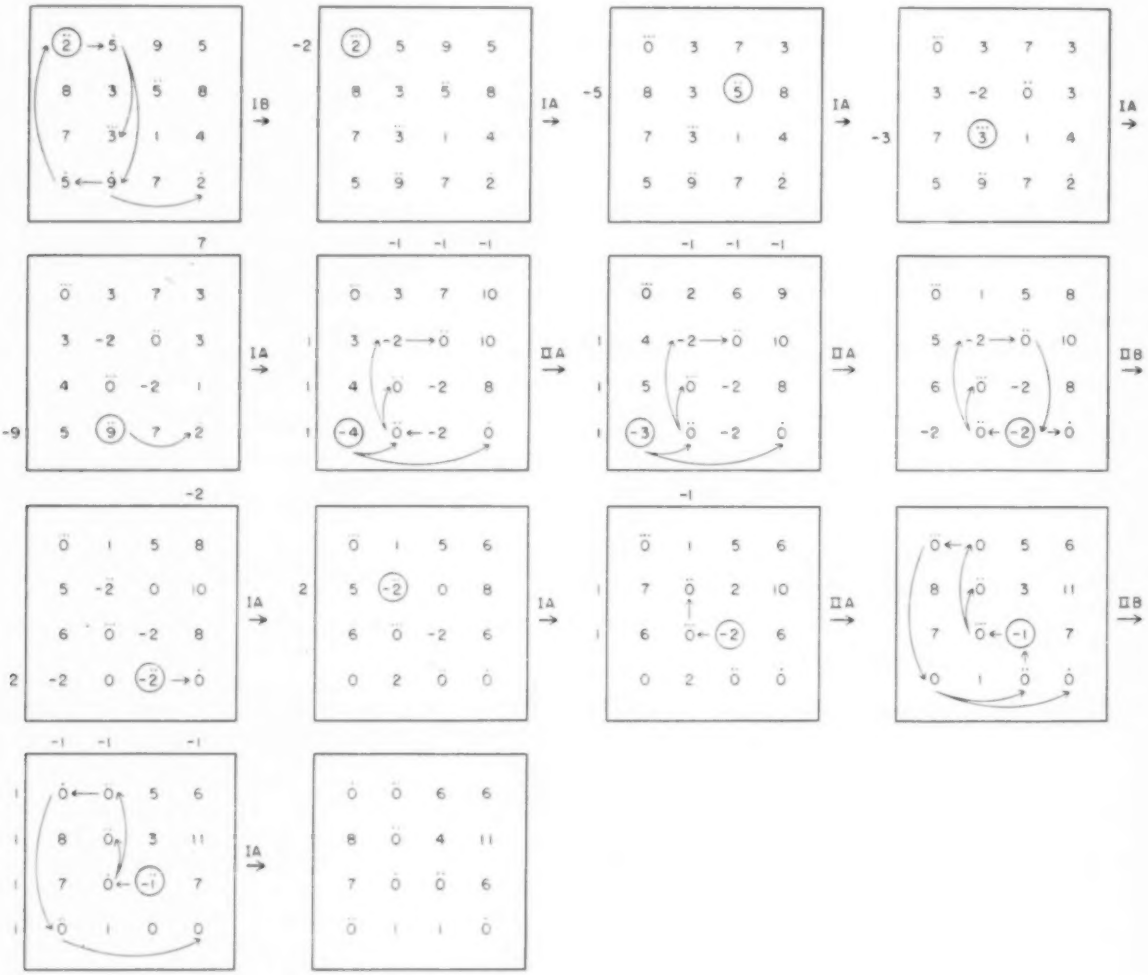

The last matrix is a solution. No closed circuit of zeros exists. Hence the solution is unique. For purposes of illustration, we have followed the method explicitly. If one permits some flexibility in choosing the sequence of operations, much faster convergence may be obtained.

The author expresses his gratitude to Alan J. Hoffman to whom he is indebted for transforming the method and proof into the algebraic form given here.

[4] Numbers on borders at matrices are quantities added to the indicated row or column. Circles drawn about an element indicate the first element of the tree.

WASHINGTON, April 23, 1954.

Journal of Research of the National Bureau of Standards Vol. 54, No. 4, April 1955 Research Paper 2584

An X-Ray Study of the System Uranium Monocarbide-Uranium Dicarbide-Beryllium Carbide

M. D. Burdick, H. S. Parker, R. S. Roth, and E. L. McGandy

Mixed carbide preparations within the system uranium monocarbide-uranium dicarbide-beryllium carbide were investigated after heating and quenching. X-ray diffraction methods were used to identify the phases found and to determine the degree of interaction. Carbide alloys were studied after treatments at 1,700° and 1,900° C, and a constitutional diagram for the 1,700° C level is presented. No ternary compounds were identified within the system. The limit of solubility of beryllium carbide in uranium monocarbide at 1,700° and 1,900° C was found to be 20 mole percent and 40 mole percent, respectively. Lattice parameters based on X-ray patterns in the back-reflection region failed to indicate any other interactions, but evidence is presented to indicate some solid solution among the uranium carbides without lattice parameter change. The room-temperature stability of uranium sesquicarbide (U_2C_3), which has been reported by other investigators, was verified. X-ray diffraction data were obtained for this cubic compound, using CuK_α radiation.

1. Introduction

Uranium, as a metal and in the form of various compounds, is the usual source of energy in nuclear reactors. As a moderator and structural material for piles operating at temperatures above the useful range for metals, some form of beryllium is among the foremost of the ceramic materials considered because of favorable cross-sectional properties and high thermal conductivity. For applications other than reactors, the carbides of these elements have been investigated and have been found to be suitable for special high-temperature applications, for example, crucibles.

An uranium carbide, later shown to have been UC_2, was prepared by Moissan [1] [1] in 1896. Other workers [2, 3, 4, 5, 6, 7, 8, 9, 10, 11] established the structure and determined some of the properties of the three uranium carbides, UC, U_2C_3, and UC_2. Beryllium carbide, discovered in 1895 by Lebeau [12], remained almost a laboratory oddity until recently. Stackelberg and Quatrum [13] in 1934 published the crystallographic structure of Be_2C, and Kielland and Tronstad [14] found it served a useful purpose as an intermediate product in the production of beryllium chloride. Beryllium carbide was little used as a refractory because other materials were available, which were more stable with respect to air and moisture and were less toxic.

In nuclear reactors, temperatures must be maintained at the highest possible levels for good efficiency. The materials used in the construction of reactors must, therefore, be stable at the temperatures involved, and, in addition, must be compatible with each other. The favorable nuclear properties of the uranium carbides and beryllium carbide made desirable an investigation of combinations of these materials. The present study was undertaken to determine the constitution of alloys resulting from solid-state reaction within the system UC-UC_2-Be_2C.

[1] Figures in brackets indicate the literature references at the end of this paper.

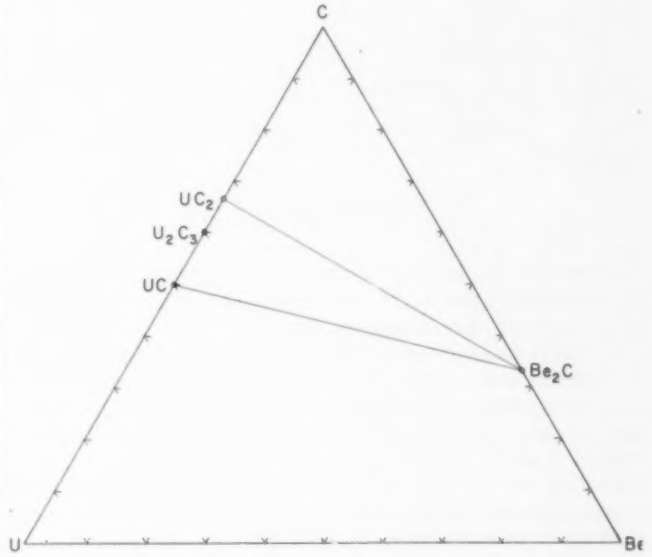

FIGURE 1. *Relation of the end members of the system* UC-UC_2-Be_2C *to that of the constituent elements, in mole percent.*

Figure 1 shows the relation of the end members of this system to that of the constituent elements (U, Be, and C).

2. Materials

The uranium-carbon alloys used in this study were supplied by Battelle Memorial Institute. They were prepared by melting the materials in an induction furnace and remelting in argon in an arc furnace. The uncombined carbon of the arc-melted alloys was usually not over 0.03 percent by weight. The chemical compositions of the starting materials are given in table 1. The uranium-carbon alloys, designated by A following the alloy number in table 1, were made available for this study by M. W. Mallett et al. [9,11] after the completion of work

TABLE 1. *Chemical composition of materials*

Material	Chemical composition (percentage by weight)[a]						
	U [b]	C	Free C	BeO	N_2	H_2O	Be
	%	%	%	%	%	%	%
Alloy 361	95.28	4.72	.....	.....	.....	.....	.....
Alloy 369	88.3	11.7	.....	.....	.....	.....	.....
Alloy 137A	95.6	4.4	.....	.....	.....	.....	.....
Alloy 112A	93.68	6.32	.....	.....	.....	.....	.....
Alloy 66A	93.07	6.93	.....	.....	.....	.....	.....
Alloy 81A	92.5	7.5	.....	.....	.....	.....	.....
Alloy 100A	91.0	9.0	.....	.....	.....	.....	.....
Be_2C	.....	[c]39.35	0.67	0.61	0.01	0.14	59.22

[a] The uranium-carbon alloys were supplied and analyzed by Batelle Memorial Institute. The beryllium carbide was supplied and analyzed by Brush Beryllium Co.
[b] Uranium by difference.
[c] Carbon by difference.

on the uranium-carbon system. Alloys 361 and 369 were freshly prepared for this study, after it was found that the older alloys had "aged" and no longer gave reproducible results. The data in this report were obtained on mixtures of alloys 361, 369, and beryllium carbide.

The beryllium carbide was of 98.3-percent purity, which was the highest quality available at the time of its purchase. The impurities were beryllia (BeO), carbon, beryllium nitride (Be_3N_2), and moisture.

3. Equipment

Figure 2 shows the inductively heated quenching furnace used for all heat treatments in this study. The base of the furnace consists of a 12-in. cube made of ¼-in. steel plate with all-welded construction. A fused-silica tube, with a 5-in. inside diameter, is set in a groove in the top of the base, and a vacuum-tight seal is obtained by means of a neoprene "O" gasket and a clamping ring. The furnace head is attached to the top of the silica tube by means of a similar arrangement and is water-cooled. An induction coil, consisting of eight turns, is placed concentric with and midway along the silica tube.

The prism and window on the furnace head provide a means for temperature measurement and observation of specimens with an optical pyrometer mounted in a horizontal position. A neoprene "O" gasket forms a vacuum-tight seal between the tempered glass window and the furnace head. The optical pyrometer was calibrated with the window and prism in the line of sight by the Temperature Measurement Section of the National Bureau of Standards. A Kovar insulated terminal is soldered in place through the head to act as a fuse-wire support and electrode for the quenching current. The head itself serves as the other electrode.

The susceptor and other structural parts of the furnace were machined from suitable carbon shapes. The susceptor assembly is mounted concentric with the silica tube at its midpoint, and the assembly is supported by a carbon pipe 1½-in. outside diameter by 1-in. inside diameter, which extends to a hole in the top of the furnace base. The pipe also

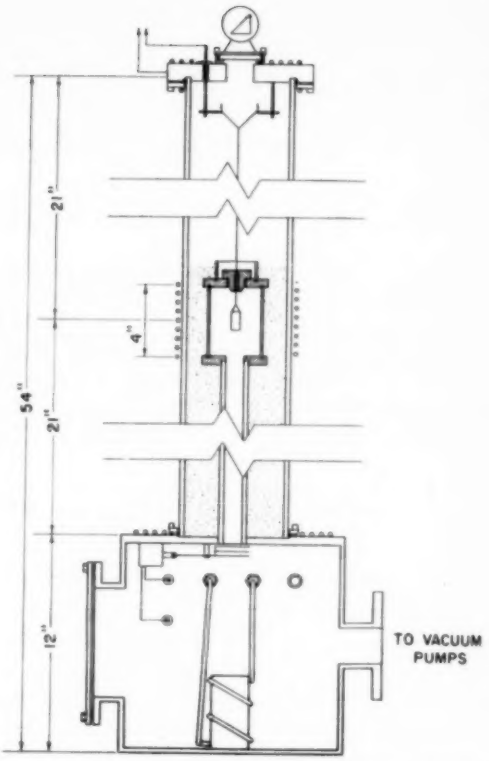

FIGURE 2. *Schematic drawing of an inductively heated furnace used for heating and quenching carbide alloys in controlled atmospheres.*

serves as a guide to direct the specimen to the quench cup and to retain the thermal insulation. The entire space above the furnace base around the pipe and susceptor assembly is solidly packed with carbon-black insulation to approximately ¼ in. below the upper rim of the stack on top of the susceptor assembly. Twelve to 14 deep holes, formed in the carbon black with a ⅛-in. rod, aid in the escape of adsorbed gases during evacuation and heating.

Within the furnace base, a solenoid-operated shutter assembly serves as a radiation sbield under the lower end of the carbon pipe. Electricity is brought into the base by means of two Kovar insulated terminals soldered through the side wall. The cup, containing about 750 ml of a quenching oil, is a thin-walled brass tube closed at the lower end. Because of the small heat capacity of the cup and the necessity for as rapid cooling as possible, a water-cooling jacket of ¼-in. copper tubing was placed around the cup. The water inlet and outlet, as well as the atmosphere inlet, consists of ¼-in. pipe nipples welded through the sidewall of the furnace base. Access to the interior of the furnace base is obtained by a 6-in. pipe flange welded to one side of the base. The flange is provided with a cover plate and rubber gasket. A standard 2-in. pipe flange welded to the opposite side of the furnace base permits connection to the vacuum system.

Specimen holders used with the furnace consist of two general types: (1) refractory metal holders sus-

pended from the furnace head, when specimens are to be quenched, and (2) carbon or graphite crucibles, when specimens are to be cooled in the furnace. When specimens are to be quenched, the sample cup consists of a hollow cylinder, ⅝-in. in diameter and 1 in. tall, with a removable bottom. The entire assembly is shaped from 0.010-in. molybdenum. A bail of 0.025-in. molybdenum wire is provided. The cylinder containing the specimen is suspended from a 0.010-in. molybdenum wire attached to a platinum fuse wire strung between two supports on the furnace head. The molybdenum support wire extends through the 3/16-in. sight hole in the susceptor cover plug. In cases where it is not necessary to quench the specimen, and a refractory metal holder is desired, the platinum fuse wire and the 0.010-in. molybdenum support wire are replaced with a 0.040-in. molybdenum wire. The second type of specimen holder used in the furnace is fabricated from graphite or carbon rods. This holder is a hollow cylindrical crucible with an external flange to support it from the susceptor cover to allow the main body of the crucible to extend well into the hot zone of the furnace.

Before heating any specimens in the furnace, the parts were outgassed by heating the furnace to 2,000° to 2,100° C in vacuum. When not in use, the furnace was continuously pumped by a small auxiliary mechanical pump to maintain a pressure of approximately 50 μ of mercury in the chamber at all times. If, however, the furnace was not to be used for an extended period, it was evacuated and filled with helium or argon. If the furnace had been maintained under reduced pressure, either during a heating period or during an idle period, it was always filled with helium or argon before exposing the interior to the air. This procedure minimized the adsorption of air on the carbon susceptor and on the carbon-black insulation. A motor-generator, rated at 75 kw at 9,600 cps, supplied power to the furnace. About 10 to 12 min. were required to reach a temperature of 1,900° C, and about 3 kw were required to maintain the temperature at that level. The specimen temperature was easily controlled to within ±5 deg C by making small manual adjustments of the field excitation of the generator.

X-ray diffraction patterns were obtained with a high-angle goniometer spectrometer, using Cu K_α radiation. The diffracted X-ray intensities were recorded on a strip chart on which 1 in. was equivalent to 1 deg 2Θ.

4. Methods

4.1. Preparation and Treatment of Alloys

The starting materials from which the preparations were compounded (see table 1) were obtained in two conditions. The uranium-carbon alloys were received in ingot form. The ingots were coarsely crushed in a "diamond" mortar, and were further reduced in a boron carbide mortar to pass a No. 325 U. S. Standard Sieve. These operations were performed in a dry box in an atmosphere of carbon dioxide. The beryllium carbide was obtained in powdered form that passed a No. 325 U. S. Standard Sieve.

Five-gram batches of the appropriate amounts of the various starting materials were weighed on an analytical balance. The powdered materials were blended by grinding together in a boron carbide mortar, within a dry box, prior to pressing. Specimens for solid-state reaction were pressed in hardened steel molds into pellet form, usually ⅜-in. diameter and approximately ⅜ to ½ in. high. The specimens were placed in graphite cups within the molybdenum cup, so that contamination due to heating in contact with molybdenum was avoided. After the furnace was assembled, with specimens in place, the chamber was "pumped down" to a pressure of 1 μ of mercury and then filled with argon. The pumping and refilling with argon was repeated once before heating was started. After a 2-hr heat treatment at the elevated temperature (either 1,700° or 1,900° C), the specimen assembly was cooled rapidly by dropping it into the cold oil. The quenching oil was removed from the specimens by soaking them overnight in carbon tetrachloride. The cleaned, dry pellets were crushed and ground in a boron carbide mortar within the dry box, to pass a No. 200 U. S. Standard Sieve. The fine powders were stored in a desiccator, usually not longer than 3 days, before they were subjected to X-ray analysis.

The results obtained for the constitution of mixed carbides within the system UC-UC_2-Be_2C, after the treatment described above, are based on room-temperature X-ray analyses of the quenched crystalline phases and on the lattice parameters.

A uniform period of 2 hr at the elevated temperature was selected, based on a series of experiments on alloy preparations involving solid-state reactions between mixtures of UC and Be_2C. The degree of reaction, as indicated by the unit-cell size of the resulting solid solutions, was evaluated after total reaction times of 2, 4, and 6 hr, with grinding and repressing between heat treatments. It is reasonable to assume that a 6-hr total reaction time with intermediate grinding and repressing at 2-hr intervals is more conducive to the attainment of equilibrium than is a single 6-hr treatment. No significant differences in lattice parameters of the UC solid solutions were observed between the alloys heated for 2, 4, or 6 hr. The shortest of these reaction periods was selected for convenience and to minimize compositional changes, such as carbon "pickup" and beryllium loss due to dissociation of the beryllium carbide.

4.2. X-Ray Methods

The lattice parameters for cubic compounds and solid solutions were evaluated by taking the average of the values obtained from the last five diffraction peaks in the back-reflection region of the X-ray pattern. The parameters of the tetragonal UC_2 compound and solid solutions were evaluated by taking the average of the values obtained from those

reflections that had the greatest contribution to the desired parameter. The "a" parameter was found by taking the average of the values obtained from the ($hk0$) reflections (200), (220), (310), (400), and (330), and the "c" parameter was found by appropriate calculations, using the formula

$$\frac{l^2}{c^2}=\frac{1}{d^2}-\frac{h^2+k^2}{a^2}$$

for the diffraction reflections (103), (004), (114), (204), (105), (215), (116), (206), (305), and (107).

4.3. Chemical Methods and Precision

Early in the investigation, it was believed that chemical analysis of the alloys after heat treatment would prove of value in interpreting the results of the X-ray analyses and in more accurately locating the phase boundaries that exist in the system UC-UC_2-Be_2C. The varying degrees of instability of the uranium-carbon alloys and of beryllium carbide, with respect to air and moisture, made it desirable to analyze preparations as soon as possible after heat treatment. Unfortunately, analytical procedures for the separation and analysis of uranium, beryllium, and carbon, in the form of mixed carbides, were not available. It was necessary to develop new techniques and adapt other techniques for use in this study.

The methods that are described for the separation and analysis of uranium, beryllium, and carbon are not intended to represent a completely developed, standard method of analysis, but are presented as a guide to other workers.

Some of the powdered, quenched preparations that were analyzed by X-ray methods were analyzed chemically for uranium, beryllium, iron, and carbon as follows:

a. Uranium

Duplicate samples of approximately 0.50 g were weighed into 125-ml Erlenmeyer flasks. Nitric and perchloric acids were added, and the sample was digested for 2 hr on a hot plate. When solution of the sample was complete, a second portion of nitric acid was added.

The solution was then transferred to a special continuous extractor, similar in design to the one described by Rodden and Warf [15], except that a Friedrichs condenser was used without an extension tube. The solution was extracted for 1½ hr with diethyl ether, at the end of which time the uranium had been quantitatively transferred to the boiler flask. The aqueous layer remaining in the extractor tube contained ammonium nitrate, beryllium, and any iron that might have been present as an impurity.

After evaporation of the ether, the uranium extract was fumed with sulfuric acid to remove any organic matter. The solution was then diluted, and the uranium was precipitated as ammonium diuranate with carbonate-free ammonium hydroxide solution. The precipitate was filtered on Whatman No. 42 filter paper, drained, and ignited in a platinum crucible at 1,000° C for 1 hr. The ignited precipitate was cooled and weighed as U_3O_8.

b. Beryllium

The aqueous layer remaining after the extraction was transferred to a beaker, evaporated to dryness, and the ammonium nitrate volatilized by the method of J. Lawrence Smith [16]. Beryllium was determined by one of two methods. If more than 2 percent by weight was indicated by the nominal composition of the sample, a gravimetric method was used, but if less was indicated, a fluorimetric method was used.

For the gravimetric determination of beryllium, the solution remaining after the ammonium nitrate volatilization was diluted, and the beryllium was precipitated with ammonium hydroxide as the hydrous oxide. The precipitate was filtered on a Whatman No. 41H filter paper, drained, and ignited in a platinum crucible at 1,000° C for 1 hr. The ignited precipitate was cooled and weighed as BeO.

For the fluorimetric determination of beryllium, the solution from the ammonium nitrate volatilization was diluted in a volumetric flask, and suitable aliquots were transferred to 50-ml volumetric flasks. These aliquots were treated according to the method of Fletcher, White, and Sheftel [17], and the fluorescence of the resulting solutions was compared with that of fluorescent uranium glass standards in a photoelectric fluorimeter designed and built at the Bureau by E. L. McGandy.

c. Iron

Iron was present in small quantities in all the alloys tested. No sample was found that contained more than 0.35 nor less than 0.10 percent of iron. Approximately, one in every three samples was tested for iron. For this determination, an aliquot was removed from the solution after ammonium nitrate volatilization and transferred to a 25-ml volumetric flask. This was treated according to a standard method described by Sandell [18], using orthophenanthroline as a colorimetric reagent. The optical density of the resulting solution was compared with that of standard solutions in a Beckman model B spectrophotometer.

d. Carbon

The carbon content of samples containing no beryllium was determined by ignition in porcelain boats in an oxygen train at 1,000° C. It was found, however, that this temperature was too low to completely decompose the samples containing beryllium carbide. Samples containing beryllium carbide were decomposed at higher temperatures, obtained in a modified inductively-heated combustion furnace, with the aid of a special flux containing copper as a combustion catalyst. In the determination of small amounts of carbon in beryllium metal, J. J. Tregonning [19] described the use of copper as a combustion catalyst.

A special flux, consisting of 0.80 g of open-hearth iron (NBS Standard Sample 55) and 0.90 g of powdered copper, was added to a combustion crucible. About 0.20 g of the carbide was then accurately weighed in the crucible, and the mixture was blended, placed in the inductively heated combustion furnace, and burned in a stream of purified oxygen. The carbon dioxide formed was absorbed in ascarite contained in a Nesbitt bulb.

Because the samples could not be dried at 110° C without some oxidation taking place, several of them were checked for moisture content by a special procedure. For this purpose, a crucible, 15 mm in diameter, 15 mm high, and having a 2-mm wall thickness, was machined from graphite. About 0.20 g of sample was weighed accurately into the crucible, and placed in the inductively heated combustion furnace. The sample was heated at approximately 1,200° C in a stream of dried helium, and the evolved moisture was absorbed in magnesium perchlorate contained in a Nesbitt bulb.

The standard deviation of an individual analysis, as well as the estimated precision that might be obtained when 2 or 3 determinations are made, is given in table 2. These data were derived from the uranium, beryllium, and carbon analyses made of the mixed carbide alloys. The lack of standard samples of these mixed carbides and the time limitation imposed by the expiration of the investigation prevented the accumulation of sufficient data to justify any definite statements concerning the accuracy of the analytical methods.

The results of analyses of various preparations in the system UC-UC_2-Be_2C are given in table 3. The data were selected as being typical of the results obtained, as well as indicating the compositional range over which the various elements occurred in the alloys. The nominal composition was included in the table to show that the analyzed compositions were in reasonably good agreement with the intended compositions. The uranium and beryllium percentages are the average of duplicate determinations, and the carbon values represent the average of three determinations. The sum of the percentages of the constituent elements found is less than 100 percent in every case. The departure from 100 percent is found, in general, to increase with increasing amounts of beryllium carbide in the alloy. In most instances smaller departures from 100 percent were found for the alloys heat-treated at 1,900° C than for the alloys heat-treated at 1,700° C. The results have been corrected for the small amount (less than 2% by weight) of moisture found and are expressed on the basis of the dry material. The

TABLE 2. *Estimated standard deviation and precision of analytical methods*

Element	Compositional range (% by weight)	Method of analysis	Degrees of freedom on which standard deviation is based [a]	Estimated standard deviation of an individual analysis [b]	Estimated standard deviation of average [c] for—	
					$n=2$	$n=3$
U	55 to 95	Gravimetric	53	0.34	0.24	0.20
Be	0 to 2	Fluorimetric	22	.036	.025	.021
Be	2 to 12	Gravimetric	34	.21	.15	.12
C	4 to 12	Combustion	146	.088	.062	.051

[a] See [21] for definition of statistical terms and description of methods.

[b] Standard deviation of an individual analysis = $\sqrt{(\text{sum of squares})/(\text{degrees of freedom})}$.

[c] Standard deviation of average = (standard deviation of individual analysis)/$\sqrt{(\text{number of determinations})}$.

TABLE 3. *Typical analyses of alloys within the system* UC-UC_2-Be_2C

Alloy	Temperature of heat treatment	Nominal composition						Analyzed composition [a] (percentage by weight)			
		Mole percent			Percentage by weight						
		UC	UC_2	Be_2C	U	Be	C	U	Be [b]	C	Total
	°C										
85	1,700	92	8	------	94.83	------	5.17	93.4	------	4.85	98.2
85	1,900	92	8	------	94.83	------	5.17	93.9	------	5.18	99.1
187	1,700	80	20	------	94.29	------	5.71	93.8	------	5.64	99.4
187	1,900	80	20	------	94.29	------	5.71	93.8	------	5.52	99.3
150	1,700	21.7	78.3	------	91.17	------	8.83	91.7	------	7.90	99.6
150	1,900	21.7	78.3	------	91.17	------	8.83	91.2	------	7.99	99.2
101	1,700	10	90	------	91.25	------	8.75	89.6	------	8.37	98.0
101	1,900	10	90	------	91.25	------	8.75	91.0	------	8.50	99.5
118	1,700	65	25	10	92.72	0.78	5.97	92.2	0.84	6.37	99.4
118	1,900	65	25	10	92.72	.78	5.97	91.4	.64	6.33	98.4
181	1,700	35	55	10	91.30	.77	7.93	90.1	.59	8.00	98.7
181	1,900	35	55	10	91.30	.77	7.93	90.6	.64	8.10	99.3
91	1,700	50	10	40	87.49	4.42	8.09	83.6	4.44	7.61	95.6
91	1,900	50	10	40	87.49	4.42	8.09	85.6	4.41	8.09	98.1
92	1,700	45	15	40	87.17	4.40	8.43	83.6	3.97	7.11	94.7
92	1,900	45	15	40	87.17	4.40	8.43	85.9	3.99	8.61	98.5
93	1,700	40	20	40	86.85	4.39	8.76	81.8	4.14	7.52	93.5
93	1,900	40	20	40	86.85	4.39	8.76	84.5	4.46	8.72	97.8
98	1,700	15	45	40	85.29	4.31	10.40	81.0	3.87	9.69	94.6
98	1,900	15	45	40	85.29	4.31	10.40	83.6	3.98	10.1	97.8
108	1,700	25	5	70	73.89	13.06	13.05	71.0	10.6	11.1	92.7
109	1,700	20	10	70	73.43	12.98	13.58	69.6	10.7	11.5	91.8
111	1,700	10	20	70	72.54	12.82	14.64	67.4	11.9	13.7	93.0

[a] The uranium and beryllium values are the average of two determinations; the carbon values are the average of three determinations.

[b] Beryllium was determined by a fluorimetric method for amounts less than 2 percent by weight, and by a gravimetric method for amounts greater than 2 percent by weight.

percentage of iron, in those specimens which were analyzed for iron content, was found to be too low (less than 0.35% by weight) to account for the departure from 100 percent.

Both the uranium carbides [1] and beryllium carbide are known to be unstable in the presence of air and moisture. The alloys heat-treated at 1,700° C were stored in desiccators for several months longer than those heat-treated at 1,900° C. In view of the instability of these carbides with respect to air, it is reasonable to assume that the departure of these analyses from 100 percent may be attributed, in part, to oxidation of the specimens that occurred during storage periods of as long as 18 months. In all cases, the specimens were ground to pass a No. 200 U. S. Standard Sieve for X-ray analysis shortly after heat treatment and were stored in this condition. The expiration of the investigation prevented the determination of oxygen content.

The results of the chemical analyses of the alloys were not substituted for the nominal compositions for several reasons:

First, due to oxidation or hydration, the chemical composition of the samples is believed to have changed during the interval between X-ray and chemical analyses.

Second, some doubt exists concerning the cause of the failure of the analysis to total 100 percent. Even if the cause is definitely attributed to oxygen, there are no valid assumptions that can be made to permit the calculation of the composition that existed at the time of heat treatment.

Third, all of the heated alloys were not analyzed, and confusion would result from the attempt to correlate data in which part of the alloys were considered on the basis of nominal composition, and part on the basis of analyzed composition.

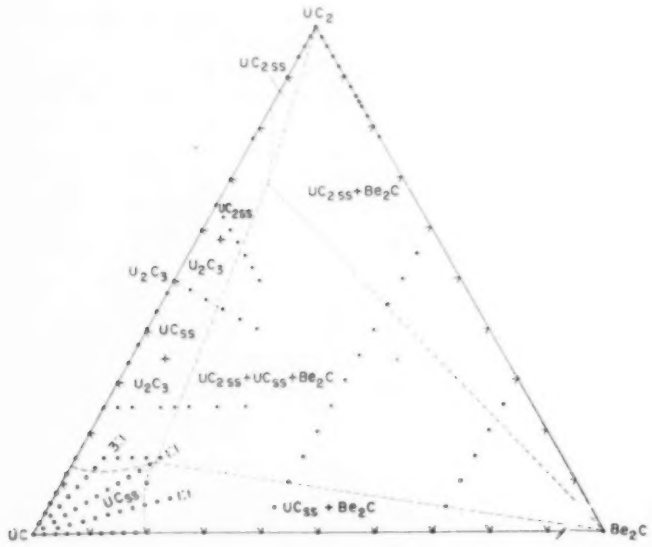

FIGURE 3. *Phases identified in the system* $UC\text{-}UC_2\text{-}Be_2C$, *in mole percent.*

The alloys were heated for 2 hours at 1,700° C, in argon and then oil-quenched. Dots refer to preparations studied.

5. Results and Discussion

5.1. Isothermal Section at 1,700° C

An isothermal section at 1,700° C was made of interactions within the system $UC\text{-}UC_2\text{-}Be_2C$ and in the binary boundary systems that are included. A constitutional diagram, prepared from the data, is shown in figure 3. This figure represents the constitution of alloys after a 2-hr heat treatment at 1,700° C and is not intended to represent an equilibrium phase diagram.

a. The Binary System $UC\text{-}Be_2C$

Data are presented in table 4 and figure 4 showing the relation between lattice parameters and composition in the system $UC\text{-}Be_2C$ after quenching in oil from 1,700° C. It can be seen that small additions of Be_2C increase the unit-cell size of the UC phase. At the limit of solubility, 20 mole percent (or 2.9 wt percent) of Be_2C, the volume of the UC unit-cell was increased by 1.6 percent. The broken line in figure 4 represents the type of results obtained early in the

TABLE 4. *Composition and* UC *lattice parameters in the system* $UC\text{-}Be_2C$

Preparations were heated 2 hr at 1,700° C in argon and then oil-quenched.

Alloy	Nominal composition		UC_{ss} parameters	
	Be_2C	UC	Oil-quenched (rapid cooling)	Quenched in less rapid cooling media [a]
	Mole %	*Mole %*	*A*	*A*
44	0	100	4.962	4.963
55	2	98	4.964	4.965
56	4	96	[b] 4.967	4.968
57	6	94	[b] 4.970	4.972
59	8	92	4.972	.....
43	10	90	4.974	4.973
173	12	88	4.979	.....
174	14	86	4.981	.....
42	20	80	4.988	4.972
41	30	70	4.985	4.972
40	40	60	4.989	4.972
39	50	50	4.988	4.973
37	70	30	4.992	4.974

[a] These data obtained on specimens that were cooled either in molten tin (mp 232° C) or on tantalum wool.
[b] Pellets missed oil quench-cup. They were cooled less rapidly than those which were oil-quenched.

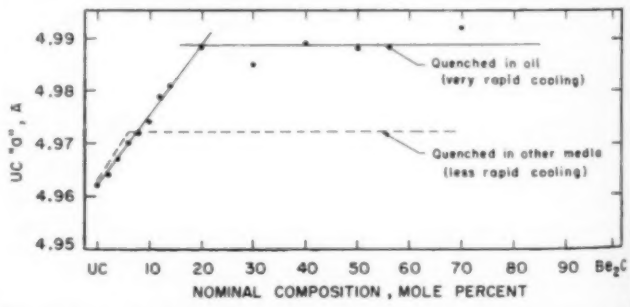

FIGURE 4. *Lattice parameters of uranium carbide solid solutions in mixtures of* UC *and* Be_2C.

The preparations were heated for 2 hours at 1,700° C in an argon atmosphere and then quenched in oil.

investigation, when the specimens were dropped onto tantalum wool or into molten tin in a cooler part of the furnace rather than into quenching oil. The furnace quench, which resulted in a less rapid cooling, indicated a much lower solubility limit for Be_2C in UC (6 mole percent) than was obtained with the oil quench (20 mole percent). Because precipitation or ex-solution occurs readily in these alloys, it seems likely that X-ray examination with high-temperature equipment might show a still higher solubility for the same temperature.

b. The Binary System UC-UC_2

The uranium-carbon system has been studied in other laboratories [10, 11]. The conflicting nature of the proposed diagrams, the need for determining lattice parameter values, and the degree of interaction between phases made desirable a reinvestigation of that portion of the system between UC and UC_2.

Uranium sesquicarbide, U_2C_3, was observed in the present investigation consistent with the conditions of stress and temperature described by Mallett, Gerds, and Vaughan [9]. The X-ray diffraction pattern described by Mallett was obtained with Fe K radiation and contained 23 lines with $a=8.088 \pm 0.001$ A. The pattern, obtained with Cu Kα radiation, in this study, contained 14 additional high-angle reflections with $a=8.089 \pm 0.001$ A, based on the high-angle reflections. Because the pattern, obtained with Cu Kα radiation, has not been published, it is given in table 5. The pattern was obtained from a sample consisting of 50 mole percent of UC_2 and 50 mole percent of UC heated at 1,600° C in argon and cooled to room temperature in the furnace.

The results obtained in the present study are given in table 6. The data indicate that UC enters into a solid-state reaction with as much as 27 mole percent of U_2C_3 (13.5 mole percent of UC_2), to yield a single-phase region of UC solid solutions. These solid solutions show no significant lattice parameter change over this range of composition. It was found that alloy mixtures, such as 194 (table 6) with a carbon content sufficient to correspond to 24 mole percent of U_2C_3, showed only the pattern of UC solid solution after heat treatment. Experiments performed, using the X-ray methods previously described, showed that 5 mole percent of U_2C_3 could easily be detected in the presence of 95 percent of UC. For this reason, the first six alloys of table 6 were considered to be one-phase solid solutions, regardless of the fact that no parameter change was observed.

An independent estimate of the limit of solid solution was obtained from a comparison of the relative intensities of U_2C_3 and UC_{ss} reflections of the X-ray patterns of two-phase alloys between 24 and 95.2 mole percent U_2C_3 (12 and 47.6 mole percent of UC_2), with the relative intensities of known, unheated mixtures of UC and U_2C_3. The (220) reflection of UC at 2θ equals 52.1° and the (510/439)

TABLE 5. *X-ray diffraction data for the cubic compound* U_2C_3 *obtained with copper* K_{α_1} *radiation*

hkl	Cu K_{α_1}	*d*	*a*
	29	*A*	*A*
211	27.00	3.300	.....
220	31.26	2.859	.....
310	35.07	2.556	.....
321	41.76	2.161	.....
400	44.80	2.021	.....
332	53.07	1.724	.....
422	55.61	1.651	.....
510/431	58.10	1.586	.....
521	62.88	1.477	.....
440	64.98	1.434	.....
530	67.46	1.387	.....
611/532	71.89	1.312	.....
620	74.06	1.279	.....
541	76.21	1.248	.....
631	80.46	1.193	.....
444	82.55	1.1676	.....
710/543	84.63	1.1442	.....
721/633/552	88.81	1.1008	.....
642	90.89	1.0809	.....
730	92.97	1.0621	.....
732/651	97.13	1.0274	.....
800	99.25	1.0111	.....
741	101.36	0.9956	.....
653	105.63	.9668	.....
660/822	107.79	.9534	.....
750/831/743	109.98	.9404	.....
752	114.48	.9159	.....
840	116.76	.9045	8.0904
833/910	119.14	.8933	8.0892
761/921/655	124.03	.8722	8.0888
664	126.56	.8623	8.0893
754/930/851	129.20	.8527	8.0891
932/763	134.79	.8343	8.0893
844	137.82	.8256	8.0887
853/941	141.01	.8171	8.0888
772/10,1,1	148.21	.8009	8.0884
862/10,2,0	152.40	.7931	8.0884
Average			8.0890

TABLE 6. *Composition and lattice parameters in the system* $UC\text{-}UC_2$

Preparations were heated 2 hr at 1,700° C in argon and then oil-quenched.

Alloy	Nominal composition		Lattice parameters of stable phases		
	UC_2	UC	UC_{ss}	U_2C_3	UC_{2ss} (a^*)[a]
	Mole %	*Mole %*	*A*	*A*	*A*
44	0	100	4.962	.....	.....
88	2	98	4.961	.....	.....
87	4	96	4.964	.....	.....
86	6	94	4.964	.....	.....
85	8	92	4.964	.....	.....
194	12	88	4.966	.....	.....
186	15	85	4.964	8.09	.....
187	20	80	4.965	8.090	.....
188	25	75	4.964	8.090	.....
84	30	70	4.965	8.089	.....
149	33.7	66.3	4.968	8.089	.....
192	40.5	59.5	4.967	8.090	.....
89	50	50	4.968	8.089	.....
146	60	40	.....	8.089	(b)
83	70	30	.....	8.090	4.196
150	78.3	21.7	.....	8.090	4.195
101	90	10	.....	.....	4.194
81	94	6	.....	.....	4.193
80	96	4	.....	.....	4.194
79	98	2	.....	.....	4.194
67	100	.....	.....	.....	4.195

[a] $a^*=\sqrt[3]{a^2c}$.
[b] Phase identified, but in an amount too small to permit a determination of the lattice parameter.

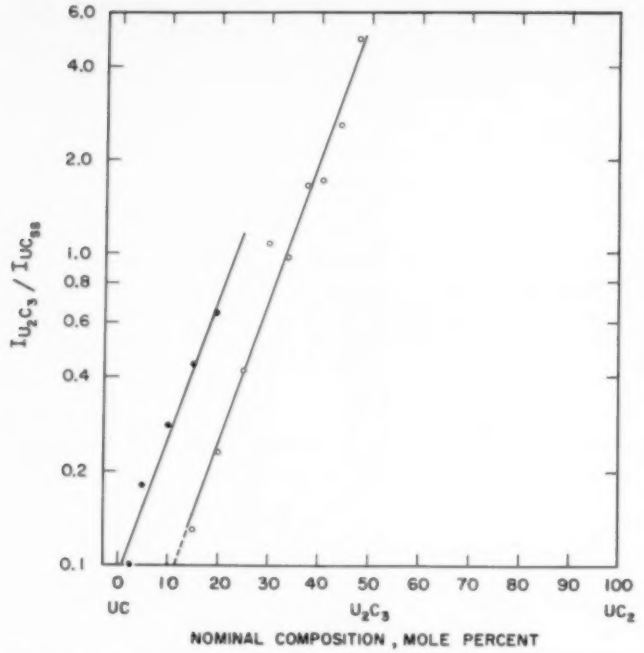

FIGURE 5. *X-ray intensity ratio as a function of composition, for alloys between* UC *and* U_2C_3.

Solid circles represent data obtained from unheated mixtures. Open circles represent data obtained from alloys heated for 2 hr at 1,700° C in argon.

reflection of U_2C_3 at 2θ equals 58.1° were selected for the intensity comparison of the heated and the unheated mixtures.

The ratios of $I_{U_2C_3}/I_{UC}$, when plotted against composition on rectangular coordinate paper, appeared to follow a curved line. When the same data were plotted on semilogarithmic paper, a more nearly linear relationship was obtained. For this reason, the data were fitted by curves of the form $y=ab^x$, using the method of least squares. These are the straight lines through the data points in figure 5.

From the curves, the intensity ratios associated with a given U_2C_3 content may be found for both the heated alloys and the known mixtures. The much smaller intensity ratio of a heated alloy, as compared with that of a known mixture of the same composition, indicate that the amount of "free" U_2C_3 has decreased as a result of the heat treatment. The distance between the curves, measured parallel to the x-axis, represents the amount of decrease in "free" U_2C_3. The value obtained from the curves in this way, about 20 mole percent of U_2C_3 (10 mole percent of UC_2), may be used as an estimate of the solubility limit of U_2C_3 in UC, and confirms the presence of solid solubility without parameter change.

The single-phase region of UC_2 solid solutions extends to about 32 mole percent of U_2C_3 (16 mole percent of UC), without appreciable parameter change. An insufficient number of alloys was examined in the field $UC_{2ss}+U_2C_3$ to allow an estimate of the solubility limit based on intensity measurements. No evidence has been found for a single-phase field for U_2C_3 at 1,700° C.

TABLE 7. *Composition and lattice parameters in the system* UC_2-Be_2C

Preparations were heated 2 hr at 1,700° C. in argon and then oil-quenched.

Alloy	Nominal composition		Lattice parameters $UC_2(a^*)$[a]
	UC_2	Be_2C	
	Mole %	*Mole %*	*A*
67	100	0	4.195
74	98	2	4.196
75	96	4	4.196
76	94	6	4.193
77	92	8	4.194
66	90	10	4.195
195	88	12	4.194
196	86	14	4.195
78	85	15	4.194
197	84	16	4.194
198	82	18	4.196
199	78	22	4.195
62	30	70	4.195

[a] $a^*=\sqrt[3]{a^2c}$.

c. The Binary System UC_2-Be_2C

Data are presented in table 7 for alloy preparations in the UC_2-rich end of the system. It can be seen that Be_2C has no effect on the UC_2 unit-cell size in the quenched alloys obtained after heating 2 hr at 1,700° C. in argon. In this particular binary system, involving the carbides of a very heavy metal and a very light metal, the X-ray method for the identification of phases is especially inadequate because of the wide difference in X-ray absorption characteristics. On the basis of X-ray evidence alone, there is no indication of solubility of Be_2C in UC_2.

d. Ternary Alloys Within the System UC-UC_2-Be_2C

The data obtained on ternary alloys along several sections within the system UC-UC_2-Be_2C are given in tables 8 and 9. Although the alloys are not identified by number in figure 3, the compositions given in the tables should identify the individual alloys along the respective section lines.

The alloys described in table 9 are, with few exceptions, within the UC single-phase field. The data give a satisfactory representation of the parametric surface within this region. It can be seen that the parameter increase along the sections, in the direction away from UC, is greatest along the 1:1 section. Vertical sections through the parametric surface, perpendicular to the 1:1 section, would show parameter maxima near the 1:1 section.

Five sections were studied (table 8), which extend into or cross the three-phase field in figure 3. For alloys along the sections, the UC_{ss} parameters increased to a value of $a=5.002\pm0.005$ A and then remained essentially constant. Those alloys that had UC_{ss} parameters within these limits were considered to be within the three-phase area and were used in locating the three-phase boundary. Along those sec-

TABLE 8. *Composition and lattice parameters along several sections within the system* UC-UC_2-Be_2C

Preparations were heated for 2 hr at 1,700° C in argon and then oil-quenched.

Alloy	Nominal composition			Lattice parameters			
	UC	UC_2	Be_2C	UC_{ss}	UC_{2ss} (a^*)[a]	U_2C_3	Be_2C
	Mole %	*Mole %*	*Mole %*	*A*	*A*	*A*	*A*
40	60	.....	40	4.989	(b)	.....	.....
90	55	5	40	4.987	(b)	.....	.....
91	50	10	40	4.998	(b)	.....	.....
92	45	15	40	5.000	(b)	.....	.....
93	40	20	40	5.002	4.198	.....	(b)
94	35	25	40	5.005	4.197	.....	(b)
95	30	30	40	5.007	4.196	.....	.....
96	25	35	40	5.005	4.194	.....	(b)
97	20	40	40	5.001	4.195	.....	.....
98	15	45	40	.....	4.191	.....	(b)
99	10	50	40	.....	4.192	.....	(b)
100	5	55	40	.....	4.192	.....	(b)
37	30	.....	70	4.992	(b)	.....	4.342
108	25	5	70	5.000	(b)	.....	4.342
109	20	10	70	5.000	(b)	.....	4.342
110	15	15	70	5.001	4.198	.....	4.342
111	10	20	70	.....	4.195	.....	4.342
112	5	25	70	.....	4.197	.....	4.341
62	.....	30	70	.....	4.195	.....	4.342
177	35	65	.....	(b)	4.196	8.090	.....
178	35	62.5	2.5	.....	4.196	8.089	.....
179	35	60	5	.....	4.198	8.090	.....
180	35	57.5	7.5	(b)	4.197	8.089	.....
181	35	55	10	5.004	4.196	.....	.....
182	35	52.5	12.5	5.002	4.198	8.091	.....
183	35	50	15	5.003	4.197	.....	.....
188	75	25	.....	4.964	(b)	8.090	.....
189	72.5	25	2.5	4.970	(b)	8.089	.....
117	70	25	5	4.976	(b)	8.088	.....
118	65	25	10	4.991	(b)	8.089	.....
190	62.5	25	12.5	5.002	(b)	8.090	.....
119	60	25	15	5.003	(b)	.....	.....
120	55	25	20	5.004	(b)	.....	.....
121	50	25	25	5.002	(b)	.....	.....
68	48.1	48.1	3.8	4.976	4.197	8.090	.....
69	46.2	46.2	7.6	4.995	4.200	.....	.....
70	44.9	43.6	11.5	5.007	4.195	.....	.....
71	42.9	41.6	15.4	5.005	4.201	.....	.....
72	40.2	40.3	19.5	5.005	4.198	.....	.....

[a] $a^*=\sqrt[3]{a^2c}$.

[b] Phase identified but in an amount too small to permit a determination of the lattice parameter.

TABLE 9. *Composition and lattice parameters of* UC *solid-solution alloys within the system* UC-UC_2-Be_2C

Preparations were heated 2 hr at 1,700° C in argon and then oil-quenched.

Alloy	Nominal composition		Lattice parameters	
	UC	UC_2:Be_2C	UC	U_2C_3
	Mole %	*Mole %*	*A*	*A*
151	95	3:1	4.966	.....
152	92.5	3:1	4.968	.....
153	90	3:1	4.967	.....
154	87.5	3:1	4.969	.....
155	85	3:1	4.971	(a)
156	82.5	3:1	4.974	.....
157	80	3:1	4.972	8.090
158	97.5	1:1	4.963	.....
159	95	1:1	4.966	.....
160	92.5	1:1	4.969	.....
161	90	1:1	4.969	(a)
162	87.5	1:1	4.976	.....
163	85	1:1	4.977	(a)
164	82.5	1:1	4.984	.....
165	80	1:1	4.989	.....
204	77.5	1:1	4.992	.....
205	75	1:1	4.993	.....
206	72.5	1:1	4.997	.....
203	70	1:1	4.998	.....
166	95	1:3	4.969	.....
167	92.5	1:3	4.972	.....
168	90	1:3	4.976	.....
169	87.5	1:3	4.981	.....
170	85	1:3	4.981	.....
171	82.5	1:3	4.987	.....
172	80	1:3	4.982	.....
208	77.5	1:3	4.986	.....
209	75	1:3	4.988	.....
210	72.5	1:3	4.989	.....
200	77.5	2:1	4.980	8.090
201	75	1.5:1	4.992	.....
202	72.5	1.2:1	4.997	.....
207	75	1:1.5	4.992	.....

[a] Phase identified, but in an amount too small to permit a determination of the lattice parameter.

tions where U_2C_3 and UC_{ss} were identified, the disappearance of U_2C_3 indicated that the boundary of the three-phase area had been crossed and was used in locating the boundary.

The stability relations of uranium sesquicarbide are not clearly understood. The conditions of stress and temperature necessary to form or stabilize U_2C_3, as described by Mallett et al. [9], were verified in the present work with the same alloys. As these alloys "aged," the sesquicarbide failed to appear, either in binary or ternary mixtures. Mixtures made from the freshly prepared alloys, 361 and 369, however, gave results compatible with those reported by Mallett.

U_2C_3 was found in the present experiments as a constituent phase in only a limited portion of the ternary diagram. It was not found in any preparation that contained more than 12.5 mole percent of Be_2C.

Three possible forms of an equilibrium phase diagram might be postulated. In the first such form, figure 6, a join would connect U_2C_3 and Be_2C. In this form of diagram the absence of U_2C_3 within the central portion of the system, under the conditions of the present experiments, would result from the nonattainment of equilibrium, and U_2C_3 would increase at the expense of UC_2 or UC as equilibrium was approached. In the second form of an equilibrium diagram, U_2C_3 would not appear. The presence of the U_2C_3 phase in the alloys would be a nonequilibrium condition, and the amount of U_2C_3 would decrease as equilibrium was approached. Another possible explanation of the occurrence of U_2C_3, within the ternary system, is one requiring the postulation of a compound in the UC-Be_2C system at about 25 to 35 percent of Be_2C. X-ray patterns within this region indicate a cubic, single-phase material with parameters slightly larger than UC, and have been interpreted merely as a solid solution of Be_2C in UC, with beryllium substituting for carbon in the interstitial uranium-carbon compound. It is possible, however, that a compound $3UC{\cdot}Be_2C$ or $2UC{\cdot}Be_2C$ may exist and form a complete series of solid solutions with pure UC. Binary joins would exist between both U_2C_3 and UC_2 and the postulated compound. This explanation would satisfactorily explain the observed occurrence of U_2C_3, without postulating varying amounts of stress on a material that does not seem to have a varying composition. The possible occurrence of a hypothetical compound is suggested as a convenient method for making the results compatible with the phase rule, but no defi-

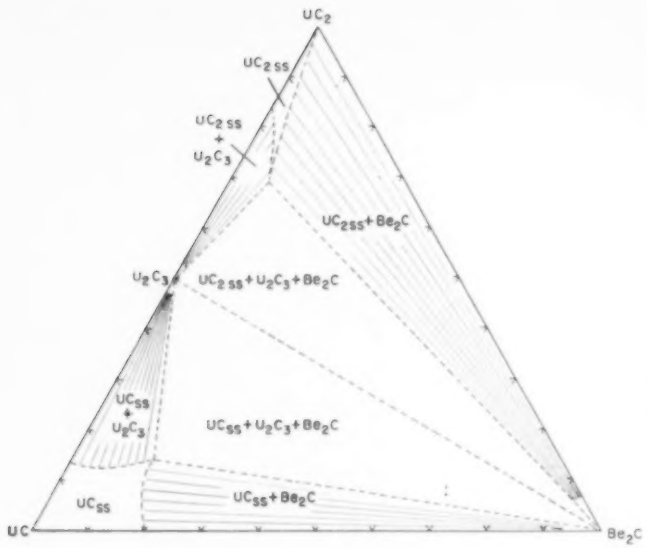

FIGURE 6. *Most probable equilibrium diagram for the system* $UC\text{-}UC_2\text{-}Be_2C$ *at 1,700 ° C, in mole percent.*

nite evidence of its occurrence was found. Of these three possible forms of an equilibrium diagram for the system, it is believed that the first, figure 6, is the most probable.

The boundary between the fields of UC_{ss} and $UC_{ss}+U_2C_3$ is clearly established because 1- and 2-phase alloys in these regions can be readily differentiated by X-ray methods. The boundary between the fields of UC_{ss} and $UC_{ss}+Be_2C$, on the other hand, can only be approximated, because the X-ray method fails to distinguish between 1- and 2-phase ternary alloys involving UC_{ss} and Be_2C.

The data and discussion of alloys in table 6 indicate the extent of the UC_2 single-phase alloys in the binary system $UC\text{-}UC_2$. Evidence has not been obtained to prove or to disprove the existence of single-phase UC_2 alloys in the binary system $UC_2\text{-}Be_2C$. The assignment of a field to single-phase UC_2 alloys is in recognition of its existence rather than an approximation of the extent of the field.

5.2. Isothermal Study at 1,900° C

a. The Binary System $UC\text{-}UC_2$

The composition and lattice parameters of constituent phases of the alloys heated at 1,900° C are given in table 10. All preparations intermediate between the carbide end members are shown to consist of the two phases UC and UC_2. There is no apparent relation between composition and unit-cell size.

b. The Binary System $UC\text{-}Be_2C$

The composition and X-ray data for alloys between UC and Be_2C are given in table 11. Alloys 35, 36, and 37 are not on the join between UC and Be_2C because of an excess of carbon. With the starting materials then available, additions of either beryllium or uranium metal would have been required to yield compositions on the join. Both the volatilization of beryllium and the gain in carbon from the specimen holder, during heating, could have resulted in further departures from the binary join. The occurrence of UC_2 in the alloys at the Be_2C end of the system may have resulted from these types of compositional changes. The tabulated data show UC solid solutions with increasing lattice parameters between 0 and 40 mole percent (7.4 wt percent) Be_2C. The marked change in slope of the parameter-composition curve at 40 mole percent of Be_2C indicates the limit of solubility of Be_2C in UC. Thus, it can be seen that the solubility of Be_2C in UC is twice as large at 1,900° C as it was found to be at 1,700° C. An explanation for the smaller slope within the two-phase region is given in section 5.3.

TABLE 10. *Composition and lattice parameters in the system* $UC\text{-}UC_2$

Preparations were heated 2 hr at 1,900° C in argon and then oil-quenched.

Alloy	Nominal composition		Lattice parameters	
	UC	UC_2	UC	UC_2 (a^*)[a]
	Mole %	*Mole %*	*A*	*A*
44	100	------	4.963	------
85	92	8	4.965	(b)
187	80	20	4.967	(b)
84	70	30	4.968	4.207
192	59.5	40.5	4.963	4.199
89	50	50	4.966	4.201
146	40	60	4.964	4.200
83	30	70	4.963	4.197
150	21.7	78.3	4.965	4.199
101	10	90	(b)	4.197
67	------	100	(b)	4.202

[a] $a^*=\sqrt[3]{a^2c}$.
[b] Phase identified but in an amount too small to permit a determination of the lattice parameter.

TABLE 11. *Composition and lattice parameters in the system* $UC\text{-}Be_2C$

Preparations were heated for 2 hr at 1,900° C in argon and then oil-quenched.

Alloy	Nominal composition			Lattice parameters		
	UC	UC_2	Be_2C	UC_{ss}	UC_2	Be_2C
	Mole %	*Mole %*	*Mole %*	*A*	*A*	*A*
44	100	------	------	4.963	------	------
43	90	------	10	4.970	------	------
42	80	------	20	4.978	------	------
41	70	------	30	4.982	------	------
40	60	------	40	4.990	------	------
39	50	------	50	4.987	(a)	------
38	40	------	60	4.993	(a)	(a)
37	29.6	0.4	70	4.995	(a)	(a)
36	19.3	.7	80	4.996	(a)	(a)
35	9.1	.9	90	5.002	(a)	4.342
26	------	------	100	(a)	(a)	4.343

[a] Phase identified, but in an amount too small to permit a determination of the lattice parameter.

c. The Binary System $UC_2\text{-}Be_2C$

The data obtained for the alloys within this system, reacted at 1,900° C, are given in table 12. The lattice parameters of the UC_2 phase showed no systematic variation with composition. Be_2C could be positively identified only in those mixtures made up to contain 40-mole percent (7 wt percent) or more

TABLE 12. *Composition and lattice parameters in the system* UC_2-Be_2C

Preparations were heated for 2 hr at 1,900° C in argon and then oil-quenched.

Alloy	Nominal composition		Lattice parameters		
	UC_2	Be_2C	UC_2 (a^*)[a]	UC	Be_2C
	Mole %	*Mole %*	*A*	*A*	*A*
67	100	------	4.202	(b)	------
66	90	10	4.196	(b)	(b)
65	80	20	4.200	(b)	(c)
73	70	30	4.197	(b)	(c)
64	60	40	4.198	(b)	(b)
63	50	50	4.196	(b)	(b)
47	40	60	4.200	(b)	(b)
62	30	70	4.199	(b)	(b)
61	20	80	4.199	(b)	4.343
60	10	90	4.202	(b)	4.343
26	------	100	(b)	(b)	4.343

[a] $a^* = \sqrt[3]{a^2c}$.
[b] Phase identified, but in an amount too small to permit a determination of the lattice parameter.
[c] Identification of the phase questionable.

TABLE 13. *Composition and lattice parameters along several sections within the system* UC-UC_2-Be_2C

Preparations were heated for 2 hr at 1,900° C in argon and then oil-quenched.

Alloy	Nominal composition			Lattice parameters		
	UC	UC_2	Be_2C	UC	UC_2 (a^*)[a]	Be_2C
	Mole %	*Mole %*	*Mole %*	*A*	*A*	*A*
40	60	------	40	4.990	------	(b)
90	55	5	40	4.995	(b)	------
91	50	10	40	4.989	(b)	------
92	45	15	40	4.998	(b)	------
93	40	20	40	4.999	(b)	(b)
94	35	25	40	5.002	(b)	------
95	30	30	40	5.004	(b)	------
96	25	35	40	4.998	4.203	------
97	20	40	40	5.005	(b)	------
98	15	45	40	(b)	4.198	------
99	10	50	40	(b)	4.200	------
100	5	55	40	(b)	4.195	(b)
64	------	60	40	------	4.198	(b)
179	35	60	5	4.982	4.204	------
181	35	55	10	4.992	4.204	------
183	35	50	15	4.992	4.204	------
117	70	25	5	4.986	(b)	------
118	65	25	10	4.993	(b)	------
119	60	25	15	5.005	(b)	------
120	55	25	20	4.998	(b)	------
121	50	25	25	5.005	(b)	------

[a] $a^* = \sqrt[3]{a^2c}$.
[b] Phase identified, but in an amount too small to permit a determination of the lattice parameter.

of Be_2C. UC reflections could be identified in the X-ray patterns of all mixtures. The persistent occurrence of UC, in these alloys, may reflect the need for still more rapid cooling to prevent the dissociation of UC_2. The data indicate no solubility in the system UC_2-Be_2C.

d. Ternary Alloys in the System UC-UC_2-Be_2C

A limited number of ternary alloy preparations on three sections were reacted at 1,900° C, and the data obtained are given in table 13. There appears to be little change in the parameters of either UC or UC_2 in the alloys heated at 1,900° C. All of the ternary alloys, however, do have somewhat larger UC_{ss} parameter values than do those alloys consisting only of UC and UC_2 (table 10).

The dissociation temperature of uranium sesquicarbide [9] is 1,800° C, and therefore this phase does not appear in alloys reacted at 1,900° C. Thus, the disappearing phase technique cannot be employed in the location of a three-phase region.

5.3. Discussion of X-Ray Results

The diffraction intensities, obtained by the X-ray Geiger counter method, for the carbides of uranium are, in general, rather weak. Although the X-ray patterns for cubic UC and U_2C_3 are sharp, the pattern for tetragonal UC_2 is diffuse, making accurate parameter determinations difficult. All of the solid solutions formed in this system give comparatively weak intensities, the preparations increasingly distant from the pure compounds having increasingly poor patterns. These weak intensities are due, primarily, to the greater degree of disorder that is generally found in solid solutions.

Another difficulty encountered in the interpretation of the X-ray patterns is the inability to identify small amounts of Be_2C in the presence of large amounts of any of the uranium carbides. This is due to the fact that beryllium is a much lighter element than uranium and has much less diffracting power. Free beryllium carbide cannot be recognized in the diffraction pattern in amounts less than about 25 to 35 mole percent. Therefore, the limits of solid solution must be found by changes in the slope of the parameters of the uranium-carbide component plotted against composition, as in figure 4. The disappearing phase method is of no value in locating the boundary between single-phase and two-phase areas where one of the phases is beryllium carbide.

Very heavy and very light atoms differ greatly in abilities to reflect and transmit X-rays. Because the uranium carbides are practically opaque to X-rays, the X-ray beam is diffracted from the extreme surface of the X-ray spectrometer sample. In beryllium carbide, on the other hand, the X-ray beam may penetrate readily, and diffraction occurs throughout the whole thickness of the sample. This results in broadened peaks, the centers of which are slightly in error. When an X-ray sample is composed of a small amount of a heavy material, such as uranium monocarbide, and a large amount of a light material, such as beryllium carbide, the position of the UC diffraction peaks will be effectively displaced toward lower 2 θ angles or larger d values. The end result is to cause an error in the parameter measurement of the UC, which is a function of the amount of dilution with Be_2C. The slope of the UC_{ss} parameter curve within the two-phase region (alloys 35 to 39, table 11) can be partly attributed to this error of "dilution."

X-ray results indicate that Be_2C enters into solid solution in UC to a considerable extent, resulting in an increase of the lattice parameter of the UC. As the beryllium atom has a much smaller radius than that of the uranium atom, this increase in parameter cannot be due to a substitution of Be for U. The beryllium atom, however, is slightly larger than the carbon atom and could partially replace carbon in the interstitial sites between the uranium atoms in six-fold coordination. The only other available positions for the beryllium atoms in the UC structure are those of the empty sites comparable to those occupied by fluorine in the fluorite-type structure. The beryllium atoms occupy these latter positions in Be_2C, which has the antifluorite-type structure. It seems highly unlikely that the beryllium atom could occupy the same position in the UC solid solution that has the NaCl-type structure, where both the corners and the faces of the unit-cell are occupied by uranium atoms, with carbon atoms filling the interstices.

Equilibrium conditions seem to be very difficult to obtain in this system. Small amounts of UC_2 were almost always indicated in the X-ray patterns for samples that might be expected to consist of a single UC phase. The reason for this occurrence is not clear, but probably represents an unmixing reaction during quenching.

Uranium dicarbide has the same crystallographic structure as CaC_2 and other alkaline-earth dicarbides, which all undergo a phase transformation to a cubic form at elevated temperatures [20]. These cubic forms are stable only at elevated temperatures. It is possible that UC_2 also has a cubic form at some elevated temperature. The possibility of such a phase transformation might well be tested with high-temperature X-ray equipment.

5.4. General Observation

Suitable compacts were obtained by pressing fine-powder mixtures at a pressure of 60,000 psi in hardened steel molds without binders. The specimens, so formed, were free from cracks and strong enough to permit handling. After the heat treatment at either 1,700° or 1,900° C, the pellets were hard and sound, even after the rather extreme thermal shock as a result of oil-quenching.

It was found that soaking in carbon tetrachloride was required to remove completely the quenching oil. This suggested the presence of some open pores in the heated specimens.

During the heating period the carbides were extremely sensitive to small amounts of oxygen in the furnace atmosphere. Crumbling of the pellet surface was an indication of oxygen contamination. Any oxygen contamination in the specimen was also shown by the presence of uranium-dioxide reflections in the X-ray pattern.

A comparison of the lattice parameters of the UC solid solutions in preparations heated in contact with graphite, molybdenum, or tantalum was made. The smaller parameters, which resulted from heating in contact with molybdenum or tantalum, indicated that reactions occurred for these combinations. For this reason, graphite cups were used to avoid reactions with the refractory metals.

6. Summary

Alloys within the system $UC\text{-}UC_2\text{-}Be_2C$ were prepared, heat-treated in the solid state in argon at 1,700° and 1,900° C, and analyzed by X-ray methods to determine the crystalline phases present. The findings may be summarized as follows:

1. Uranium monocarbide forms single-phase alloys with as much as 20 mole percent of beryllium carbide at 1,700° C, and approximately 40 mole percent at 1,900° C.
2. Solid solutions of Be_2C in UC have larger lattice parameters than either of the end members. It is believed that beryllium atoms partially replace the smaller carbon atoms of the UC structure.
3. Uranium monocarbide interacts with as much as 27 mole percent of uranium sesquicarbide (13.5 mole percent of uranium dicarbide) during the treatment at 1,700° C to form single-phase alloys.
4. Uranium dicarbide interacts with as much as 32 mole percent of uranium sesquicarbide (16 mole percent of uranium monocarbide) during the treatment at 1,700° C to form single-phase alloys.
5. No solubility of either the monocarbide or the dicarbide of uranium in uranium sesquicarbide is indicated.
6. The limitations of the X-ray methods prevent any definite statement about the interaction of Be_2C and UC_2.
7. Several possible explanations are offered with regard to the occurrence of U_2C_3 within a very restricted portion of the system.
8. The various interactions outlined above have shown no deleterious effects on the physical structure of the mixed carbide alloys. The preparations were hard and sound, even after the rather extreme thermal shock due to oil-quenching. In a like manner, the solid-solution alloys showed no improvement, insofar as was incidentally observed, in their stability to air and moisture over the individual pure carbides.

The continued interest and encouragement of R. F. Geller, Chief, Porcelain and Pottery Section of the National Bureau of Standards, and the assistance of Martha S. Richmond of the Analytical Chemistry Section is gratefully acknowledged.

Acknowledgment is made to the U. S. Atomic Energy Commission for their support of this investigation and for permission to publish these results.

The uranium-carbon alloys were obtained through the courtesy of Battelle Memorial Institute, and their cooperation is gratefully acknowledged.

7. References

[1] H. Moissan, Study of uranium carbide, Compt. rend. **122,** 247 (1896).

[2] P. Lebeau, The formula of uranium carbide, Compt. rend. **152,** 955 (1911).

[3] O. Ruff and A. Heinzelmann, Uranium hexafluoride from uranium carbide and elementary fluorine with chlorine as catalyst, Z. anorg. u. allgem. Chem. **72,** 63 (1911).

[4] E. P. Polushkin, Alloys of iron and uranium, Iron Steel Inst. (London) Carnegie Schol. Mem. **10,** 129 (1920).

[5] G. Hagg, Regularity in crystal structure of hydrides, borides, carbides and nitrides of the transition elements, Z. physik Chem. [B] **12,** 33 (1931).

[6] R. E. Rundle, N. C. Baenzinger, A. S. Wilson, and R. A. McDonald, The structure of the carbides, nitrides and oxides of uranium. J. Am. Chem. Soc. **70,** 2, 99 (1948).

[7] L. M. Litz, A. B. Garrett, and F. C. Croxton, Preparation and structure of the carbides of uranium, J. Am. Chem. Soc. **70,** 1718 (1948).

[8] H. A. Wilhelm, P. Chiotti, A. L. Snow, and A. H. Daane, The carbides of uranium and thorium, J. Am. Chem. Soc. Suppl. No. 2, 318 (1949).

[9] M. W. Mallett, A. F. Gerds, D. A. Vaughan, Uranium sesquicarbide, J. Electrochem. Soc. **98,** 505 (1951).

[10] R. E. Rundle, A. S. Wilson, N. C. Baenzinger, and A. D. Tevebaugh, X-ray analysis of the uranium-carbon system, AECD–2325, Declassified.

[11] M. W. Mallett, A. F. Gerds, and H. R. Nelson, The uranium-carbon system, BMI–63, Declassified.

[12] P. Lebeau, On a carbide of beryllium, Compt. rend. **121,** 496 (1895).

[13] M. V. Stackelberg and F. Quatrum, The structure of beryllium carbide, Z. Physik Chem. **27,** 50 (1934).

[14] J. Kielland and L. Tronstad, The production of anhydrous beryllium chloride from beryllium oxide via beryllium carbide, Kgl. Norske Videnskab. Selskabs, Forh, **8,** 147 (1935) (published in 1936); C. A. **30,** 72885 (1936).

[15] C. J. Rodden, Analytical chemistry of the manhattan project, p. 33 (McGraw-Hill Book Co., Inc., New York, N. Y., 1950).

[16] W. F. Hillebrand, G. E. F. Lundell, H. A. Bright, and J. I. Hoffman, Applied inorganic analysis, p. 133 (John Wiley & Sons, Inc., New York, N. Y., 1953).

[17] M. H. Fletcher, C. E. White, and M. S. Sheftel, Determination of beryllium in ores, Ind. Eng. Chem., Anal. Ed. **18,** 179 (1946).

[18] E. B. Sandell, Colorimetric metal analysis, p. 271 (Interscience Publishers, Incorporated, New York, N. Y., 1944).

[19] C. J. Rodden and J. J. Tregonning private communication).

[20] M. A. Bredig, J. Phys. Chem. **46,** 801 (1942).

[21] W. J. Youden, Statistical methods for chemists, p. 12 (John Wiley & Sons, New York, N. Y. 1951).

WASHINGTON, July 1, 1954.

Journal of Research of the National Bureau of Standards Vol. 54, No. 4, April 1955 Research Paper 2585

An Analysis of Within-the-Hour Fading in 100- to 1,000-Mc Transmissions

H. B. Janes

An analysis is made of the fading range of 100- to 1,000-Mc transmissions received both within and beyond the radio horizon. The measurements were made during August 1952 over the various Cheyenne Mountain Field Station paths and over the Cedar Rapids, Iowa,-Quincy, Ill. path. Fading range is defined as the ratio in decibels of the signal levels exceeded 10 and 90 percent of an hour. For each of the four frequencies studied, the extent to which median fading range and median signal level depend on the angular distance and time of day is shown in the form of graphs and sample recordings. The data show that beyond the region where diffraction is considered to be the dominant mechanism, the signal level distributions closely resemble the Rayleigh distribution in both fading range and general shape. Deviations from the 13.4-db fading range of a Rayleigh distribution are thought to be due to changes in the average signal power during the hour. The method developed by Norton for estimating from the fading range the ratio of the Rayleigh-distributed component of signal to the constant diffracted component is applied to a sample of the data, and the techniques for applying the method to these particular data are discussed.

1. Introduction

The Bureau's Central Radio Propagation Laboratory has been conducting a long-term program of propagation measurements at its Cheyenne Mountain Field Station in Colorado Springs, Colo. Included in these measurements are frequencies ranging from 100 to 1,000 Mc, and propagation over both optical and nonoptical paths. Several transmitting antenna heights are employed so conditions that might be encountered in both ground-to-ground and air-to-ground transmissions can be simulated. Similar long-term measurements have been carried out at a frequency of 418 Mc over the 134-mile path between Cedar Rapids, Iowa, and Quincy, Ill.

The analysis of these data has included a study of the short-term fading, which, in general, characterizes VHF and UHF signals transmitted beyond and, to a lesser extent, within the radio horizon. For the purpose of this investigation, short-term fading is defined as those fluctuations in instantaneous signal level that occur within a period of an hour's recording. The two principal factors of interest in studying short-term fading are the extent or range of fading and the rate at which these variations occur. The data recorded during August 1952 have been selected for a rather detailed study of fading range. An attempt has been made to show for these particular frequencies and paths and this time of year, the variation of fading range with time of day and the angular distance, θ. θ is defined as the angle in the great circle plane between the horizon rays from the transmitting and receiving antennas as determined for a standard atmosphere.

Figure 1 shows examples of within-the-hour fading in 100-Mc transmissions made during alternate hours from two widely separated transmitting antenna elevations and received at three receiving sites. A description of the various transmission paths is given in section 2. These samples serve to illustrate the wide variety of fading characteristics to be observed with various combinations of antenna height and path length. In figure 2, cumulative distributions of instantaneous signal level are plotted, corresponding to two of the hours, 10 to 11 a. m. and 11 to 12 noon, shown in figure 1. All the recorded data were reduced in this way to hourly cumulative distributions of instantaneous signal level, and these distributions were used as the basis of the fading study. Figure 2 also shows graphically the definition of fading range used here; i. e., the ratio, in decibels, of the level exceeded 10 percent of the hour to the level exceeded 90 percent of the hour.

2. General Description of the Propagation-Measurement Facilities

Figure 3 shows the location of the several transmitting and receiving sites on the Colorado-Kansas path. The profile has been drawn on the basis of a 4/3 earth's radius to allow for standard atmospheric refraction. Transmissions were made at a frequency of 100 Mc from three sites on or near Cheyenne Mountain. The lowest one was a rhombic antenna located about 40 ft above local terrain at the base of Cheyenne Mountain on the Camp Carson military reservation. The middle antenna is a corner reflector located near the summit of Cheyenne Mountain at an elevation of 8,805 ft, or approximately 2,500 ft above the surrounding plains. At the summit of Pikes Peak, a yagi antenna was located at an elevation of 14,115 ft, or approximately 7,800 ft above the plains. In addition, transmissions were made at 192.8 and 1,046 Mc from the Cheyenne Mountain summit site.

The receiving sites of interest in this study are those at Karval, Colo.; Haswell, Colo.; Garden City, Kans.; and Anthony, Kans. They are located at distances from Cheyenne Mountain of 70, 97, 226,

and 393 miles, respectively. Half-wave dipoles were used on all frequencies at Karval, Haswell, and Garden City. The heights above local terrain of the 100-, 192.8-, and 1,046-Mc antennas at these three sites were 18.8, 17.5, and 42.7 ft, respectively. At Anthony, rhombic antennas located approximately 40 ft above ground were used for the two lower frequencies. A half-wave dipole, mounted in a 10-ft parabolic reflector with its axis 8.5 ft above ground, was used for the 1,046-Mc recordings. A more complete description of the Cheyenne Mountain project facilities is given in [1].[1]

Figure 4 shows a similar profile for the Cedar Rapids-Quincy path. Three corner reflector receiving antennas were mounted at heights of 30, 365, and 665 ft above ground near Quincy. The transmitting antenna at Cedar Rapids was a pyramidal horn mounted approximately 40 ft above ground.

With the exception of Anthony, received power data at all the receiving sites were recorded by Esterline-Angus recorders having a chart speed of 3 in./hr. At Anthony, chart speeds ranging from 1½ to 6 in./min were used. In addition, at Garden City, Anthony, and Quincy, time-totalizing recorders were employed because the wide and rapid fading encountered at these sites made graphical analysis of Esterline-Angus chart data difficult, if not impossible [2].

3. The Parameter θ

In figures 3 and 4, the angular distance, θ, mentioned previously is shown as the angle formed by the lines drawn between the transmitting and receiving antennas and their respective horizons in the great circle plane. This angle has been found to be a useful means of describing the extent to which a receiving antenna lies within or beyond the radio horizon of a given transmitting antenna. This has been found preferable to expressing path length in terms of distance in miles, because θ takes into account the path length, antenna heights and the slope of the terrain between an antenna and its horizon determined with an effective earth's radius factor of 4/3. The angular distance, θ, is an important parameter in both diffraction and scattering theories [3]. Table 1 lists the values of θ for each transmission path used in this study.

TABLE 1. *θ Values for transmission paths used in fading-range study*

(θ computed with an earth's radius factor of 4/3 to allow for standard atmospheric refraction)

Receiving site	Transmitting sites and frequencies				
	Camp Carson 100 Mc	Cheyenne Mountain			Pikes Peak 100 Mc
		100 Mc	192.8 Mc	1,046 Mc	
	Colorado-Kansas paths				
	deg	*deg*	*deg*	*deg*	*deg*
Karval	0.489	−0.076	−0.083	−0.077	−0.523
Haswell	.661	.103	.096	.100	−.307
Garden City	2.197	1.611	1.608	1.532	1.183
Anthony	3.895	3.353	3.346	3.428	2.917
Cedar Rapids-Quincy path					
Receiving antenna height					θ
ft					*deg*
30					1.148
365					1.002
665					0.898

[1] Figures in brackets indicate the literature references at the end of this paper.

4. Median Fading Range and Median Signal Level

Most of the data presented in this report are the medians of the individual hourly values of fading range and of signal level. Figure 5 shows an example of a distribution from which such a median value of fading range was obtained. The fading ranges for each hour at a given site and frequency were tabulated and a distribution plotted to obtain the median of the hourly fading ranges. This was done for each hour of the day to show the diurnal variation of the median fading range. In addition, the values for all hours of the day were combined (as in the case of fig. 5) to obtain the over-all median values shown in figure 7.

A similar procedure was used in the signal-level analysis. In this instance, tabulations of individual hourly median levels were made, the hourly median levels being taken from the cumulative distributions of instantaneous signal level, such as those shown in figure 2. From each of these tabulations a distribution of hourly median levels was drawn. Figure 6 is an example of such a distribution. The medians of these hourly medians were used in figure 8 and in the subsequent diurnal-variation curves.

5. Fading Range Versus θ

Figure 7 shows the variation of fading range with θ for the 100-, 192.8-, and 1,046-Mc transmissions over the Colorado-Kansas path and the 418-Mc transmissions over the Cedar Rapids-Quincy link. Each point on the plot represents the median of the individual hourly fading-range values measured during August 1952 on a particular frequency and path. Negative values of θ indicate a propagation path lying entirely within the radio horizon. The values of θ shown in this graph range from $-0.52°$ for the 100-Mc Pikes Peak-Karval path to $+3.90°$ for the Camp Carson-Anthony path. It will be seen that the most rapid increase in fading range with θ occurs just below the radio horizon in the so-called diffraction region (i. e., for values of θ from 0° to about 1°). When θ exceeds a value of about 1°, the receiving antenna is so far below the horizon that

the predominant part of the signal is received as a result of some mechanism such as atmospheric scattering, in which the received power is small in magnitude and the fading deep and rapid. The dashed line represents the fading range (13.4 db) of a Rayleigh-distributed signal. Such a distribution would result, if the incoming signal consisted of a number of component waves in random relative phase and had a constant average power. For values of θ greater than about 1° the fading range appears to level off at very nearly the Rayleigh distribution value of 13.4 db. It is interesting to note that for signals received near the radio horizon (i. e., for the Cheyenne Mountain-Karval path, $\theta = -0.08°$ and for the Cheyenne Mountain-Haswell path, $\theta = 0.1°$), the fading range appears to be a function of frequency. This is not true of the longer paths, such as Cheyenne Mountain-Garden City ($\theta = 1.6°$) and Cheyenne Mountain-Anthony ($\theta = 3.4°$).

For purposes of comparison, figure 8 shows a corresponding plot of the median attenuation relative to free space versus θ for each of the paths and frequencies represented in figure 7. As in the case of fading range, the attenuation increases most rapidly in the diffraction region and levels off considerably in the scattering region far beyond the horizon.

6. Diurnal Variation of Median Fading Range and of Median Signal Level

Figures 9, 10, and 11 show the variation of median fading range and of median signal level versus time of day for the various paths and frequencies. These curves were obtained from the monthly distributions of fading range and median signal level for each hour of the day; i. e., the lines join points, each of which represents a median of the hourly values recorded during that particular hour.

Figure 9 shows the diurnal variation of signal level and fading range at Karval, Haswell, Garden City, and Anthony for the 100-Mc transmissions from each of the three transmitting elevations used. The value of θ for each path is indicated on the figures along with the number of hours of recording on which the curves are based. Unfortunately, there were not sufficient hours of Pikes Peak transmissions recorded at Karval or at Garden City to justify a diurnal analysis. There is a very apparent diurnal pattern in both the median signal level and median fading range for the Cheyenne Mountain and Camp Carson transmissions recorded at Karval and Haswell. These paths range in θ from −0.076° to 0.661°, which means that the receiving antennas were located either just within the radio horizon or slightly beyond the horizon in the region where diffraction is considered to be the dominant propagation mechanism.

For smaller values of θ, such as −0.307° for the Pikes Peak-Haswell path, although there is still a definite diurnal pattern in the median signal level, the fading range has decreased to a very small value, and there is no apparent variation in it with time of day, at least as far as could be detected by these measurements. Similarly, for larger values of θ, such as the Garden City recordings from Camp Carson and Cheyenne Mountain (θ equals 2.20° and 1.61°, respectively), there is clearly a diurnal variation in median signal level, but the fading range appears to be influenced very little or perhaps not at all by time of day. In the data recorded at Anthony from Pikes Peak, Cheyenne Mountain, and Camp Carson (θ equals 2.92°, 3.35°, and 3.90°, respectively), there is a diurnal pattern in the median signal level and what appears to be a slight variation in fading range. The latter effect may be caused by a partial mixing of the weak afternoon signal with noise at this most distant recording site. This would result in an apparent rise in the 90-percent level and a corresponding decrease in fading range. The mixture of signal and noise was not a problem at the nearer sites.

Figure 10 shows similar diurnal-variation curves for the 100-, 192.8-, and 1,046-Mc transmissions from Cheyenne Mountain received at each of the four receiving sites. It will be seen that not only is the median signal level apparently a function of frequency at Karval and Haswell, as was mentioned previously, but the extent of the diurnal variation of fading range likewise appears to be a function frequency.

Figure 11 shows the diurnal variation information for the 418-Mc transmissions from Cedar Rapids, Iowa, received at three antenna heights at Quincy, Ill. The angle θ for the three antenna heights ranges from 0.90° to 1.15°. Here, as in the case of the Garden City data shown in figures 9 and 10, there is no apparent diurnal variation in fading range, although the median signal level shows very wide variation for all three antenna heights.

7. Average Distribution of Instantaneous Signal Level

The data thus far have consisted only of median values of fading range. In some practical applications, it might be desirable to know more about the expected cumulative distribution of instantaneous signal levels than merely the fading range as defined here. In order to obtain a representative distribution for a given hour of the day, transmission path, and frequency, each individual hourly distribution was tabulated in terms of received power relative to the median signal level for that hour. Specifically, they were tabulated in terms of the percentage of time that the signal exceeded each of 10 levels spaced at 2-db intervals above and below the median. These percentages were then averaged for each of the 10 levels, and an "average" distribution of instantaneous levels was drawn. For the Cheyenne Mountain-Haswell and Pikes Peak-Haswell paths, where the range of variation was comparatively small, intervals smaller than 2-db were used.

In figure 12 average distributions are shown for each of the propagation conditions studied at Haswell (i. e., 3 transmitting antenna heights for 100 Mc and the 3 frequencies transmitted from Cheyenne Mountain). An early morning and an early afternoon hour were chosen because in general the signal level is at a maximum and minimum, respectively, during these periods. These curves are principally intended to illustrate the general character of the distributions of instantaneous signal level for the various paths and frequencies. However, they also serve to point out some of the effects discussed in connection with the diurnal-variation curves and the fading range versus θ plot. For example, on 100 Mc, the slope of the curve, and hence the fading range, increases sharply with increasing θ. There is also a slight increase in slope with increasing frequency, but, as can be seen more clearly in the Haswell curves in figure 10, this effect is noticeable only during the night and early morning hours. Figure 13 shows the corresponding curves for the Garden City site. Here, in contrast to Haswell, a change in θ or in frequency appears to have little effect on the fading range, and the same is true in general of the Anthony and Quincy distributions shown in figures 14 and 15. On each of the graphs, the dashed line represents the Rayleigh distribution.

It should be pointed out that fading ranges obtained from these curves should probably be termed the "expected" fading ranges, whereas the values plotted in the previous figures were the medians of the individual hourly fading ranges. It has been found, however, that in most cases these expected values obtained from the average distribution curves varied only a small amount from the median fading ranges.

From the standpoint of practical application it might seem desirable to have defined fading range as the ratio of the 1- to the 99-percent level. However, obtaining fading-range data based on this definition would have involved considerable extrapolation of the hourly distribution curves derived from the time-totalizing recorders. For this reason, it is felt that the 10- and 90-percent levels provide a much more accurate and more easily obtainable measure of fading range. Estimates of the 1- and 99-percent levels could be obtained by extrapolating the average distribution curves, and they would probably be no less accurate than the values obtained by extrapolation of the individual hourly distributions.

If it is assumed that the signal is composed of a steady component superimposed on a Rayleigh-distributed signal, the slope of the resulting signal-level distribution plotted on Rayleigh graph paper will be decreased. Norton [3,4] has developed a method for estimating from the slope of the distribution, the ratio of the rms magnitude of the Rayleigh-distributed component to the magnitude of the steady component to give the resulting distribution. This is illustrated in figure 16, which shows a comparison of the distribution for the hour 1 to 2 p. m. over the Cheyenne Mountain-Haswell path with the computed distribution for K equal to -19 db, where K is the ratio in decibels of the rms Rayleigh-distributed signal to the constant component. Such a small value of K would be expected here because Haswell lies only slightly below the horizon of Cheyenne Mountain, and during the afternoon the predominant part of the signal probably arrived by way of diffraction. It should be pointed out that estimating K from the slope of the distribution curve is valid only if the average energy contained in either component does not vary during the hour [4]. Determination of the ratio of constant to Rayleigh-distributed component from the observed fading range is illustrated in figure 42 of NBS Circular 554 [1].

8. Discussion of the Chart Samples

Figure 1 and figures 17 through 23 are samples of Esterline-Angus chart records, which were chosen as being typical of the various paths and frequencies included in this study. Figure 1 shows 100-Mc signals received at Karval, Haswell, and Garden City and transmitted alternate hours from Camp Carson and Cheyenne Mountain. Figure 17 shows signals transmitted from Cheyenne Mountain and Pikes Peak and received at Haswell and Garden City. They serve to illustrate the fact that for small values of θ, both the median signal level and the fading range are very critical to changes in θ. However, for larger values of θ, such as those at Garden City, the signal level and, more particularly, the fading range is affected comparatively little by changes in θ.

Figures 18 to 20 show sample recordings at 100, 192.8, and 1,046 Mc received at Karval, Haswell, and Garden City. From these it is evident that not only is fading range a function of frequency at Karval and Haswell (i. e., near the radio horizon); but, if we define the rate of fading as the number of times the signal level crosses the median level in a given period, it is seen that the rate of fading is also a function of frequency at all three sites. Figures 21 and 22 show similar samples recorded at Anthony on the same frequencies. These were made at much more rapid chart speeds, and it is evident that the dependence of fading rate on frequency holds even for these large values of θ. These samples also show that there can be wide variations in fading rate from day to day. The signals in figure 21 were recorded during the morning hours of August 16 and those in figure 22, during the afternoon of the next day while there were local thunderstorms in the vicinity of Anthony. This variation in fading rate with time of day is also illustrated in figure 23, which shows sample 418-Mc recordings at Quincy. Although the characteristics of the fading appear to be approximately the same for all three antenna

heights at Quincy, there is a very marked decrease in fading rate during the early evening hours.

In connection with fading rate, it should be noted that the time constant of the recording circuits used is approximately 1 sec., the limiting factor being the time constant of the recording meter itself.

9. Conclusions

When plotted as functions of θ, fading range and signal attenuation relative to free space exhibit some very similar properties. Within the radio horizon, $\theta<0$, the fading range is very small, the median value for all hours of the day being in all cases studied less than 2 db. Beyond the radio horizon in the so-called diffraction region, fading range and signal attenuation both increase very rapidly with θ. For values of θ greater than approximately 1°, the signal attenuation increases much more slowly, and the fading range levels off at very nearly the Rayleigh distribution value of 13.4 db.

It was found that there is a definite diurnal variation in fading range measured in the vicinity of the radio horizon. The fading range increases during the evening hours, drops again in the morning, and reaches a minimum during the afternoon at about the same time the signal level is also at a minimum. The amount of nocturnal rise in fading range near the radio horizon appears to be a function of frequency.

The diurnal variation of fading range tends to disappear as the receiving terminal is moved farther below the radio horizon; i. e., for paths having values of θ equal to, or greater than, about 1°.

It was pointed out previously that, assuming the received signal consists of a constant component plus a Rayleigh-distributed component, it is possible to estimate the ratio K of the magnitudes of the two components from the slope of the distribution curve; i. e., from the fading range. The difficulty in applying this method to an hourly distribution is that what would normally be called the "constant" component often varies considerably during an hour's time. For example, the diurnal variation in fading range near the radio horizon is largely due to relatively slow and deep fades occurring during the night.

If some smaller increment of time, say 5 or 10 min., were employed in this fading analysis, the results could be expected to be substantially different from those reported herein. In fact, the diurnal variation in fading range at Haswell, for example, might be completely inverted if the time interval were sufficiently small. This is because the fading at night is so slow that a time interval that would include numerous fades during the afternoon might include only a small portion of a fade at night. This would suggest the desirability of further fading studies in which a variety of time increments would be employed. In this way an increment could be chosen for a particular group of data, which would permit analysis of the constant and random components. Such a study would necessarily deal with fading rate as well as fading range.

This paper is an expanded and revised version of one entitled "An analysis of short-term fading in 100–1000 Mc propagation measurements beyond the radio horizon," by A. P. Barsis, H. B. Janes, and C. J. Roubique, which was presented at the joint URSI-IRE meeting in Washington, D. C., April 27 to 30, 1953. The author thanks Barsis and Roubique for their valuable assistance in the initial phases of the study, and Georgia J. Haines, R. W. Hubbard, and M. T. Decker for their work in analyzing the data.

10. References

[1] A. P. Barsis, J. W. Herbstreit, and K. O. Hornberg, Cheyenne Mountain tropospheric propagation experiments, NBS Circular 554 (Jan. 1955).

[2] R. P. Decker, Notes on the analysis of radio propagation data, Proc. IRE **22,** 1382 (Nov. 1951).

[3] K. A. Norton, The role of angular distance in tropospheric radio wave propagation. Unpublished paper presented at the IRE Convention, San Francisco, Calif., Aug. 19 to 21, 1953.

[4] K. A. Norton, Propagation over rough terrain, p. 101, Report of Symposium on Tropospheric Wave Propagation, U. S. Navy Electronics Laboratory, San Diego, Calif. (July 1949).

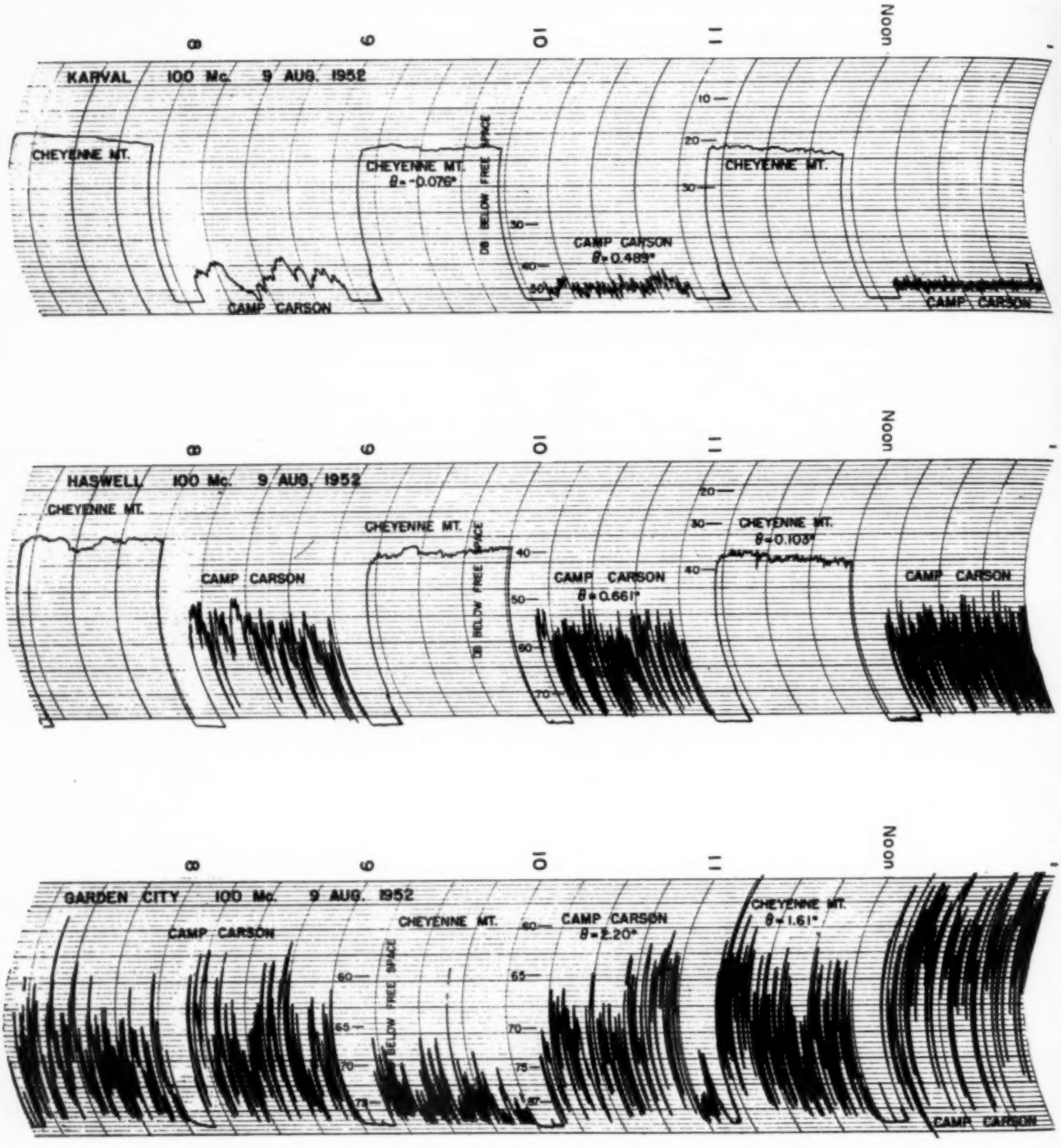

FIGURE 1. *Comparison of fading characteristics in relation to angular distance below the radio horizon.*

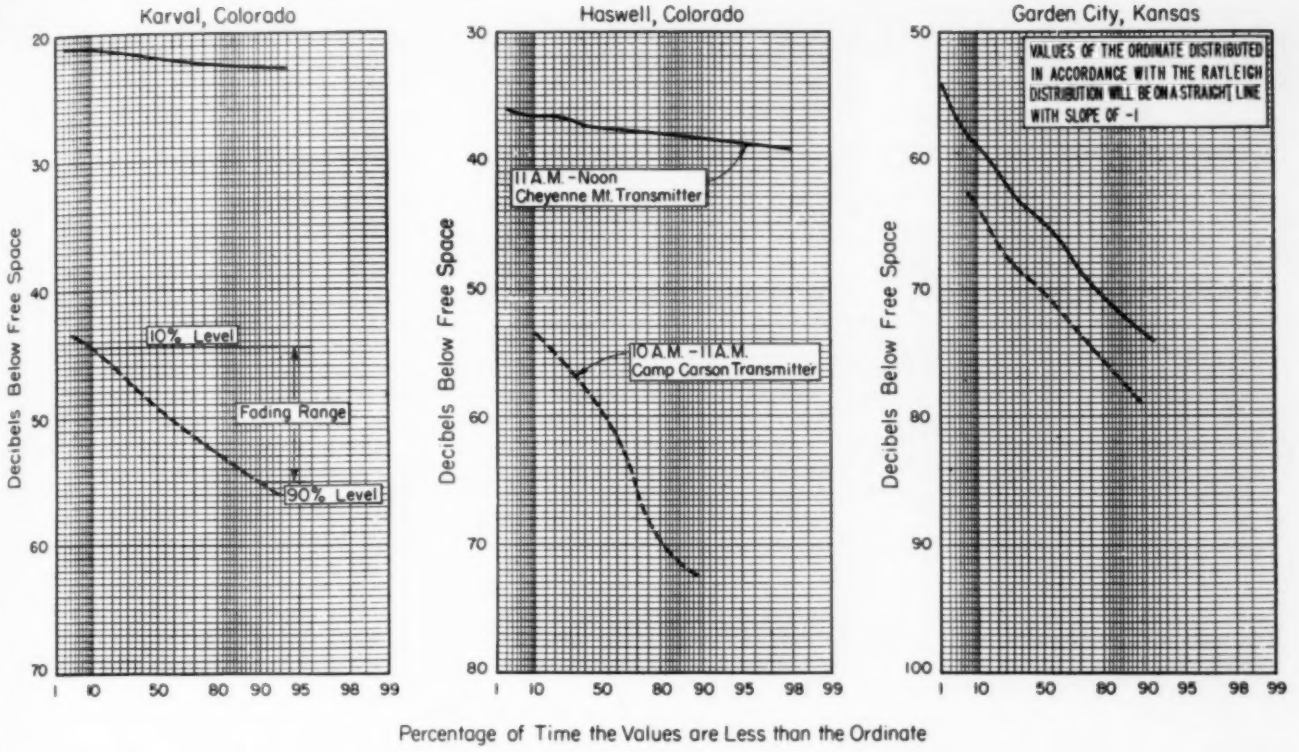
Karval, Colorado
Haswell, Colorado
Garden City, Kansas
Decibels Below Free Space
10% Level
Fading Range
90% Level
11 A.M. - Noon
Cheyenne Mt. Transmitter
10 A.M. - 11 A.M.
Camp Carson Transmitter
VALUES OF THE ORDINATE DISTRIBUTED IN ACCORDANCE WITH THE RAYLEIGH DISTRIBUTION WILL BE ON A STRAIGHT LINE WITH SLOPE OF -1
1 10 50 80 90 95 98 99
Percentage of Time the Values are Less than the Ordinate

FIGURE 2. *Sample distributions of instantaneous signal levels for two of the hours shown in figure 1, August 9, 1952, 100 Mc*

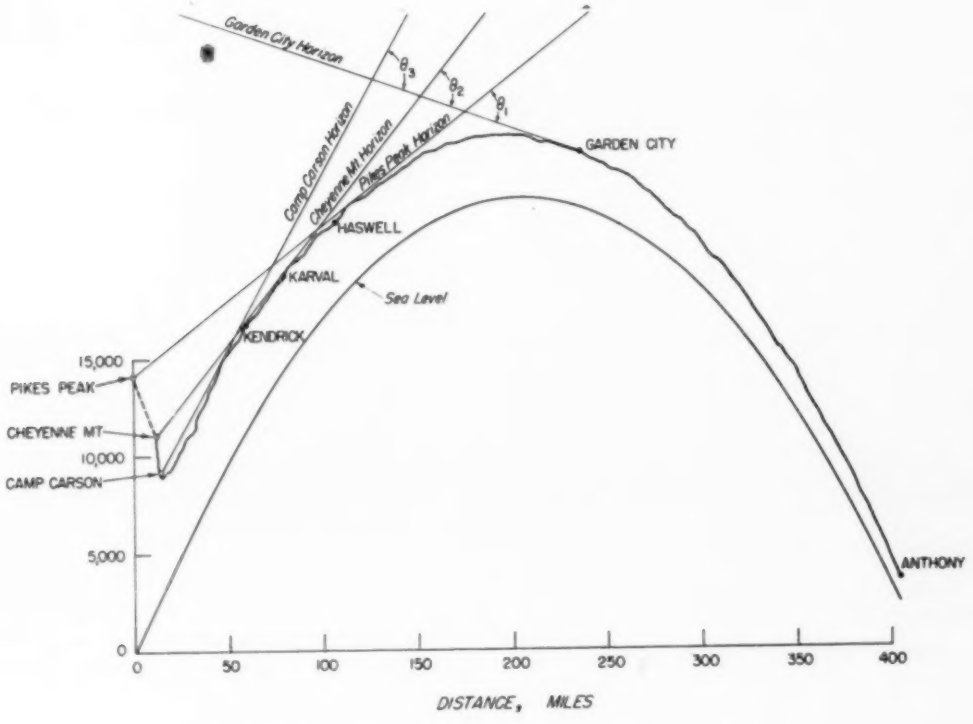

FIGURE 3. *Terrain profile of Colorado-Kansas paths.*

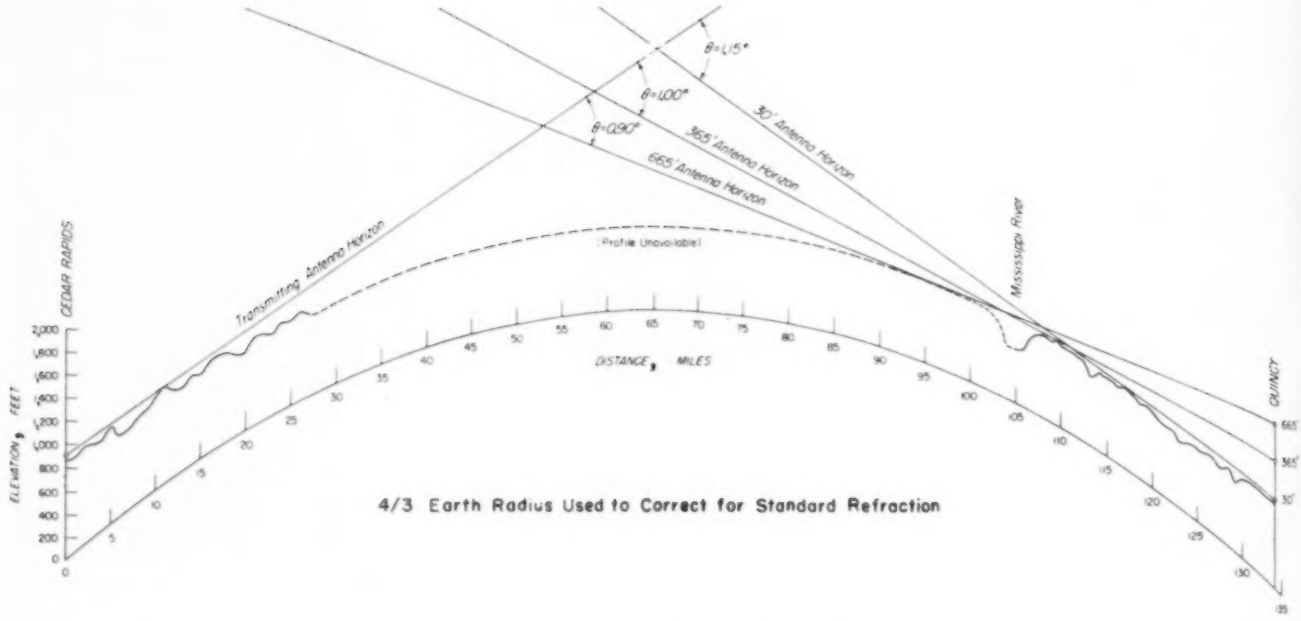

FIGURE 4. *Terrain profile of Cedar Rapids-Quincy path.*

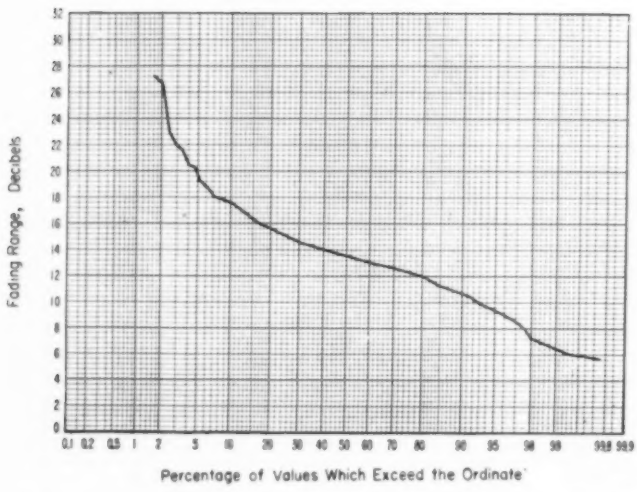

FIGURE 5. *Distribution of fading-range values, Cedar Rapids-Quincy path, August 1952, 418 Mc.*

Receiving-antenna height, 365 ft.

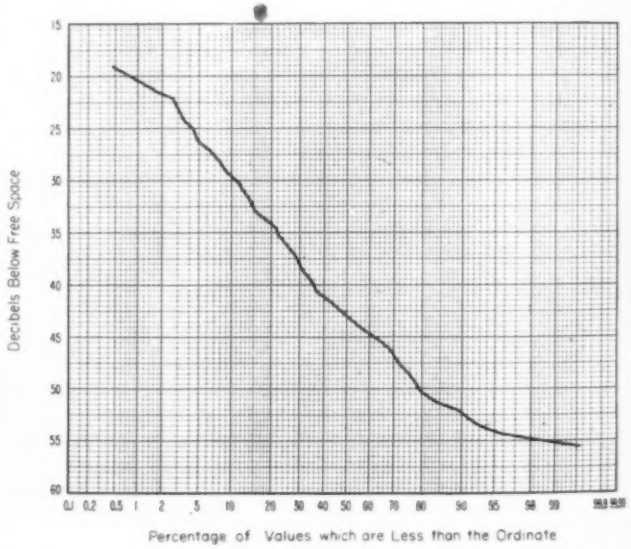

FIGURE 6. *Distribution of hourly median signal levels, Cedar Rapids-Quincy path, August 1952, 418 Mc.*

Receiving-antenna height, 365 ft.

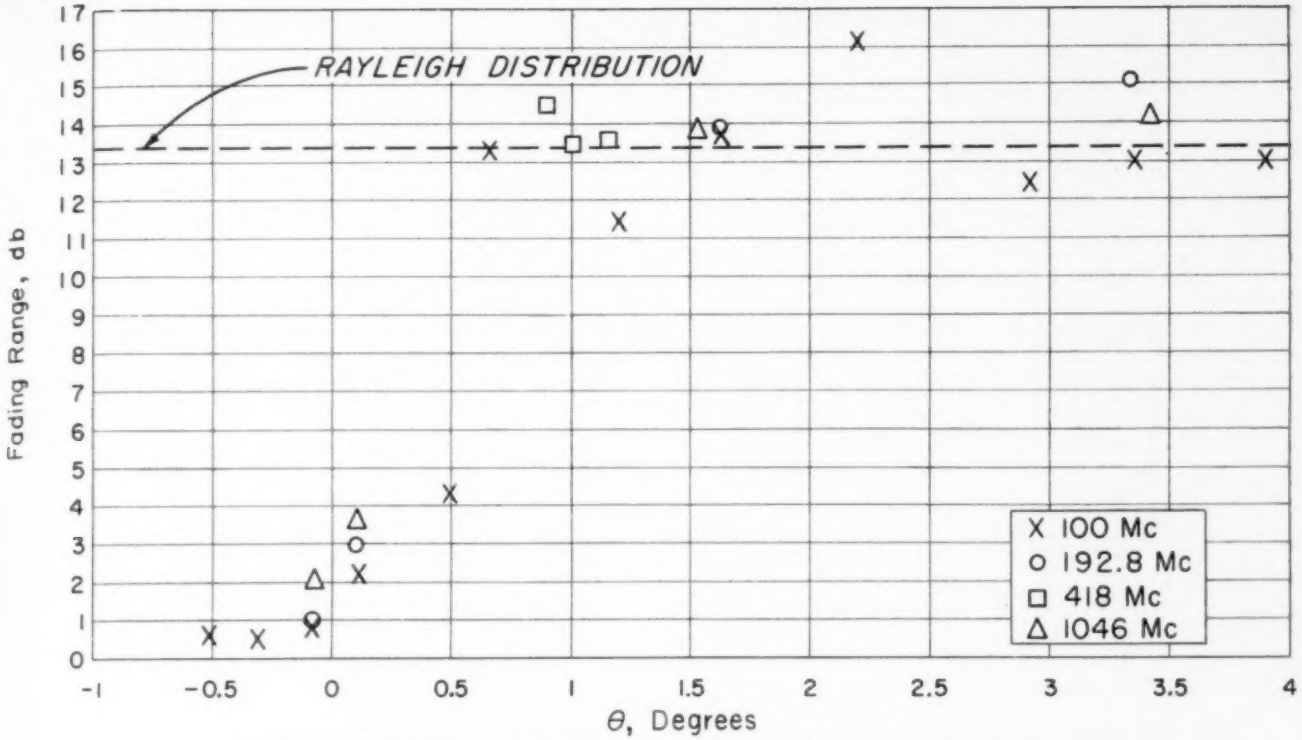

FIGURE 7. *Dependence of fading range on the angular distance below the horizon.*
θ calculated, assuming standard atmospheric refraction, August 1952 data.

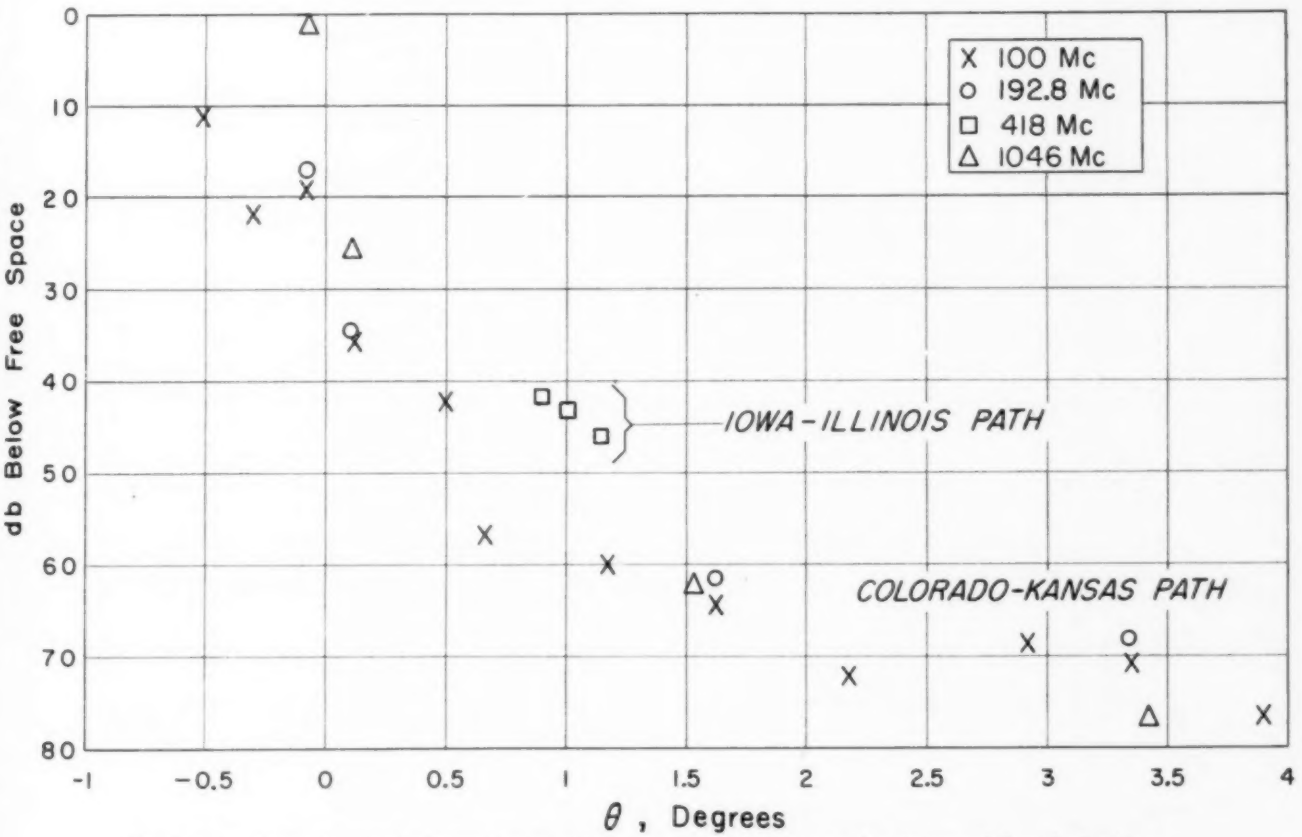

FIGURE 8. *Dependence of attenuation relative to free space on the angular distance below the horizon.*
θ calculated, assuming standard atmospheric refraction, August 1952 data.

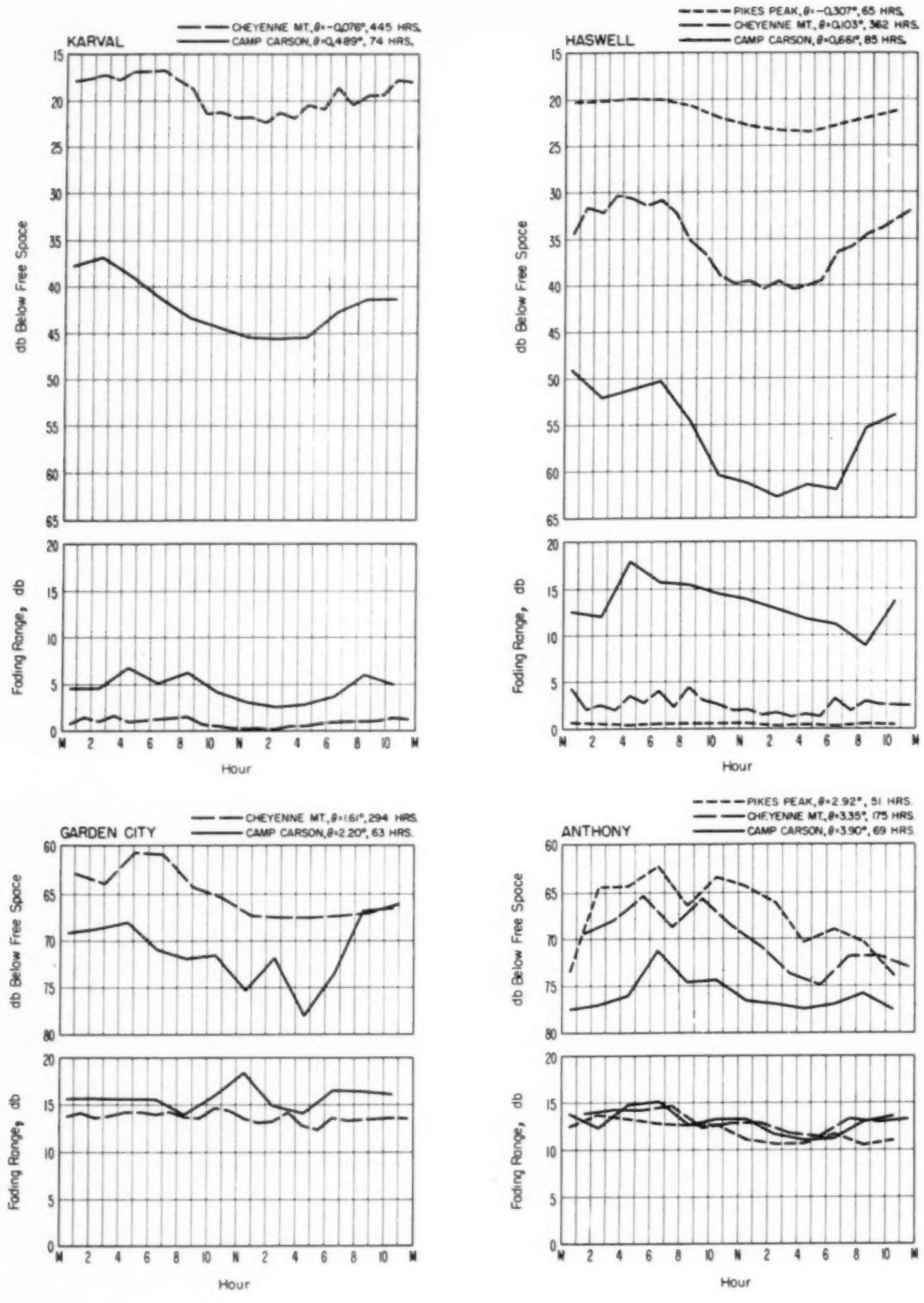
KARVAL
CHEYENNE MT., θ=-0.076°, 445 HRS.
CAMP CARSON, θ=0.489°, 74 HRS.
HASWELL
PIKES PEAK, θ=-0.307°, 65 HRS.
CHEYENNE MT., θ=0.103°, 362 HRS.
CAMP CARSON, θ=0.66°, 85 HRS.
GARDEN CITY
CHEYENNE MT., θ=1.61°, 294 HRS.
CAMP CARSON, θ=2.20°, 63 HRS.
ANTHONY
PIKES PEAK, θ=2.92°, 51 HRS.
CHEYENNE MT., θ=3.35°, 175 HRS.
CAMP CARSON, θ=3.90°, 69 HRS.
db Below Free Space
Fading Range, db
Hour
M 2 4 6 8 10 N 2 4 6 8 10 M

FIGURE 9. *Diurnal variation of median attenuation and of median fading range, August 1952, 100 Mc.*

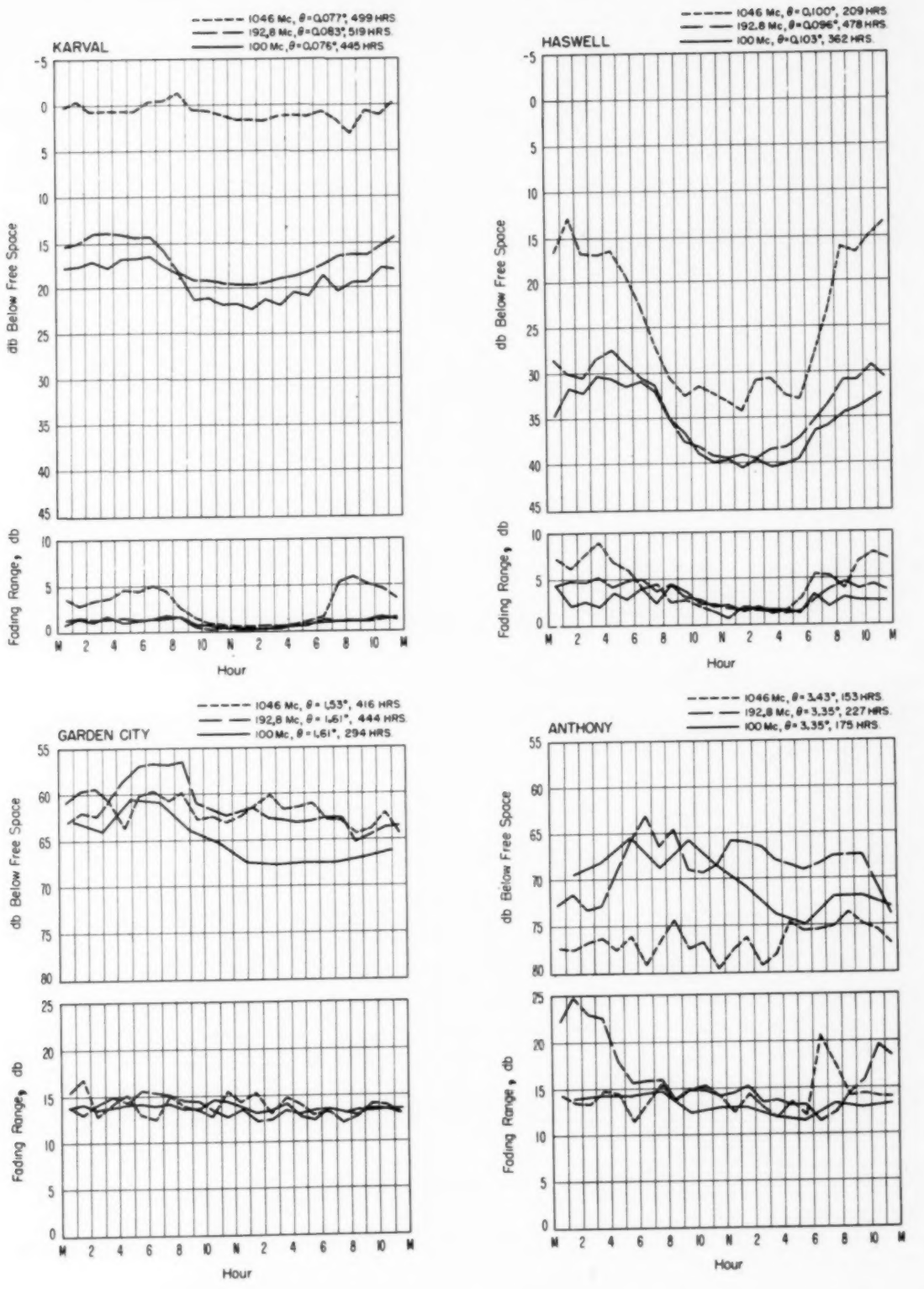
KARVAL
1046 Mc, θ=0.077°, 499 HRS.
192.8 Mc, θ=0.083°, 519 HRS.
100 Mc, θ=0.076°, 445 HRS.
HASWELL
1046 Mc, θ=0.100°, 209 HRS.
192.8 Mc, θ=0.096°, 478 HRS.
100 Mc, θ=0.103°, 362 HRS.
GARDEN CITY
1046 Mc, θ=1.53°, 416 HRS.
192.8 Mc, θ=1.61°, 444 HRS.
100 Mc, θ=1.61°, 294 HRS.
ANTHONY
1046 Mc, θ=3.43°, 153 HRS.
192.8 Mc, θ=3.35°, 227 HRS.
100 Mc, θ=3.35°, 175 HRS.
db Below Free Space
Fading Range, db
Hour
M 2 4 6 8 10 N 2 4 6 8 10 M

FIGURE 10. *Diurnal variation of median attenuation and of median fading range from Cheyenne Mountain, August 1952*

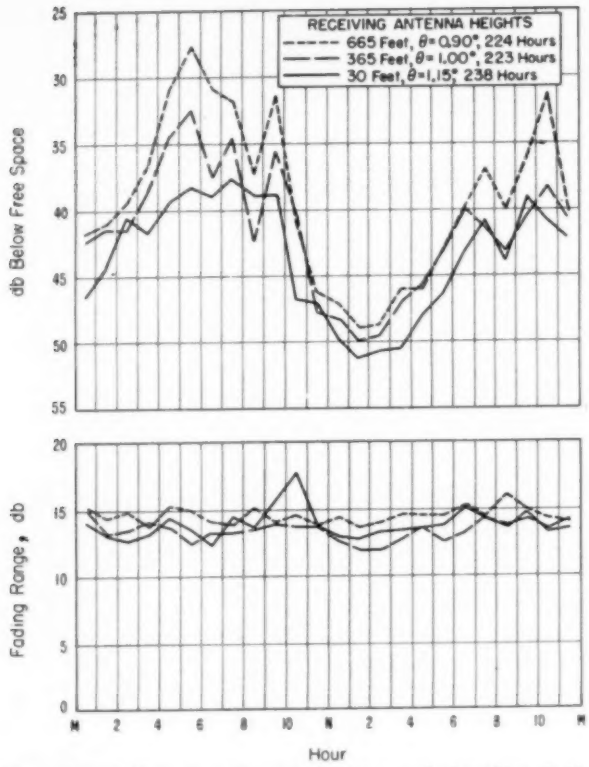

FIGURE 11. *Diurnal variation of median attenuation and of median fading range, Cedar Rapids, Iowa to Quincy, Ill., August 1952, 418 Mc.*

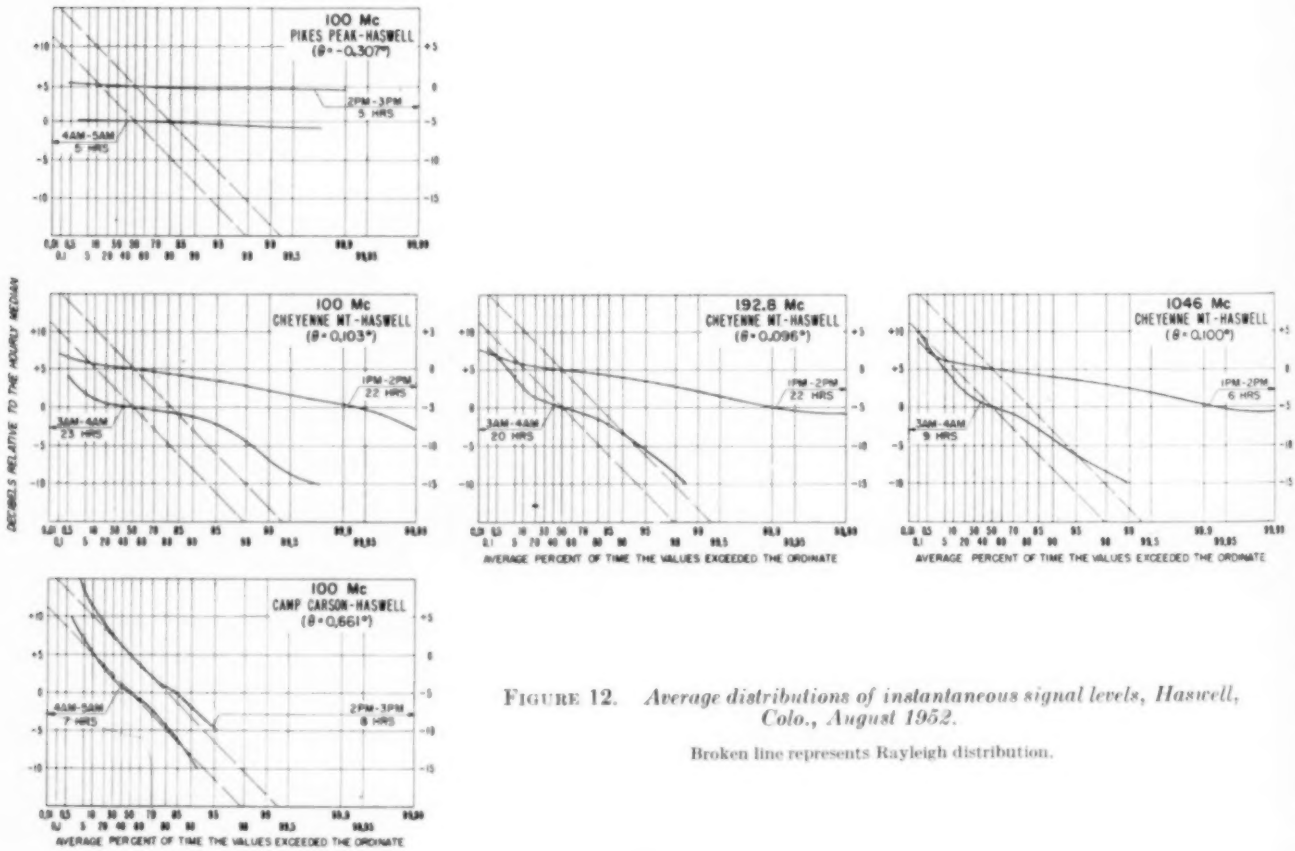

FIGURE 12. *Average distributions of instantaneous signal levels, Haswell, Colo., August 1952.*

Broken line represents Rayleigh distribution.

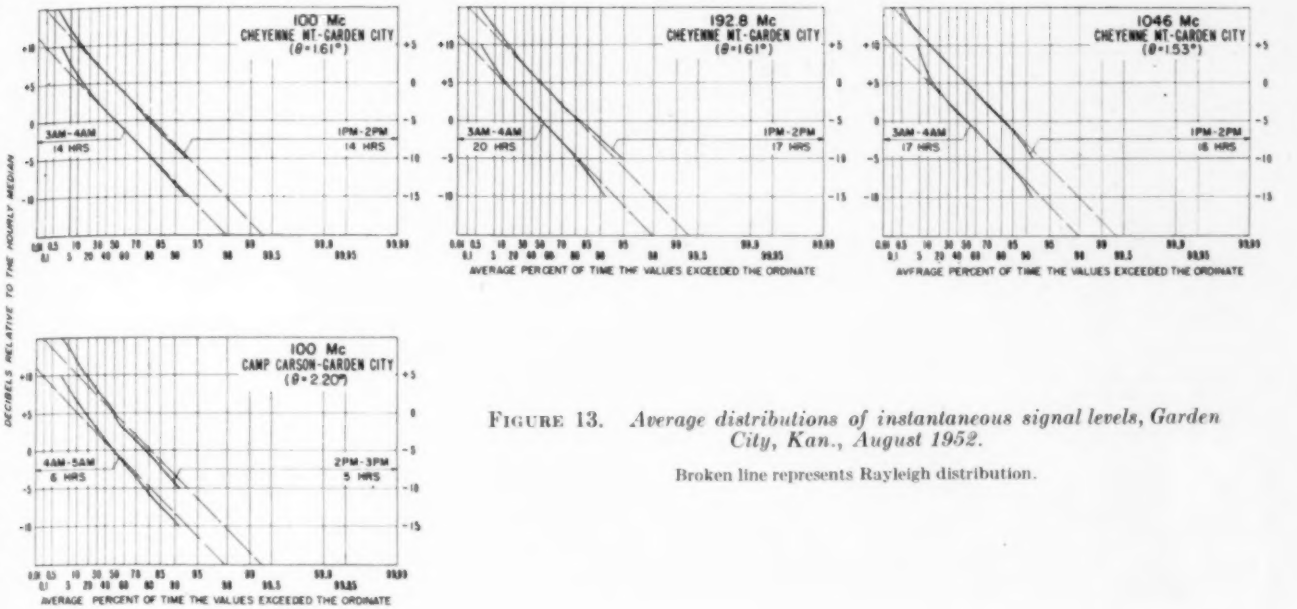

FIGURE 13. *Average distributions of instantaneous signal levels, Garden City, Kan., August 1952.*

Broken line represents Rayleigh distribution.

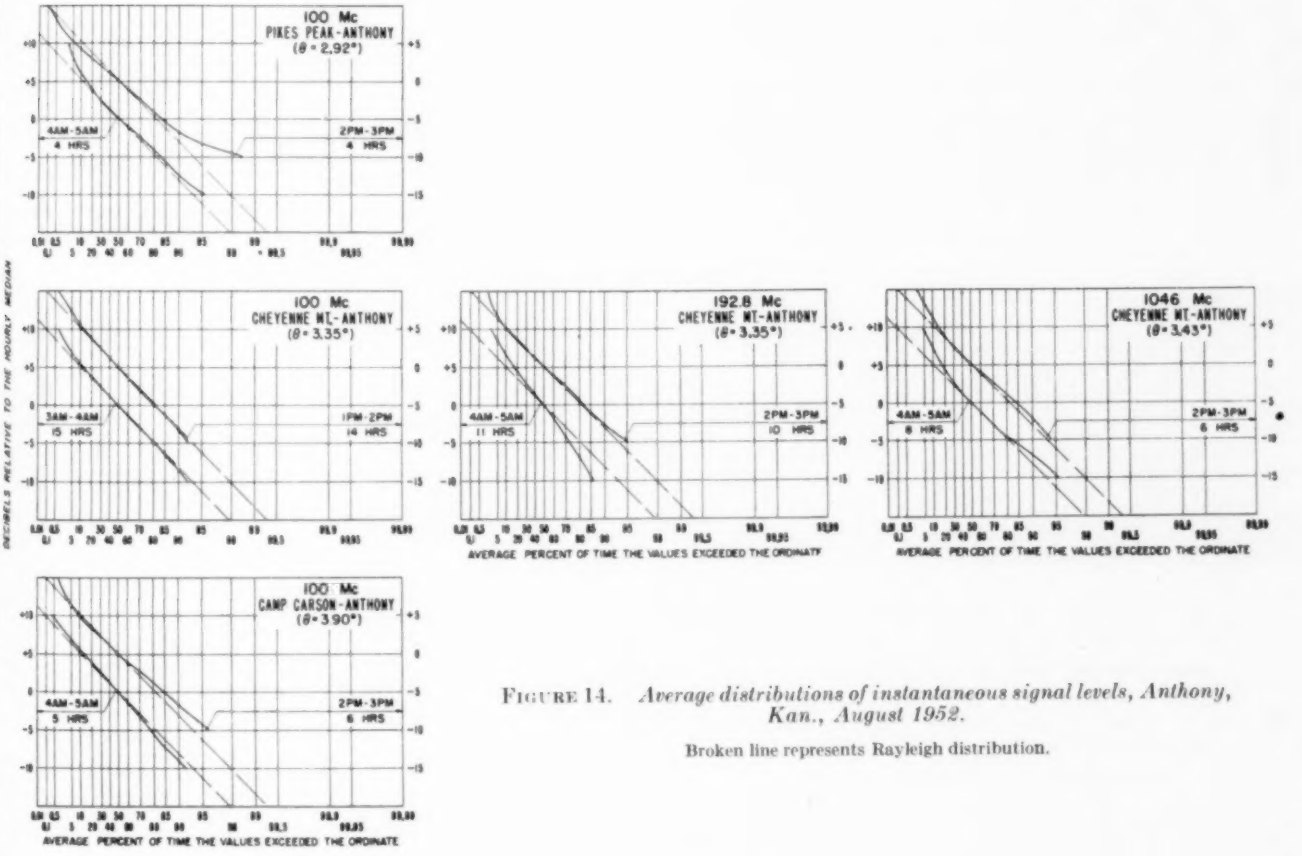

FIGURE 14. *Average distributions of instantaneous signal levels, Anthony, Kan., August 1952.*

Broken line represents Rayleigh distribution.

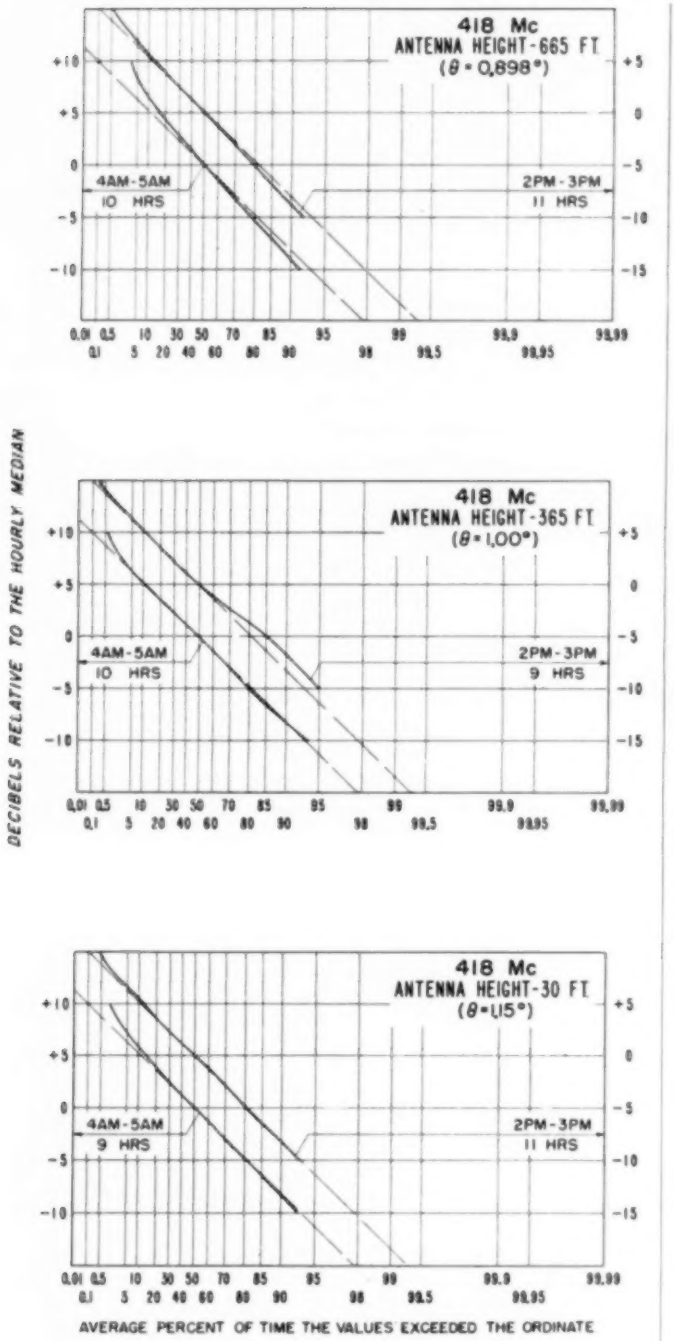

FIGURE 15. *Average distributions of instantaneous signal levels, Cedar Rapids, Iowa to Quincy, Ill., August 1952*

Broken line represents Rayleigh distribution.]

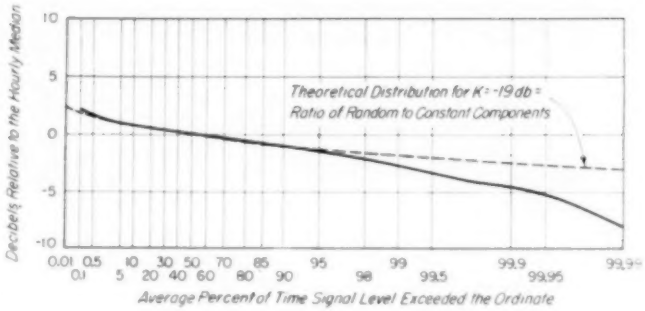
Theoretical Distribution for K = -19 db =
Ratio of Random to Constant Components
Decibels Relative to the Hourly Median
Average Percent of Time Signal Level Exceeded the Ordinate

FIGURE 16. *Average distribution of instantaneous signal levels, Cheyenne Mountain-Haswell path, August 1952, 100 Mc.*

$\theta = 0.103°$, 1 to 2 p. m., 22 hr.

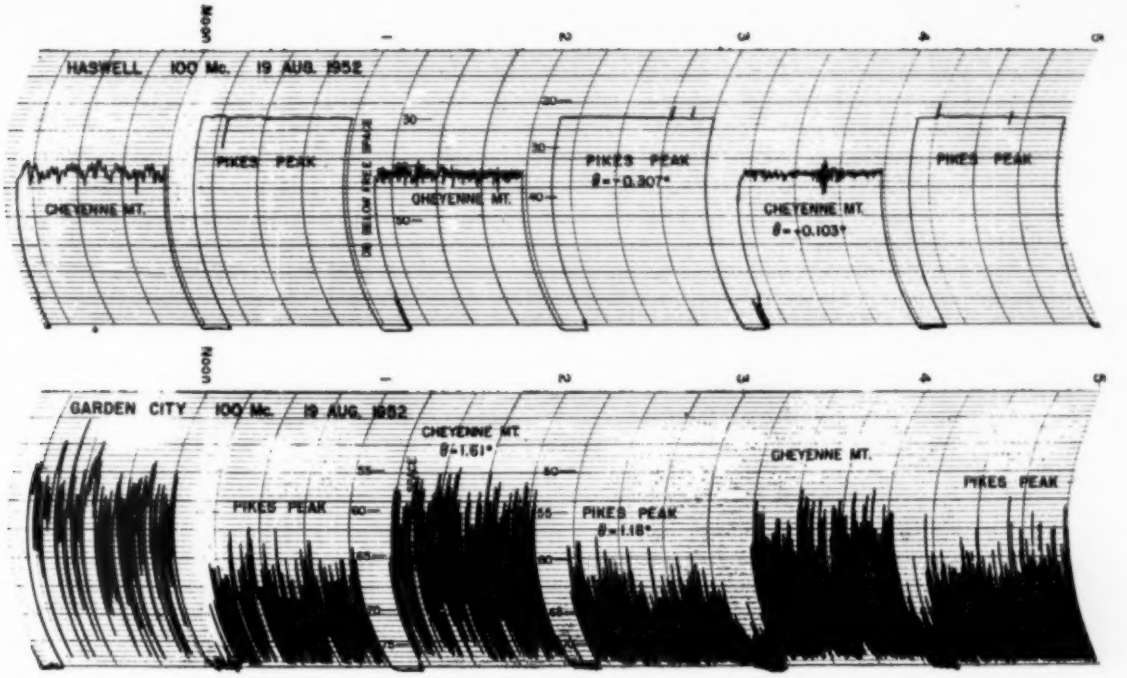

FIGURE 17. *Comparison of fading characteristics in relation to angular distance below the radio horizon.*

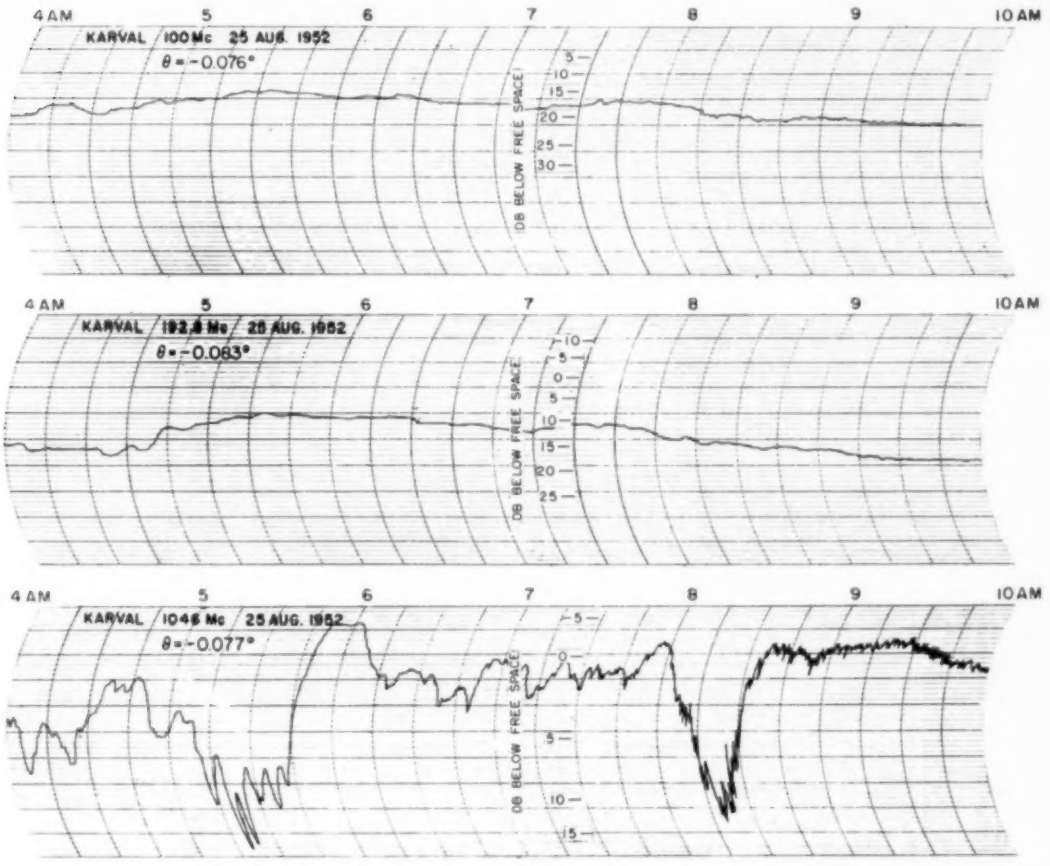

FIGURE 18. *Sample fading characteristics of three radio frequencies, Cheyenne Mountain-Karval path.*

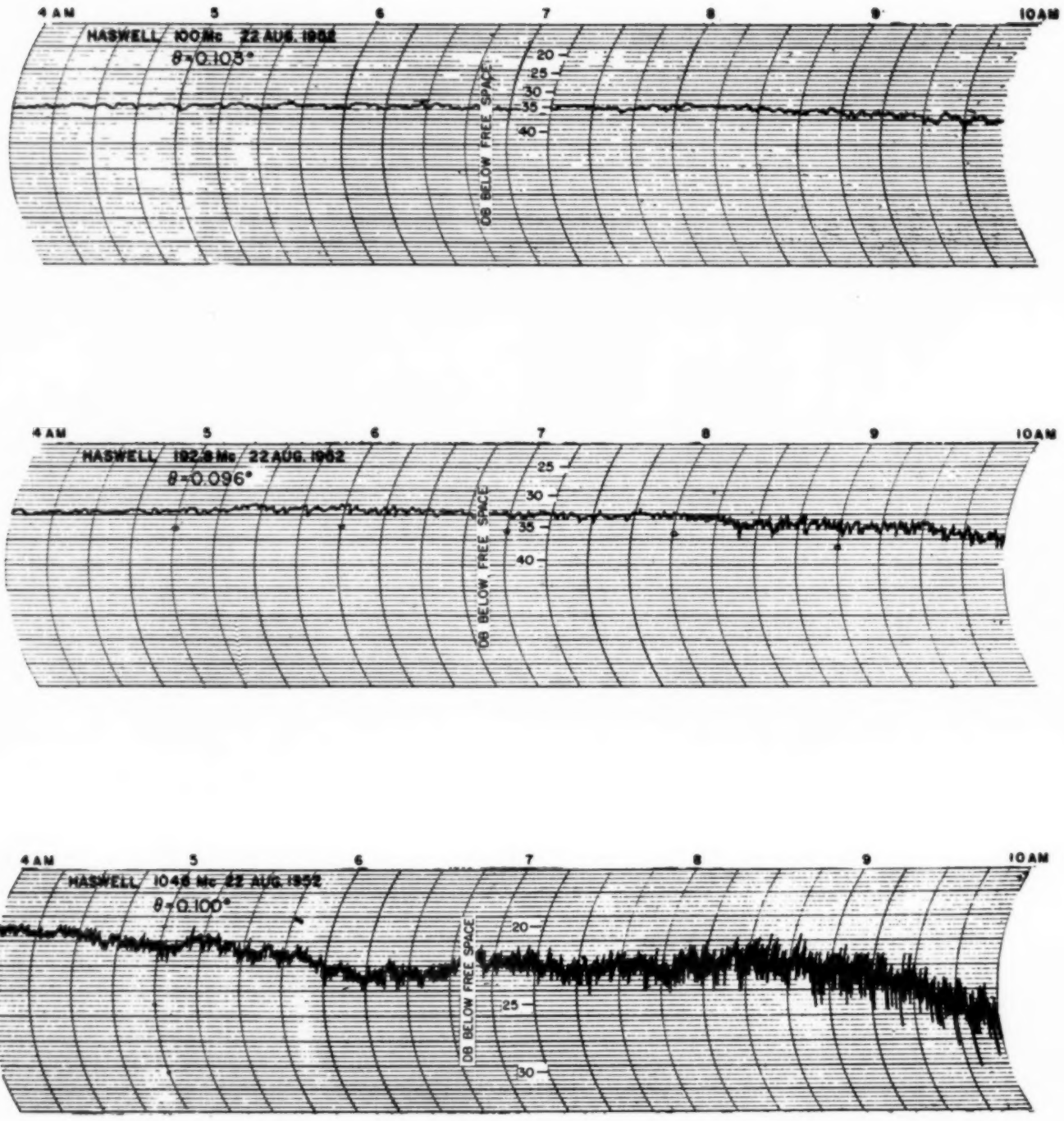

FIGURE 19. *Sample fading characteristics for three radio frequencies, Cheyenne Mountain-Haswell path.*

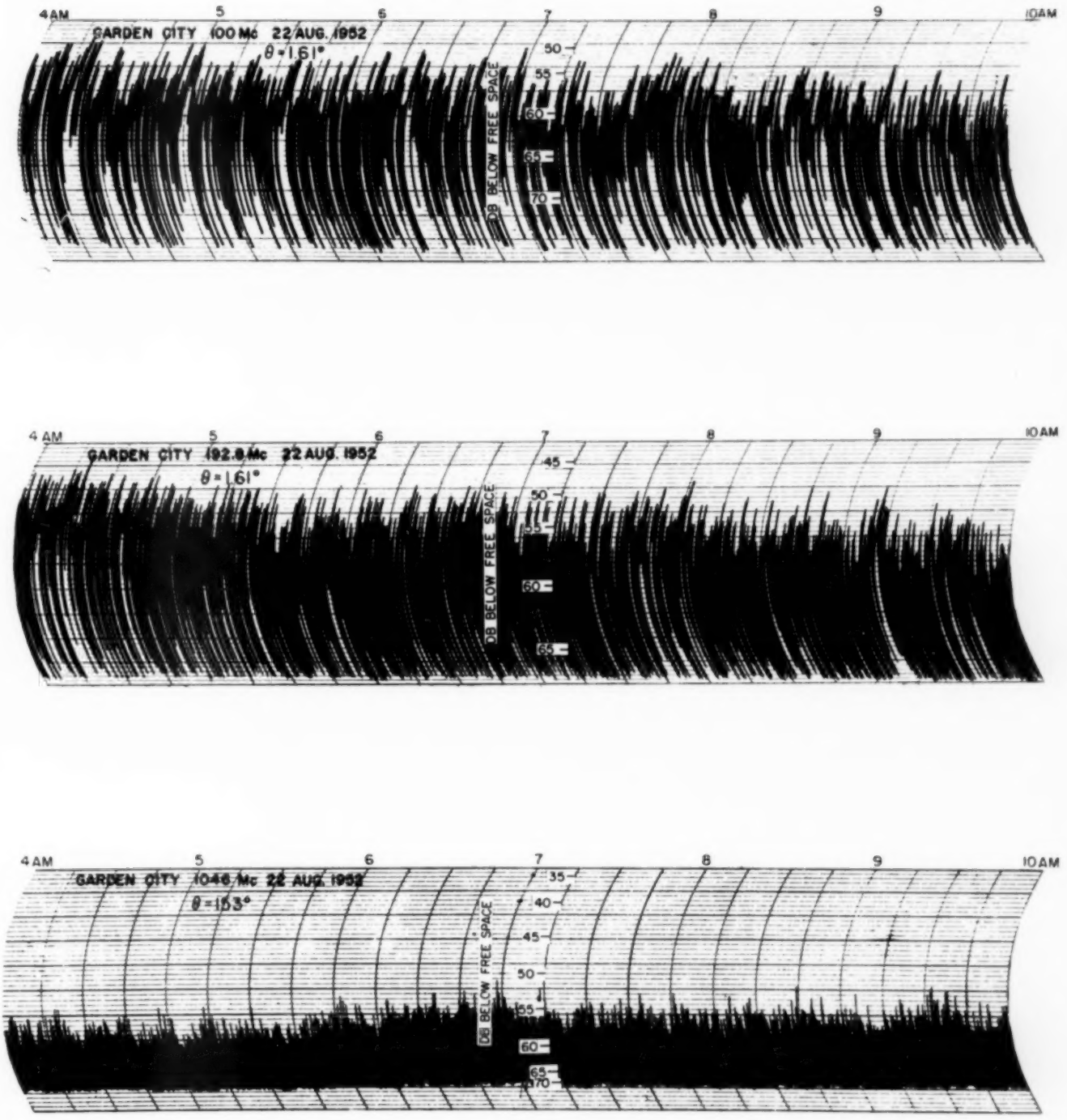

FIGURE 20. *Sample fading characteristics for three radio frequencies, Cheyenne Mountain-Garden City path.*

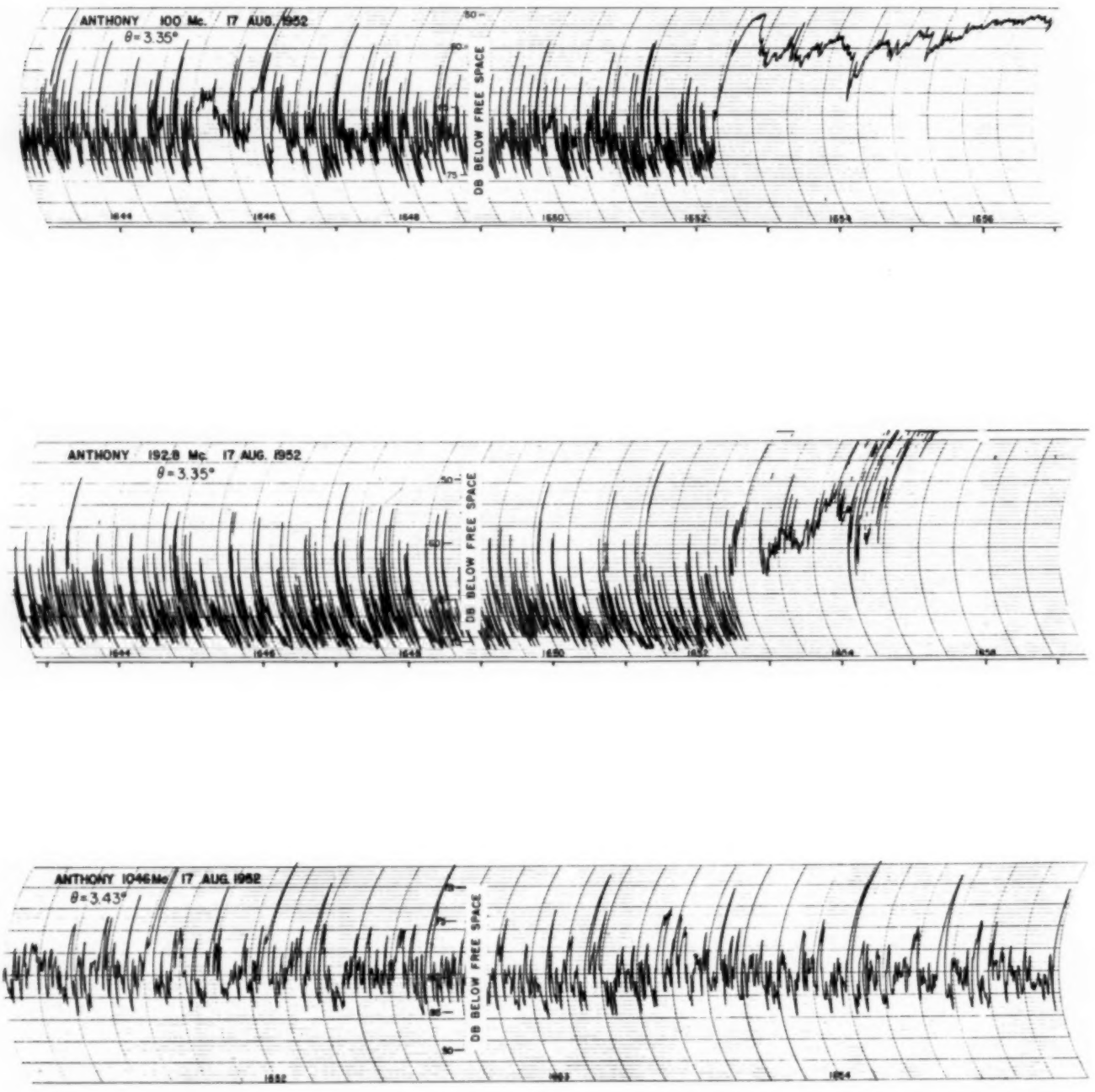

FIGURE 21. *Sample fading characteristics for three radio frequencies, Cheyenne Mountain-Anthony path.*

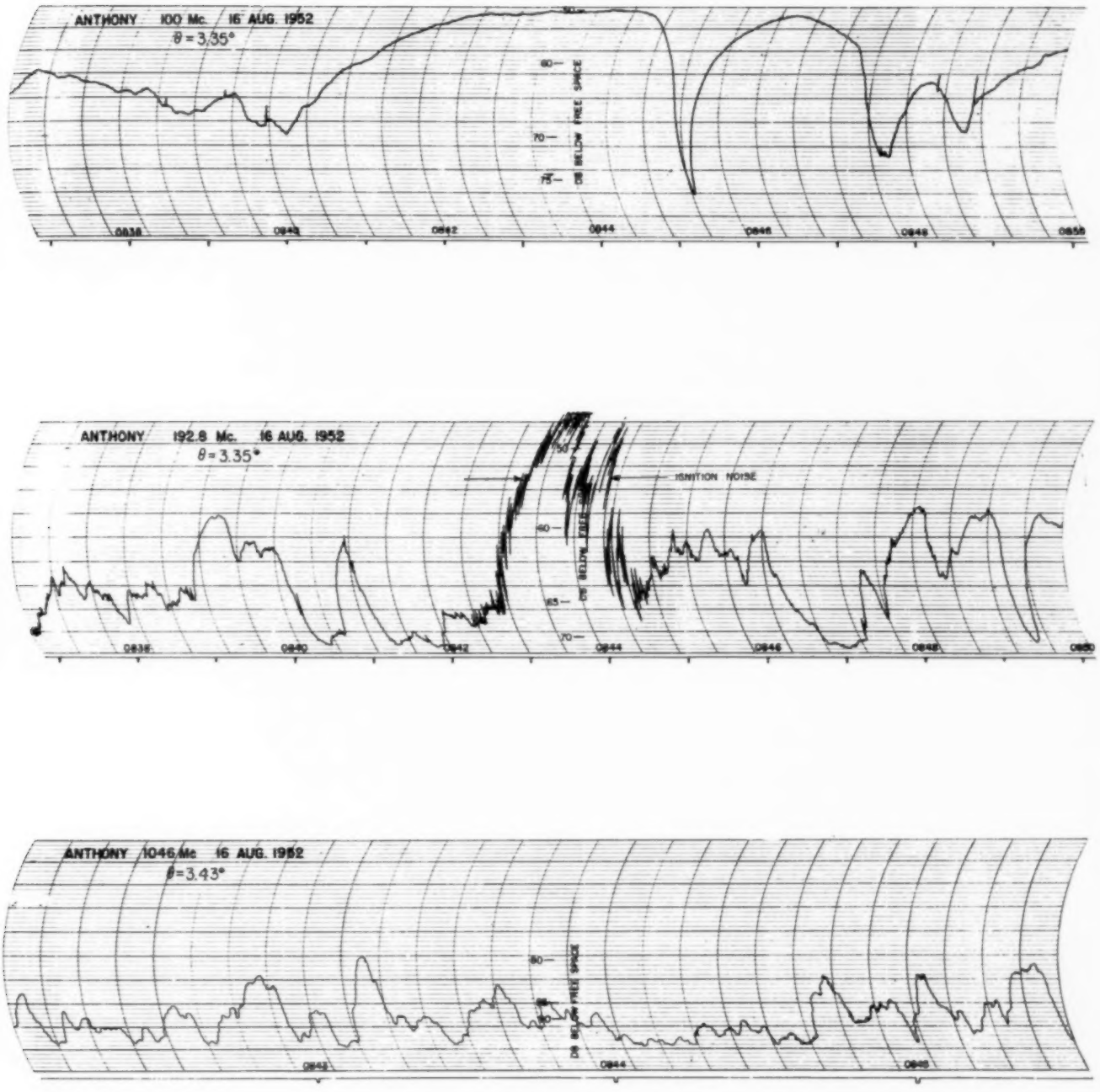
ANTHONY 100 Mc. 16 AUG. 1952
θ = 3.35°
DB BELOW FREE SPACE
ANTHONY 192.8 Mc. 16 AUG. 1952
θ = 3.35°
IGNITION NOISE
DB BELOW FREE SPACE
ANTHONY 1046 Mc 16 AUG. 1952
θ = 3.43°
DB BELOW FREE SPACE

FIGURE 22. *Sample fading characteristics for three radio frequencies, Cheyenne Mountain-Anthony path.*

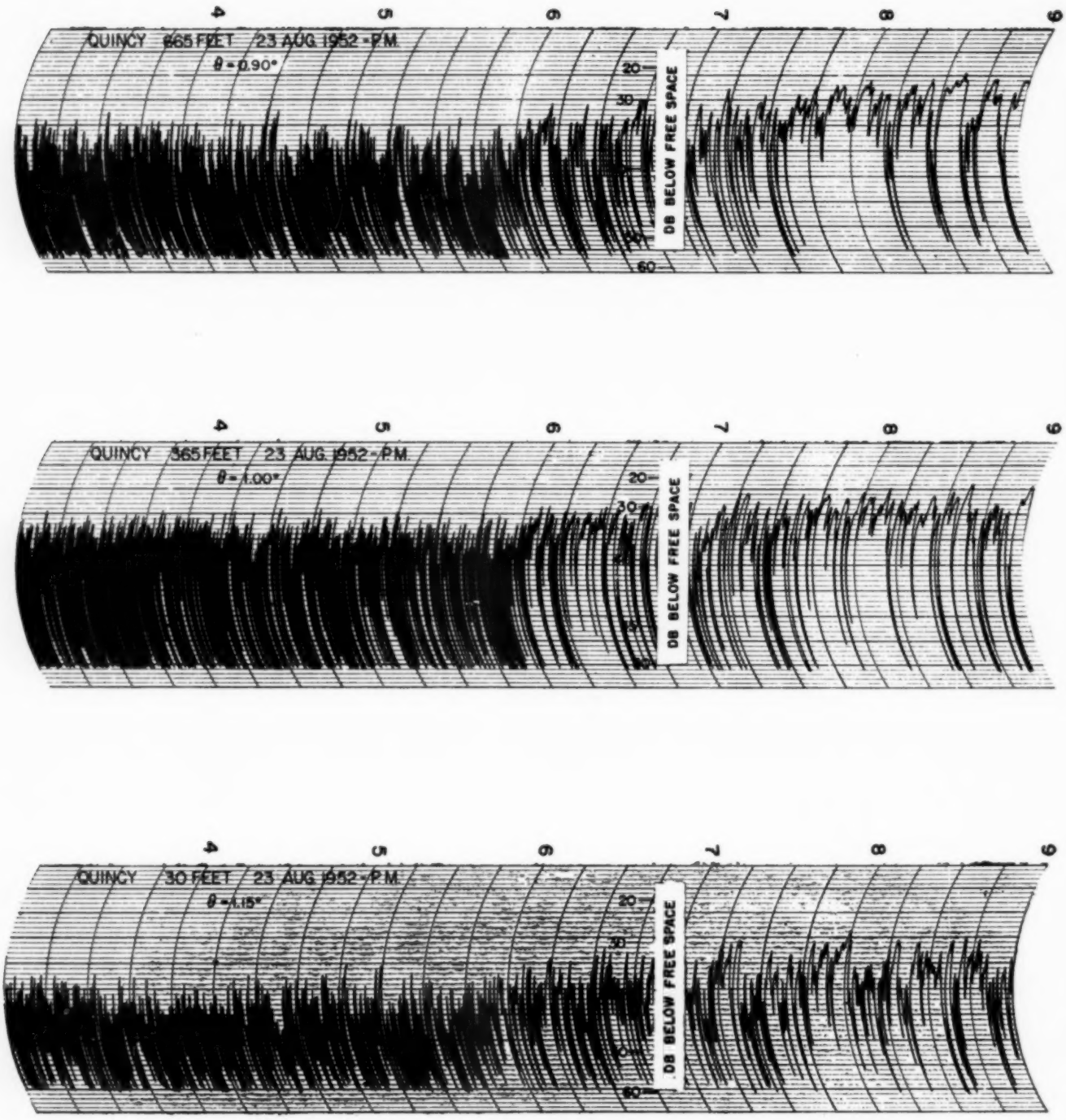

FIGURE 23. *Sample fading characteristics at 418 Mc for three receiving antenna heights, Cedar Rapids-Quincy path.*

BOULDER, Colo., December 1, 1954.

U. S. GOVERNMENT PRINTING OFFICE: 1955